HEAT FLOW AND MAGNETIZATION IN THE OCEANIC LITHOSPHERE

By

Kjell Lennart Hayling

A dissertation Presented in Partial Fulfillment
of the Requirements for the Degree
Doctor of Philosophy

UNIVERSITY OF MIAMI

Coral Gables, Florida

December, 1988

HEAT FLOW AND MAGNETIZATION IN THE OCEANIC LITHOSPHERE

By

Kjell Lennart Hayling

A dissertation Presented in Partial Fulfillment
of the Requirements for the Degree
Doctor of Philosophy

UNIVERSITY OF MIAMI

Coral Gables, Florida

December, 1988

UNIVERSITY OF MIAMI

A dissertation submitted in partial fulfillment of
the requirements for the degree of
Doctor of Philosophy

HEAT FLOW AND MAGNETIZATION IN THE OCEANIC LITHOSPHERE

Kjell Lennart Hayling

Approved:

Christopher G.A. Harrison
Professor of Marine Geology and
Geophysics
Chairman of Dissertation Committee

Jo Anne K. Hecker
Associate Dean of the
Graduate School

Keir Becker
Assistant Professor of Marine
Geology and Geophysics

Harry A. DeFerrari
Professor of Applied
Marine Physics

Donald B. Olson
Associate Professor of Meteorology
and Physical Oceanography

John R. Southam
Associate Professor of
Marine Geology and
Geophysics

HAYLING, KJELL L. (Ph.D. Marine Geology and Geophysics)
HEAT FLOW AND MAGNETIZATION IN THE OCEANIC LITHOSPHERE
(December, 1988).
Abstract of a doctoral dissertation at the University of Miami.
Dissertation supervised by Professor Christopher G. A. Harrison.

Two aspects of the processing and interpretation of satellite measurements of the geomagnetic field are described. One deals with the extraction of the part of the geomagnetic field that originates from sources in the earth's lithosphere. The other investigates the possibility of using the thermal state of the oceanic lithosphere to further constrain modelling and interpretation of magnetic anomalies.

We show that some of the magnetic signal in crustal anomaly maps can be an artifact of the mathematical algorithms that have been used to separate the crustal field from the observed data. Strong magnetic anomalies can be distorted but are probably real, but weak magnetic anomalies can arise from leakage of power from short wavelengths, and will also appear in anomaly maps as repetitions of the strong crustal anomaly. The distortion and the ghost anomalies follow the magnetic dip lines in a way that is similar to actual MAGSAT anomaly fields. This phenomenon will also affect the lower degree spherical harmonic terms in the power spectrum of the crustal field.

A model of the magnetic properties of the oceanic crust, that has been derived from direct measurements of the rock magnetic properties of oceanic rocks, is presented. The average intensity of magnetization in the oceanic crust is not strong enough to explain magnetic anomalies observed over oceanic areas. This is the case for both near surface observations (ship and aeromagnetic data) and satellite altitude observations. We show that magnetic sources in the part of the upper mantle that is situated above the Curie isotherm, if sufficiently strong, can produce satellite magnetic anomalies that are comparable to MAGSAT data. The method that we have developed for the study of depth to the Curie isotherm and magnetic anomalies can also be used in inverse modelling of satellite magnetic anomalies when the model is to be adjusted with an annihilator.

ACKNOWLEDGEMENTS

This disseration is the result of the work initiated by Chris Harrison with MAGSAT magnetic data. I thank Chris for giving me the opportunity to work on this project and Mark Carle for introducing me to the work he was doing with MAGSAT data and to this type of computer processing. Mark also provided me with the computer software that he had developed and assisted me when I started on this project.

I want to express my appreciation of my academic committee that always was willing to help me in my research and showed understanding in matters surrounding my stay at Rosenstiel. John Southam for mathematically steading my hand, Harry DeFerrari for introducing me to the theory of signal processing, Keir Becker for giving me a background in terrestrial heat flow, and Don Olson for focusing my attention to the leakage problem and for many helpful discussions. To Chris Harrison, chairman of my committee, I want to express my special appreciation for the assistance throughout my entire stay in Miami, not only with respect to my research but for making my stay in Miami possible in several respects. Chris was always willing to listen to my ideas, clarifying problems and to spend so much time for discussions that have been so fruitful. This stimulation and support have not only assisted me in this research project but have added new dimensions in my way of doing research. I am also grateful for the hospitality and

generosity that Chris and Martha has shown me and my family.

I thank all my friends at RSMAS, my fellow students, the faculty and staff. I specially want to mention Hank Poor and Grant Basham in the Computer Center for being so helpful and understanding.

This disseration research has been supported by grants from the National Aeronautics and Space Administration and by a fellowship from the Scandinavian-American Foundation.

All my friends in Miami have made my visit to the United States a pleasant experience. I am grateful to my family for all their support, in particular I thank my wife Marie for every time that she put things in perspective and for sharing in everything.

TABLE OF CONTENTS

LIST OF FIGURES

LIST OF TABLES

1. INTRODUCTION

Satellite altitude magnetic anomalies have helped to discover many new things about the Earth's lithosphere, but new questions have arisen and will continue to arise in the future. The scalar magnetic anomaly maps that have been derived often show a pronounced elongation that is parallel to the dip of the magnetic field. Some of the explanations forwarded for this phenomenon is that the instruments of the satellite have better resolution of magnetic anomalies that are at a 90 degree angle to the orbital track of the space craft. The simple fact that the magnetic field from a random distribution of dipoles in the Earth's lithosphere will show a certain elongation along the dip lines of the main magnetic field has also been shown (Langel, 1987). However, the extent to which the entire anomaly field will be elongated is not nearly what we can see in magnetic anomaly maps. The severity of the elongation, and also repetition of magnetic anomalies, is well demonstrated in Figure 1. Spherical harmonic expansion of the total geomagnetic field (which is used to extract the anomaly field) was expanded to a higher degree of harmonics. The harmonic terms are fitted to the observed total magnetic field in a least squares sense. Carle and Harrison (1982) pointed out some fundamental problems, in working with anomaly fields, when spherical harmonics is used to represent the core magnetic field. Any crustal magnetic

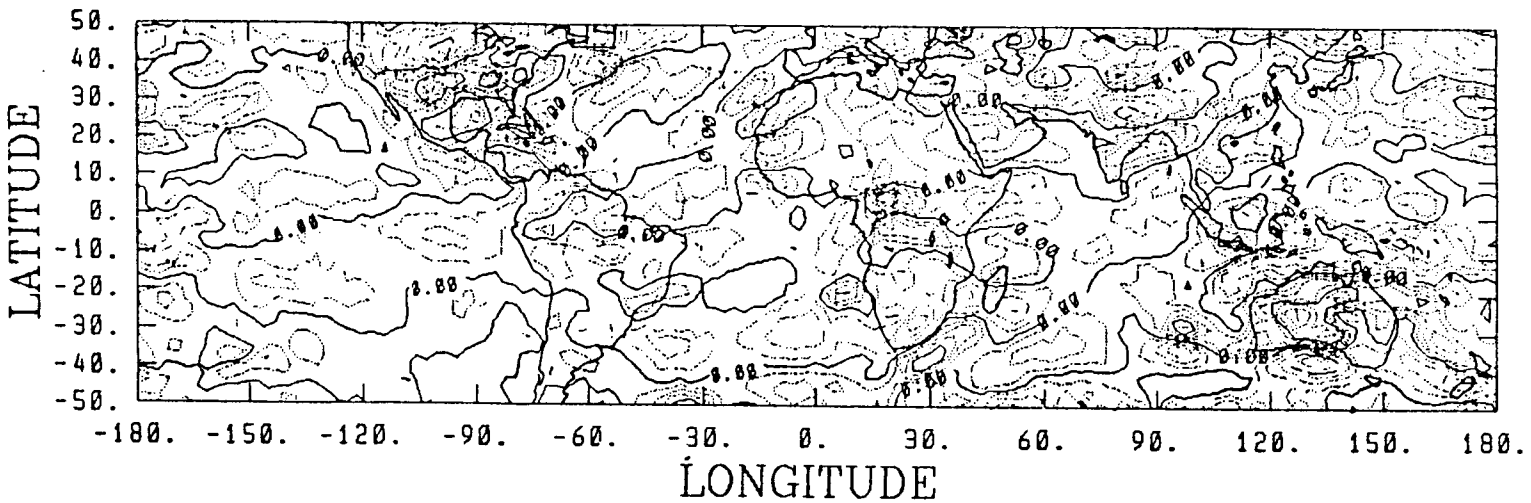

Figure 1. 2 by 2 scalar magnetic anomaly field from MAGSAT at an average altitude of about 400 km (from Langel et al., 1982).

sources that produce magnetic anomalies that have certain fractions of this anomaly in a low degree of harmonic will contribute to this coefficient of harmonic. Alldredge (1983) predict that crustal anomaly fields that are derived with the most commonly used extraction technique will be seriously distorted by crustal sources that have a lateral extension of more than a few hundred kilometers.

Another surprising characteristic of the scalar magnetic field is that there are few, if any, magnetic anomalies along continent-ocean boundaries. The assumption for magnetic anomalies along the continent-ocean boundaries is that the continental crust is many times thicker than the oceanic crust, which will cause a difference in vertically integrated magnetization between continents and oceans. Mayer et al. (1983, 1985) propose that when the main magnetic field is removed from the total field some of the signal from the Earth's crust is also removed. Usually degrees of harmonic 1 through 13 of a spherical harmonic model are used to represent the core field. Mayer et al. derived a synthetic scalar magnetic anomaly field of the Earth's crust and concluded that the spectrum of the magnetic signals from continent-ocean boundaries has power of equal amplitude down to spherical harmonic degree 5. Contrary to this hypothesis, several investigators suggest that some of the core field signal is present in degrees of harmonic higher than the usual truncation point at degree 13

(Arkani-Hamed et al., 1985; Harrison et al., 1986). Both these investigations indicate that the crustal signal becomes important at degree 18 or 19.

This dissertation deals with two important problems which arise when satellite altitude magnetic data are used in modelling large scale structures and compositional variations in the oceanic crust. The first studies whether some of the magnetic signal in satellite magnetic anomaly maps can be artifacts of the mathematical algorithms that are used when these are extracted from the original measurements of the geomagnetic field. The second problem examines if there is a correlation between the depth to the Curie isotherm and magnetization models that have been derived from satellite magnetic data. We will also discuss the possibility of finding areas in the oceanic lithosphere where the intensity of magnetization is zero or very close to zero which can be used to constrain the amount of annihilator that has to be added to the magnetization model.

In Chapter 2 we describe the processing techniques that are used in modelling crustal magnetization and how crustal magnetization can be correlated with geologic structures. In this chapter we will also discuss possible magnetic sources in the oceanic lithosphere and how these correlate with what has been found from observations of oceanic rock samples. Much of what we discuss in this chapter has been published in Harrison et al. (1986) and in Hayling and Harrison

(1986). Chapter 3 describes how we have investigated the possibility that some of the magnetic signals in magnetic anomaly maps are artifacts of the mathematical algorithms that have been used to derive these maps rather than large scale structural and compositional variations in the oceanic lithosphere. We will also investigate how the crustal magnetic might be represented in a spherical harmonic model and what the power spectrum of this type of magnetic field represents. We will compare the magnetic anomaly maps from our simulated inversions with some of the anomaly maps that have been produced from MAGSAT data. In Chapter 4 we will describe how Curie isotherm modelling can be made in the oceanic lithosphere and we will discuss how different distributions of magnetic material in the ocean lithosphere will produce magnetic anomalies at satellite altitude. In this chapter we will also investigate if Curie isotherm modelling can be used to constrain further the magnetization models when the choice of an annihilator needs to be made. Chapter 5 includes a discussion of the results from this study and of the questions raised by this work.

2. MODELLING MAGNETIC ANOMALIES

Satellite measurements of the Earth's magnetic field have been made since the late 1950's and have given the scientific community a new opportunity to study large scale structures and compositional variations in the Earth's lithosphere. The latest magnetic space observatory, MAGSAT, provided us with a unique set of global magnetic data. This space craft was put in a twilight polar orbit at an average altitude of about 400 km (352 km perigee and 561 km apogee), and completed its seven and a half month mission in 1980. Magsat carried both scalar (Cesium vapor) and vector (Fluxgate) magnetometers. Vector data of the geomagnetic field are used for spherical harmonic modelling of the main field. The vector measurements of the crustal field were made in an attempt to distinguish between remanent and induced magnetizations. Unfortunately, the attitude sensors did not work according to specifications and the vector data of the crustal field have mainly been used to construct scalar anomaly maps.

A. Extraction of magnetic anomaly fields

Isolation of an anomaly field requires that the Earth's main magnetic field (strength between 30,000 and 60,000 nT), and external magnetic fields (0 - 2,000 nT) are removed. The derived anomaly field (0 - 30 nT at satellite altitude)

has to be inverted to a magnetization model, and even when a reliable anomaly field has been obtained, there are several magnetic distributions that are able to produce the same magnetic field.

The magnetic field of the Earth is conveniently represented in terms of the scalar magnetic potential V, which is usually described by spherical harmonic analysis in the form:

$$V = a \sum_{n=1}^{N} \left(\frac{a}{r}\right)^{n+1} \sum_{m=0}^{n} \left(g_n^m \cos m\phi + h_n^m \sin m\phi\right) P_n^m(\theta) \qquad (1)$$

where r is the radial distance of the observation point, θ is the colatitude, ϕ is the east longitude, n is the spherical harmonic degree, N is the maximum expansion of spherical harmonic degree, m is the spherical harmonic order, a is a reference radius (usually the radius of the Earth), g_n^m and h_n^m are the Gauss coefficients, and $P_n^m(\cos(\theta))$ are the semi-normalized associated Legendre polynomials.

The Gauss coefficients are usually determined by least squares analysis. (A detailed description is given in Appendix A.) The number of Gauss coefficients increases rapidly with higher degrees of harmonic. Even when a super computer is used for this analysis the spherical harmonic expansion has to truncated at a fairly low degree. Even when supercomputers are used in these inversions is the processing time many hours. Langel et al. (1981) produced

a spherical harmonic model from 26,500 scalar and vector MAGSAT data, to degree and order 23. The shortest wavelength of this model is approximately 1700 km. Cain et al. (1984) determined these coefficients up to degree and order 29. Surprisingly, the anomaly field derived by Cain et al. is lower in amplitude compared to the Langel et al. (1982) anomaly field. One would expect that the greater number of high order and degree spherical harmonic coefficients that is believed to represent the crustal field (14-29 versus 14-23) would increase the average crustal component. The reason for this is unclear. Arkani-Hamed et al. (1985) produced a spherical harmonic model up to degree and order 120, by slightly modifying the expansion technique when the harmonic coefficients are derived.

When we want to study crustal magnetization, it is necessary to filter out all non-crustal sources. The first step is the removal of the main geomagnetic field, or the core field, which is usually estimated by studying the power spectrum of the geomagnetic field. The power spectrum of a potential field that is represented by a set of spherical harmonic coefficients can be determined by Equation 2, introduced by Mauersberger (1956), and developed by Lowes (1966, 1974).

$$R_n = (n+1) \sum_{m=0}^{n} \left[(g_n^m)^2 + (h_n^m)^2 \right] \qquad (2)$$

R_n is the mean square value of the magnetic field over the Earth's surface produced by the n:th degree of the SHM. The rest of the symbols are the same as in Equation 1. Figure 2 shows the power spectrum of a spherical harmonic model derived by Langel et al. (1981). The white spectrum of a magnetic source at the core mantle boundary of degrees of harmonic 1 through 13 and the rapid increase in power for higher degrees of harmonic have been the strongest arguments for a truncation of the core field at this degree. Degrees of harmonic 1 through 13 of the derived spherical harmonic model are then used to calculate the magnetic field at satellite altitude that originates in the Earth's core. The

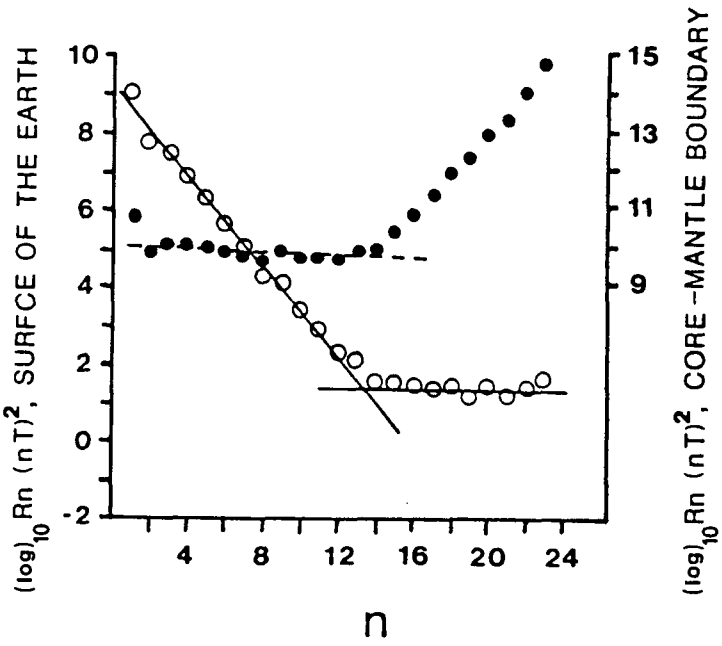

Figure 2. Geomagnetic field spectrum of MGST (10/81) SH-model. The open circles (surface of the Earth) and the solid dots (extrapolated to the core-mantle boundary) represent the total mean square contribution to the field by all harmonics of degree n.

Langel et al. (1982) scalar magnetic anomaly field (Figure 1) was derived by subtracting the main field for each individual satellite track. External fields, calculated with Equation 2 are then removed. Langel et al. also removed linear trends from each track line. These trends are believed to be caused by either additional external fields or by unremoved magnetic signal from the core. The data were then averaged in 2 by 2 degree blocks. Langel et al. (1982) used degree 1 through 13 of SH-model MGST (10/81) Langel et al., 1981). Cain et al. (1984) also removed degrees 1 through 13 of their SH-model. A different method to derive an anomaly field was used by Arkani-Hamed et al. (1985). They assumed that the direction of magnetization in the Earth's crust is equal to the field from the best fitted dipole (Gauss coefficients g_1^0, g_1^1, h_1^1) and expanded the spherical harmonic coefficients by fast Fourier transformations of MAGSAT data along longitudinal lines. The degree and order of harmonics can naturally be much higher compared to least squares inversions. Arkani-Hamed et al. derived a SHM model up to degree 120 (wavelengths down to $\sim$ 330 km) and found that the crustal field shows good coherency between harmonics 18 and 42 (wavelengths 900 to 2200 km), leaving the core field, and to some extent the field from electrojets to be represented by harmonics 1 through 17. Non-crustal sources contributing substantially to intermediate degrees of harmonics was also

suggested by Harrison et al. (1986). They performed inversions of magnetic potential from SH-models to models of crustal magnetization. These results indicate that the crustal component of the geomagnetic field becomes important at degree 18 or 19.

The external fields are greatly suppressed when data from magnetically quiet days are used. Further reduction of external fields is made by subtracting the field from magnetospheric currents that can be described by the potential function of Langel and Sweeney (1971).

$$V = a \left[\left(\frac{r}{a}\right) e + \left(\frac{a}{r}\right)^2 i \right] \cos(\theta) \qquad (3)$$

where e and i are time dependent coefficients of potential and represent external and internal sources respectively. The rest of the symbols are the same as in Equation 1.

B. Inversion of satellite magnetic anomalies.

The most adopted inversion process for satellite magnetic anomalies is a development of a technique introduced by Bott (1967). The intensity of magnetization of discrete sources in the Earth's crust is fit by least squares to an anomaly field. The sources can be spherical caps, where integration is performed in three dimensions, or magnetic dipoles, where the dipole source strength is determined. The latter is an acceptable assumption, with much less computation involved, if the dipoles are not

spaced too far apart (i.e. the spherical caps are small enough) (Carle, 1983). The thickness of the magnetized layer in the oceanic crust is usually assumed to be 6 km. The variations in magnetization can alternatively be caused by thickness variations in a uniformly magnetized layer, since the two models are indistinguishable at satellite altitude (Harrison, 1976). The direction of magnetization (or direction of the dipoles) is usually constrained to lie in the direction of the main field at the location of the source. This assumption is correct if the magnetization of the source is induced, and also is correct for remanent magnetization if the remanent magnetization was acquired in a field with a direction similar to the ambient field direction. The resulting matrix is solved by normal or modified Gaussian elimination methods. The highest resolution, or optimal solution (Mayhew et al., 1980), in equivalent source inversions has to be found by trial and error in the following way. A series of inversions is performed, where the spacing between the dipoles is varied and the standard deviation (STD) of the calculated magnetization and the root mean square (RMS) of the difference between observed and calculated anomaly fields are studied as functions of source spacing. This is demonstrated in Figure 3. The bulls-eyed pattern that can be seen in Figure 3G and 3H is an indication that oscillations have entered the solution. The optimum source

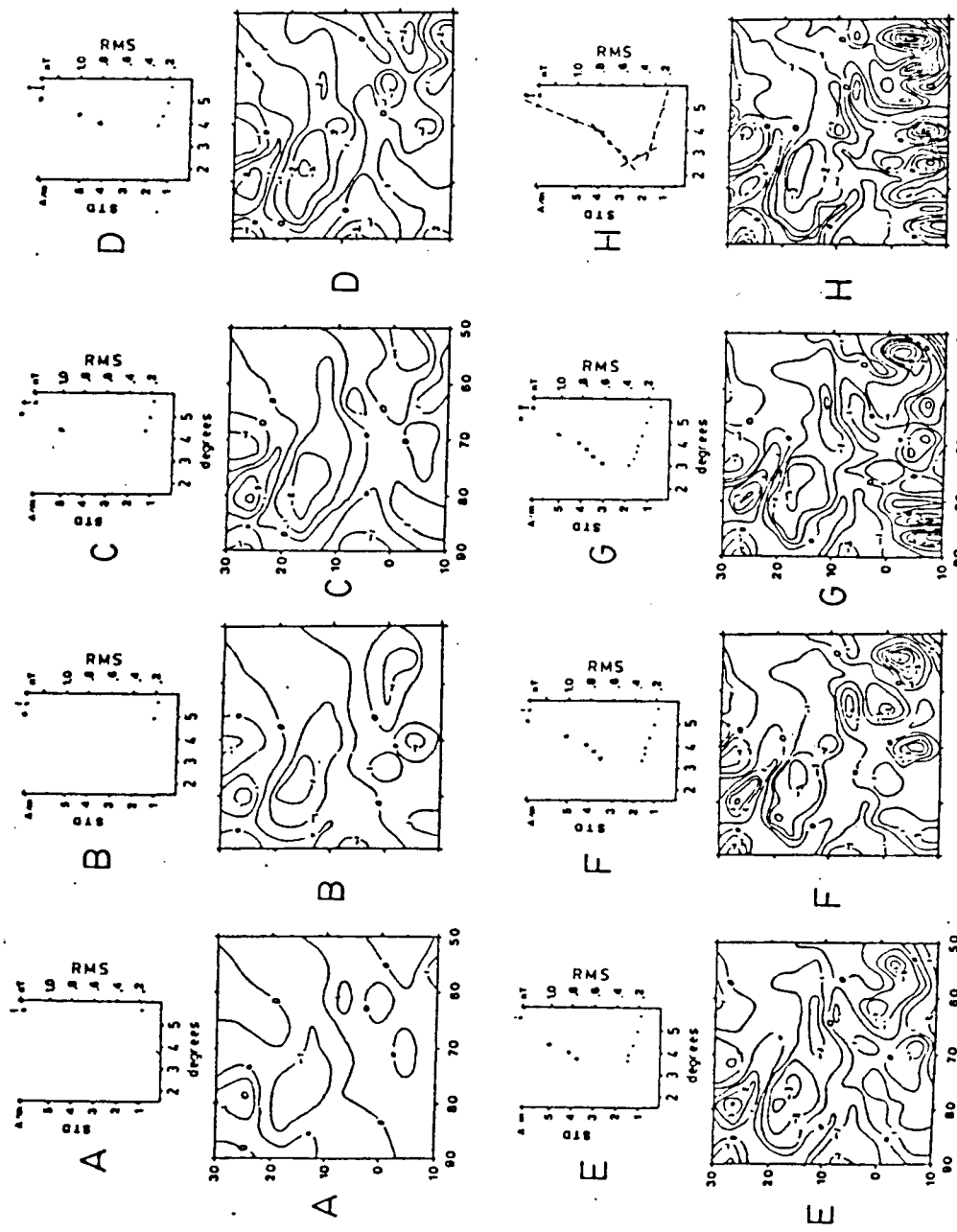

Figure 3. Standard deviation (STD) of modelled magnetization and root mean square (RMS) of the difference between modelled and observed anomaly fields, as functions of the spacing between the magnetic dipoles, in an area in the western North Atlantic. Model 3F is chosen as the optimal solution.

spacing is chosen to be just before oscillations start. Hayling and Harrison (1985) found that the source spacing at the optimum solution is related to the latitude of the inverted area (Figure 4A). Wider source spacings were found at lower latitudes for both oceanic and continental areas. The same general trend was also found in the ability of the calculated magnetizations to reproduce the anomaly field (Figure 4B). The reason for instabilities in the inversions

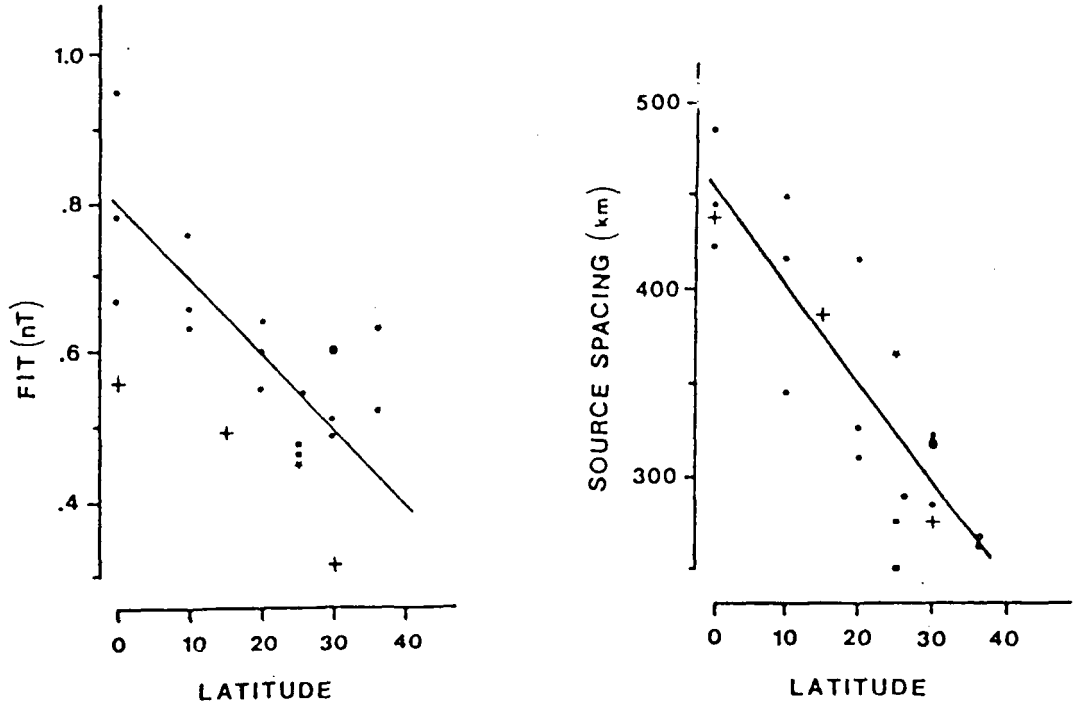

Figure 4. A. The function of the source spacing (in kilometers) at the optimal solution, to the latitudinal location of the center of the modelled area. B. The function of the fit (nT) between modelled and observed anomalous magnetic fields, at the optimal source spacing, to the latitude of the center of the inverted area. - Atlantic Ocean (Hayling and Harrison, 1986), + - Central and South Pacific (Hayling and Harrison, 1985), - Australia (Mayhew et al., 1980), ⊙ - North America (Mayhew, 1982b), o - Asia (Hayling and Harrison, 1985), * - Central North Pacific (Harrison et al., 1986).

probably arises from the relative amount of noise in the anomaly data set. A case where the source spacing at the optimum solution only depends on the spacing between the data points, in this case 2 by 2 degrees, would enable equivalent source solutions to be determined when the magnetic sources are spaced by this distance.

The calculated average magnetization in equivalent source models is approximately zero, which means that about half of all the sources have negative magnetizations, and that the direction of magnetization is antiparallel to the present field. For a model of induced magnetization this is obviously not correct. Induced magnetization is believed to be the most important magnetic source in the continental crust (e.g. Mayhew, 1985; Harrison, 1987a).

Studies of oceanic rock samples indicate that the principal magnetic source in the oceanic crust is remanent. This type of magnetization will be negative compared to the ambient field, when acquired during periods of reversed polarity. However, at satellite altitude ($\sim$400 km), only large scale variations in the intensity of magnetization are recorded. The magnetic lineations that can be seen in near surface measurements, are not detectable by satellites, except for very wide zones on constant polarity. The lower limit of the width of magnetized slabs recordable by MAGSAT is about 250 km (Harrison et al., 1986). The longest period of reversed polarity during the past 180 MY is 3.83 MY

(Berggren et al., 1985). A typical spreading rate of 30 km/MY (Minster and Jordan, 1978) will produce a reversely magnetized slab only 100 km wide. Long periods of normal polarity of the geomagnetic field occurred in the Jurassic and in the Cretaceous (Kent and Gradstein, 1985). The Jurassic normal polarity epoch (NPE) lasted for almost 10 MY ending 153 MY ago, and the Cretaceous NPE occurred between 118 and 84 MY. The width of these quiet zones in the NW Atlantic is about 250 and 700 km, respectively, depending on the distance from the rotation pole of the plates. The only remanent magnetization that will produce significant fields at satellite altitude is more or less parallel to the ambient field. Any physically plausible model of crustal magnetization, induced as well as remanent, cannot have negative magnetization values.

C. Adjustment with annihilators

In order to convert a model that contains negative magnetizations we must add a distribution of magnetic sources that does not produce a magnetic field of its own. Such a magnetization distribution is called an annihilator (Parker and Huestis, 1974). Harrison et al. (1986) adjusted an equivalent source solution in the central North Pacific to non-negative magnetizations. They also give a detailed discussion of annihilators. The adjustment technique is demonstrated in Figure 5. The intensity of

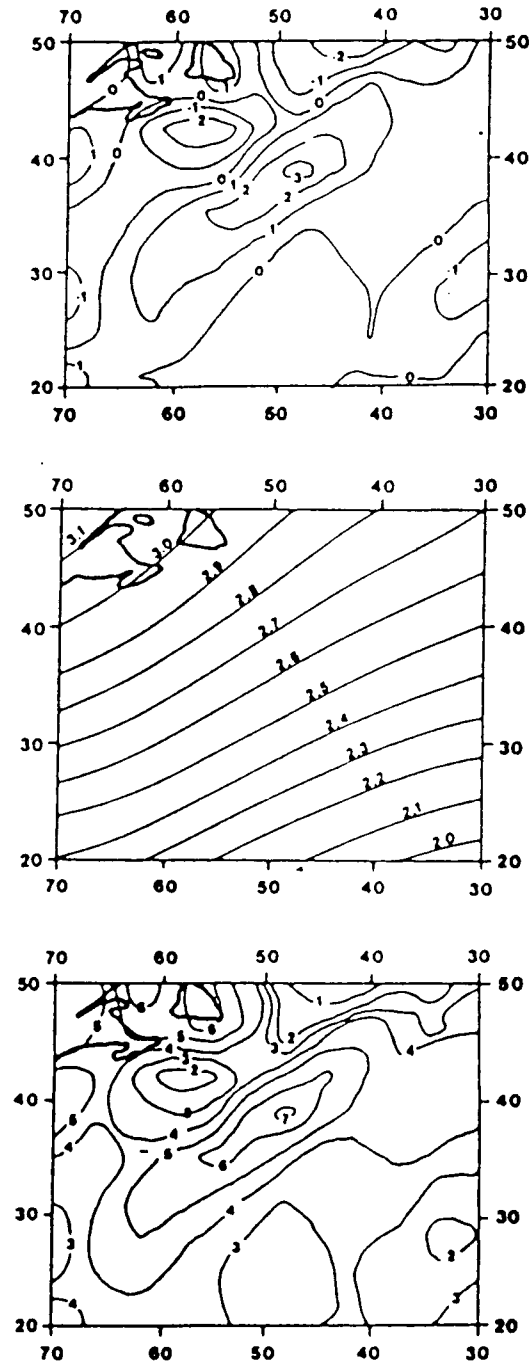

Figure 5. Adjustment of a magnetization model in the northwestern Atlantic Ocean. A. Modelled magnetization before annihilator addition. B. Intensity of magnetization of an annihilator with a strength necessary to convert the magnetization of Figure 5A to entirely positive or zero magnetizations. C. Modelled magnetization after the annihilator has been added.

magnetization in a 6 km thick source layer, determined by equivalent source inversions of the MAGSAT field in the NW Atlantic Ocean, is shown in Figure 5A. Figure 5B shows the annihilator that converts the original model to non-negative magnetizations (Figure 5C). By adding enough annihilator to remove all negative magnetizations, the model becomes physically plausible. However, just by adding an additional amount of annihilator a new magnetization model is created that will produce the same magnetic field as the original model (Figure 6). In fact, there exists an infinite number of magnetic distributions that will produce the same magnetic anomalies.

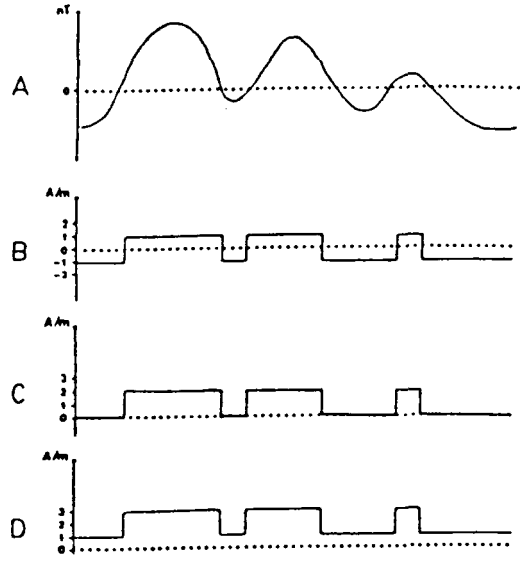

Figure 6. Ambiguity in modelling of magnetic anomalies. A. Observed magnetic anomaly. B. Modelled magnetization with an average intensity of approximately zero (usually the result from least squares inversions). C. Intensity of magnetization when an annihilator has been added, with a strength necessary to remove all negative magnetizations. D. Intensity of magnetization when an additional amount of annihilator is added.

Hayling and Harrison (1986) show how annihilators can be used to match magnetization models that have been inverted separately from different areas together. Figure 7 shows a magnetization model in the Atlantic Ocean that has been derived by matching 12 separate equivalent source models.

One of the effects when an annihilator is added is that the average intensity of magnetization is increased. The average crustal magnetization in the Atlantic is approximately 3.7 A/m. This value is similar to what has been found from inversions in the Indian ocean (Sailor and Lazarewicz, 1983), in the Sea of Japan (Yanigisawa et al., 1982), and in the Pacific Ocean (Harrison et al., 1986). There are several areas in the Atlantic that have zero magnetizations, which means that the crust totally lack magnetizable material, or an indeterminable amount of annihilator can be added to the model.

D. Sources for magnetic anomalies over oceanic crust

When interpreting the calculated intensity of magnetization there are two variables to work with, the three dimensional shape and the susceptibility or magnetization contrast of the source body. In the case of the oceanic crust, not only susceptibility but remanent and viscous magnetizations have to be considered. We will first examine the results from magnetic studies of rocks from the

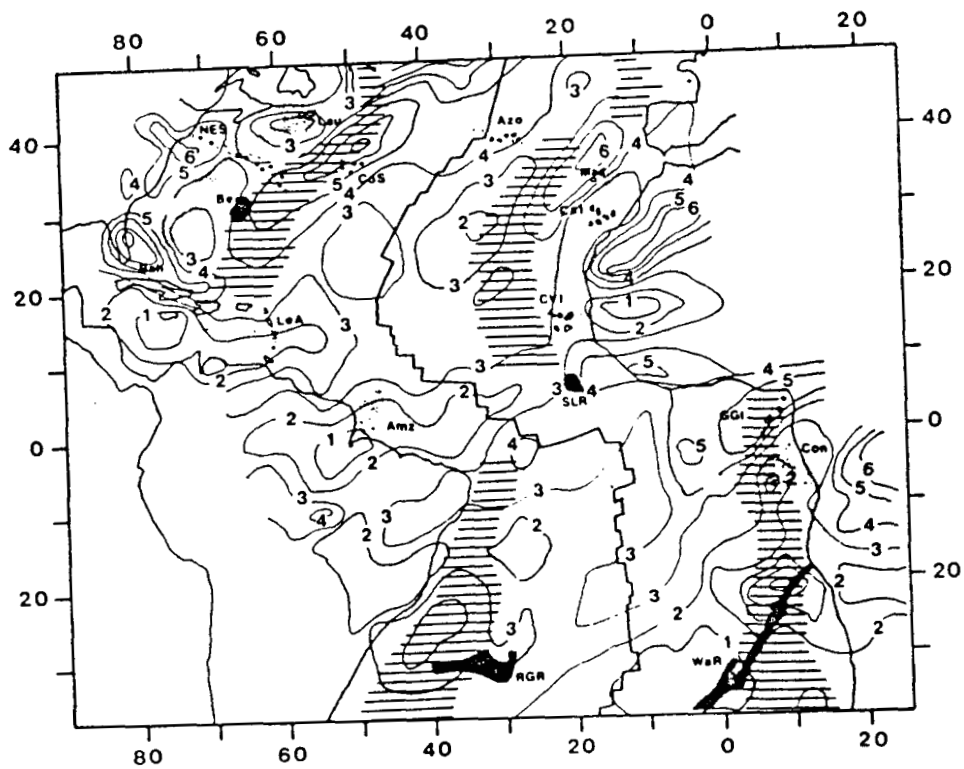

Figure 7. Intensity of magnetization in the North and Equatorial Atlantic Ocean determined by equivalent source inversions of the MAGSAT scalar magnetic anomaly field (Figure 1). The magnetization contour interval is 1 A/m. Very low magnetizations are seen over the Laurentian (Lau), Congo (Con), and Amazon (Amz) deep sea fans. The highest intensities of magnetization, seen on each side of the mid-Atlantic ridge in the North Atlantic Ocean, may be caused by the normally polarized remanent magnetization that was acquired during the Cretaceous normal polarity epoch. The derivation of the magnetization model is described in Hayling and Harrison (1986), who also discuss the correlation between intensity of magnetization and large scale geologic structures in the oceanic crust.

oceanic crust.

Several models of the magnetic crust, deduced from direct studies of oceanic rock samples, have been proposed (e.g. Kent et al., 1978; Dunlop and Prevot, 1982; Swift and Johnson, 1984; Thomas, 1985). These models have used information from ophiolitic rocks, often hundreds of millions of years old, as well as rocks recently formed at active spreading ridges. We belive that only rock samples that are appropriate for interpretation of satellite altitude magnetic anomalies should be used. The selection procedure is described by Hayling and Harrison (1986). Table 1 shows the data that were selected. The average magnetization in a normal oceanic crust is shown in Table 2. Remanent magnetization is the most important source in the oceanic crust. This type of magnetization, together with considerable thickening of the crust, is the only case in the Atlantic where the intensity of magnetization inferred from oceanic rock samples agrees with a magnetization model that is derived from satellite data. Induced magnetization is more than one order of magnitude less that the average crustal magnetization inferred from satellite modelling. Harrison (1987b) investigates in great detail the rock magnetic properties of the oceanic crust and serpentinized layer of the upper 1 to 2 km of the mantle (Lewis and Snydsman, 1977). Harrison concludes, after considering both surface and satellite magnetic anomalies, that the intensity

TABLE 1. Magnetization of Oceanic Rocks

	N	NRM, A/m	N	Induced Magnetization, A/m in 40,000nT	Reference
Basalt					
1. Ophiolites	208	0.342	208	0.3369	1
2. DSDP	122	2.64	122	0.4702	1,2
3. Dredge	309	5.37	309	0.1632	2
4. Metamorphosed	16	0.0122	16	0.0070	3,4,5,6
Gabbro					
5. Ophiolites	257	0.478	257	0.1008	7,8,9
6. Unaltered	31	0.621	31	0.4029	1,3,6,10
7. Metamorphosed/ cataclastic	47	0.894	47	0.5934	6,11
8. Serpentinized	6	0.48	6	0.1536	1
Serpentinized Peridotites					
9. Ophiolites	38	6.03	38	0.4852	7,11
10. Dredged/ Drilled	28	4.15	27	0.8873	1,3,5,6

References are 1, Dunlop and Prevot [1982]; 2, Lowrie [1974]; 3, Opdyke and Hekinian [1967]; 4, Luyendyk and Melson [1967]; 5, Irving et al. [1970]; 6, Fox and Opdyke [1973]; 7, Vine and Moores [1972]; 8, Luyendyk and Day [1979]; 9, Banerjee [1980]; 10, Kent et al. [1978]; and 11, Beske-Diehl and Banerjee [1979].

TABLE 2. Average Magnetization of the Oceanic Crust

Thickness, km	Material	NRM, A/m	Induced Magnetization, A/m in 40,000 nT
0.5	Pillows	3.6060 (see 1 below)	0.2857
1.0	Dykes	0.3090 (see 2 below)	0.3039
4.0	Gabbros	0.6040 (see 3 below)	0.2849
0.5	Serpentinites	5.0900 (see 4 below)	0.6863
Average magnetization in a 6-km-thick layer		1.18	0.322

Average, %*	Row in Table 1
1. 45	2
45	3
10	4
2. 90	1
10	4
3. 45	5
22.5	6
22.5	7
10	8
4. 50	9
50	10

*Averages for each layer are determined from the appropriate values in Table 1.

of magnetization in the oceanic crust has to be much greater than what is inferred from oceanic rock samples. He also discusses the possibility of a time dependence in the intensity of magnetization in the oceanic crust.

Viscous magnetization has been suggested to be a very important magnetic source in the oceanic crust, and make up the difference between magnetization intensities inferred from magnetic anomalies and the low intensities of magnetization in oceanic rocks. Viscous magnetization is aligned with the ambient field and will work in a way similar to induced magnetization. Thomas (1985) suggested that this type magnetization is the principal cause of oceanic crustal magnetization. Thomas proposed that the combined effect of susceptibility and viscous magnetization gives an intensity of 1.5 A/m in normal oceanic crust and 4 A/m in subducted oceanic crust. The increase of magnetization in subducted crust was assumed to be caused by thermal enhancement of the viscous component during the subduction process. Similar intensities of magnetization were needed in order to explain satellite magnetic anomalies over oceanic plateaus and subduction zones in the Pacific (e.g. Clark, 1983; Vasicek et al., 1984; Frey, 1985).

Very little is known about viscous magnetization. This type of magnetization builds up when a rock is exposed to a magnetic field for a very long time. The Earth's magnetic field has been of uniform polarity for the last 700,000

years. Experiments with viscous magnetization have usually lasted for minutes and hours, and at the most a few weeks. In practically all cases there is an increase in magnetization with time, usually as a linear function of log(t), when a rock is exposed to a magnetic field similar in strength to that of the Earth. It has also been found (e.g. Smith, 1984) that the viscous behavior changes with varying temperatures, and the increase in magnetization with time is accelerated with increased temperatures. One of the samples studied by Smith showed an almost 50% increase in viscous magnetization when exposed to 50 μT at a temperature of 105 ^{o}C for two hours. Obviously, the increase in VM must level off at some point (i.e. reach saturation) and the final intensity of magnetization might be much less than what is inferred from extrapolation studies that are more than six orders of magnitude less in time compared to the 700,000 years of normal polarity since the last now established geomagnetic reversal.

In order to get some idea of how much viscous magnetization would affect the total intensity of magnetization in the oceanic crust, we have used the results of Lowrie and Kent (1978) for basalts, and from Dunlop (1983) for gabbros and serpentinized peridotites. They predict that viscous magnetization has an amplitude of 30%-50% of the NRM for oceanic basalts, and a few percent from gabbros and serpentinized peridotites. If assuming that

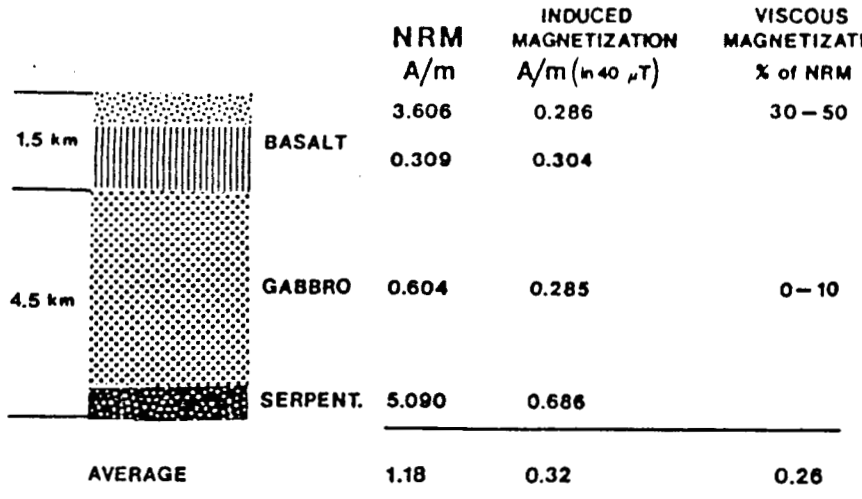

Figure 8. Magnetization of the oceanic crust. See text for further discusssion.

as much as 50% of the magnetization for basalts being viscous and 10% for gabbros and serpentinites, the average viscous magnetization in a 6 km thick crust will be 0.26 A/m (Figure 8). The sum of susceptibility and viscous magnetization will give a total of 0.58 A/m, which still is more than 6 times less than the average implied from satellite data.

Enhanced susceptibility due to a change in the crystal structure of some magnetic minerals (the Hopkinson effect), which becomes important within some 100 °C of the Curie point of a mineral (Dunlop, 1974), has been observed for several of the minerals constituting the rocks of the ocean floor. Dunlop observed that the susceptibility increased by a factor of 1.5 to 3 for magnetite, depending on the domain

structure of the mineral, and by as much as a factor of five for certain hematite minerals. The latter is of minor importance because of its very low initial susceptibility. The thermal enhancement for magnetite bearing rocks becomes important in the temperature range 420-580 °C and can occur only in subduction zones and in areas with a very thick cover of sediments. One effect of serpentinization of oceanic crust with age is that the direction of remanent magnetization of the serpentinites is very difficult to determine. There is evidence that hydrothermal circulation, with the possiblity of serpentinization, is still taking place in crust as old as 80 MY (Embley et al., 1983), and the serpentinite layer has a probability of 0.5 of becoming magnetized in an opposite direction to the rocks surrounding and above it, except during times of constant polarity. We should also keep in mind that a general increase in magnetization in the oceanic crust, arising from induced and viscous magnetization, will more or less work as an annihilator and would not produce magnetic anomalies, except where edge effects are present.

In Figure 8 we can see that the serpentinized peridotites have the highest susceptibility of the rocks in the oceanic crust. There is a possibility that these rocks are more abundant in the upper mantle than assumed in Figure 8. Arkani-Hamed and Strangway (1986b) propose that 20% serpentinization of the upper mantle is able to produce

magnetic anomalies, similar in strength to MAGSAT anomalies.

In Chapter 4 we will investigate, by forward modelling, if viscous magnetization and a magnetized upper mantle can produce anomaly fields at satellite altitude that are similar to what has been observed by MAGSAT (Figure 1).

3. DISTORTION OF MAGNETIC FIELDS WHEN SHM IS USED

Many crustal magnetic anomaly maps often show pronounced elongations that follow the dip of the main field (see Figure 2). In many cases is is difficult to correlate these anomalies with geologic structures in the Earth's crust. We have investigated if some of these signals are caused by leakage of power from high amplitude local anomalies into longer wavelengths when anomaly fields are extracted from satellite data. Our simulations of magnetic anomaly field reductions suggest that there might be a problem when spherical harmonic analysis is applied to the geomagnetic field.

Methods

Figure 9 shows a flow chart of our simulation, and Figure 10 the power spectra of three different core field models that we have used in our simulations. We use the lower degrees of harmonic of the Langel et al. (1981) SH-model to calculate the vector and scalar magnetic field at 10,800 locations for satellite altitude (400 km) between 60° South and 60° North. The scalar magnetic field is shown in Figure 11A. For the crustal magnetic field (Figure 11B) we selected the strongest anomalies from Langel et al. (1982) anomaly field (Figure 1) and placed dipoles 20 km below the Earth's surface. The dipole moments were chosen in

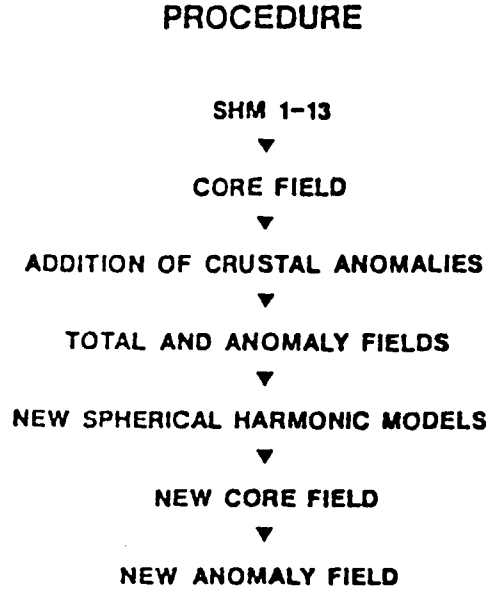

Figure 9. Flow chart of the simulation procedure to examine the possibility of leakage of power from high amplitude short wavelength anomalies into longer wavelength, and the distortion of anomaly fields, from this phenomenon. Models containing spherical harmonic coefficients 1 through 13 and 1 through 17, have been used to model initial core fields. In the SH-model 1 through 17 are the Gauss coefficients for the first 13 degrees of harmonic taken from Langel et al (1982), and degrees 14 through 17 are simulated with random numbers in such a way that the power spectrum from these coefficients remains fairly flat at the core-mantle boundary.

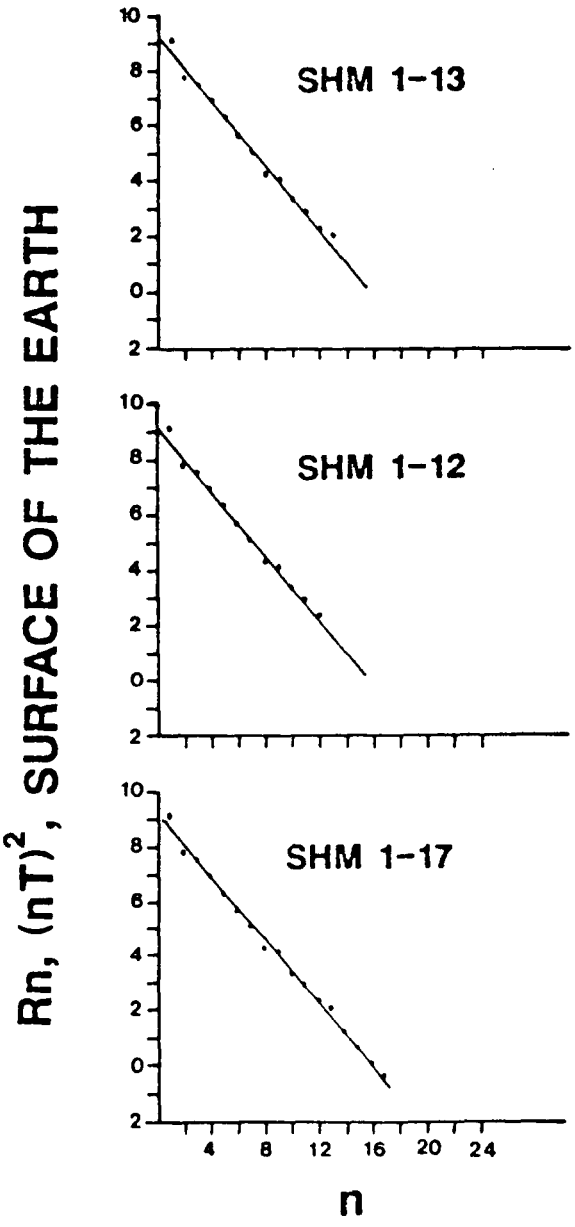

Figure 10. Power spectrum of the spherical harmonic models of the magnetic field that are used for the main field in the simulations. When downward continued to the core-mantle boundary, the spectrum of all three SH-models is fairly flat.

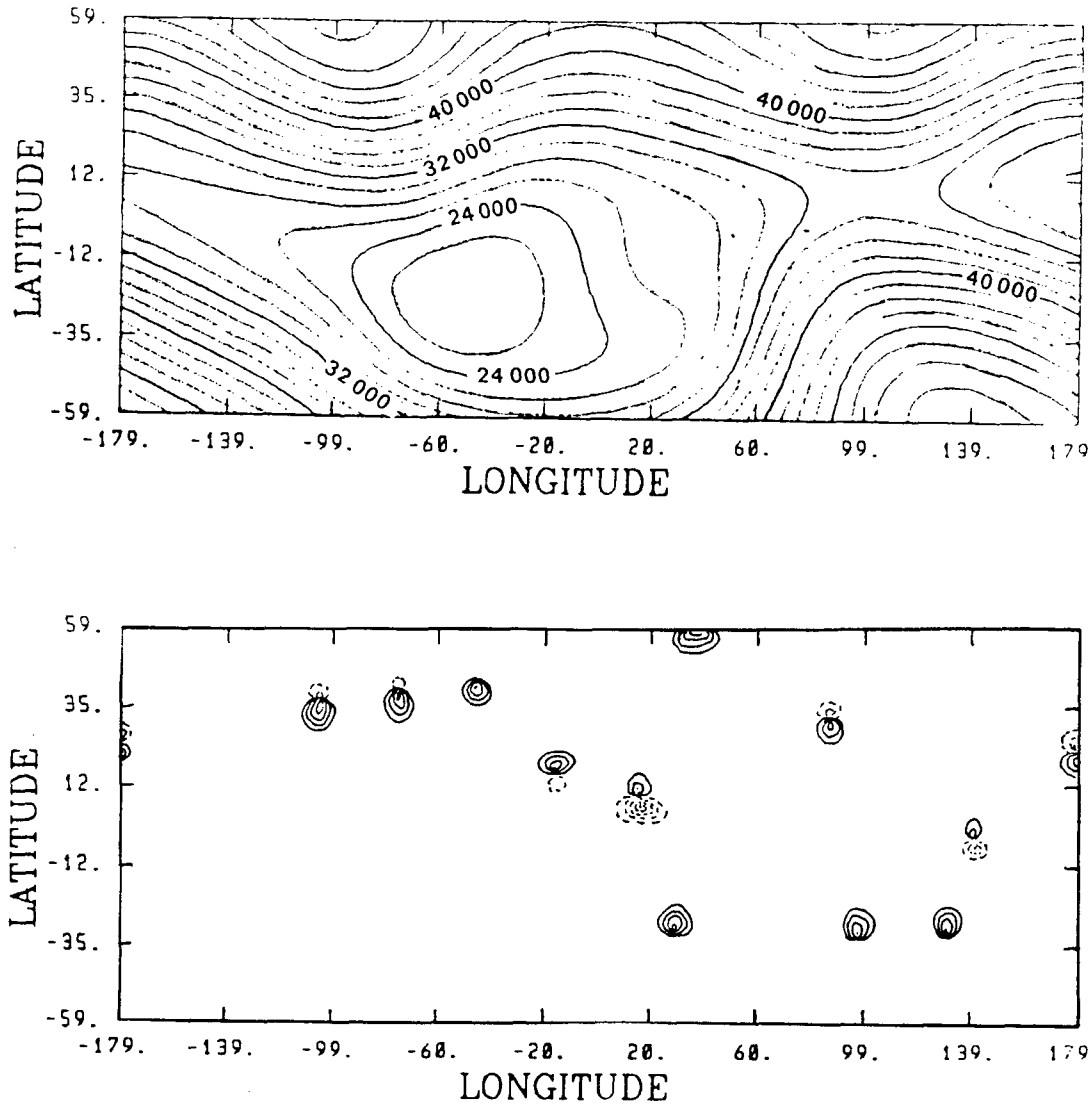

Figure 11. A. Example of a simulated scalar magnetic field from the core at satellite altitude (400 km). This looks almost the same for all three core field models, because the magnetic anomalies produced by the higher degrees of harmonics have much lower amplitudes compared to the dipole field. B. Scalar magnetic field (at 400 km altitude) from 12 dipoles that are placed at a depth of 20 km below the surface of the Earth. The locations and moments of the dipoles have been chosen is such a way that the magnetic field at satellite altitude is similar to some of the strongest anomalies that can bee seen in the MAGSAT scalar magnetic anomaly map (Figure 1).

such a way that the maximum intensity of the anomaly field is similar to the Langel et al. anomaly field, which is between 10 and 20 nT. A spherical harmonic model is then fitted to the X, Y and Z components of the total magnetic field. We have used an iterative least squares inversion method that is similar to the method used by Schmitz and Cain (1983). The least squares inversion method is described in Appendix A. In order to suppress the higher density of data points at high latitudes we have used sin Θ (where Θ is the colatitude of the data point) as a weighting function (w). This is the same function that is used when SH-models are determined from satellite measurements (e.g. Langel et al., 1981; Schmitz and Cain, 1983). Improvement in fit between the magnetic field produced by the new SH-model and the 'observed' magnetic field usually ceased after 2 to 4 iterations. The standard deviation (STD) of the difference between the magnetic field produced by the SH-model and the 'observed' field are between 0.12 and 0.17 nT.

RESULTS

Figure 12 shows the new anomaly field when SH-coefficients 1 through 13 is used for both the original core field, and the new core field. In order not to distort the resulting anomaly field by smoothing, the field is contoured at certain intensity levels. Figure 12B shows the

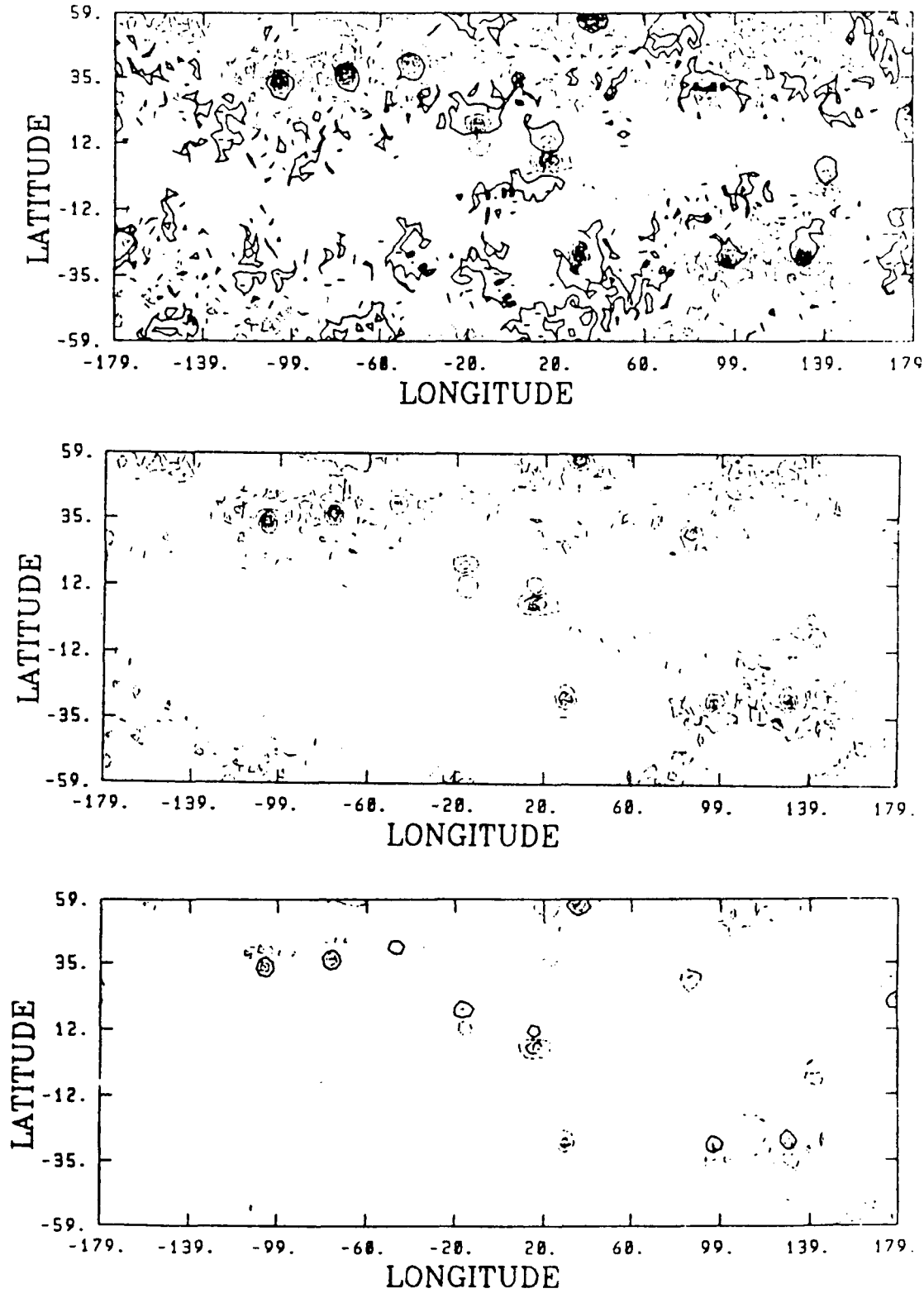

Figure 12. Scalar magnetic anomaly field at an altitude of 400 km from the first simulation. See text for further discussion.

-10, -6, -2, 2, 6, 10 nT contour lines and Figure 12C the -21, -15, -9, -3, 3, 9, 15 and 21 nT contour lines. The magnetic field from the dipoles has not changed very much, and the 'ghost' anomalies have a fairly low amplitude. This simulation suggests that if the correct degrees of harmonics are chosen to calculate the core field, which then is subtracted from the total field, only minor distortions of the anomaly field occur.

In the second inversion we simulate a situation when some of the core field signal remains in the anomaly field. The original core field is the same as in the first simulation, but the new core field is determined by spherical harmonic degrees 1 through 12 of the new spherical harmonic model. Figure 13A shows the new anomaly field with a contour interval of 4 nT, Figure 13B shows the contour levels of -22, -18, -14, -10, -6, -2, 2, 6, 10, 14, 18, 22 nT, and Figure 13C the -20, -12, -4, 4, 12, 20 nT contour levels. The field from the dipoles have approximately the same amplitude as the original anomaly field, but some of them have been elongated and there are several ghost anomalies with relatively high amplitudes.

In our third simulation we use the same harmonic coefficients of degrees 1-13 as in the two cases just described, but have added spherical harmonic coefficients 14 through 17. These coefficients have been generated from random numbers and constrained in such a way that the power

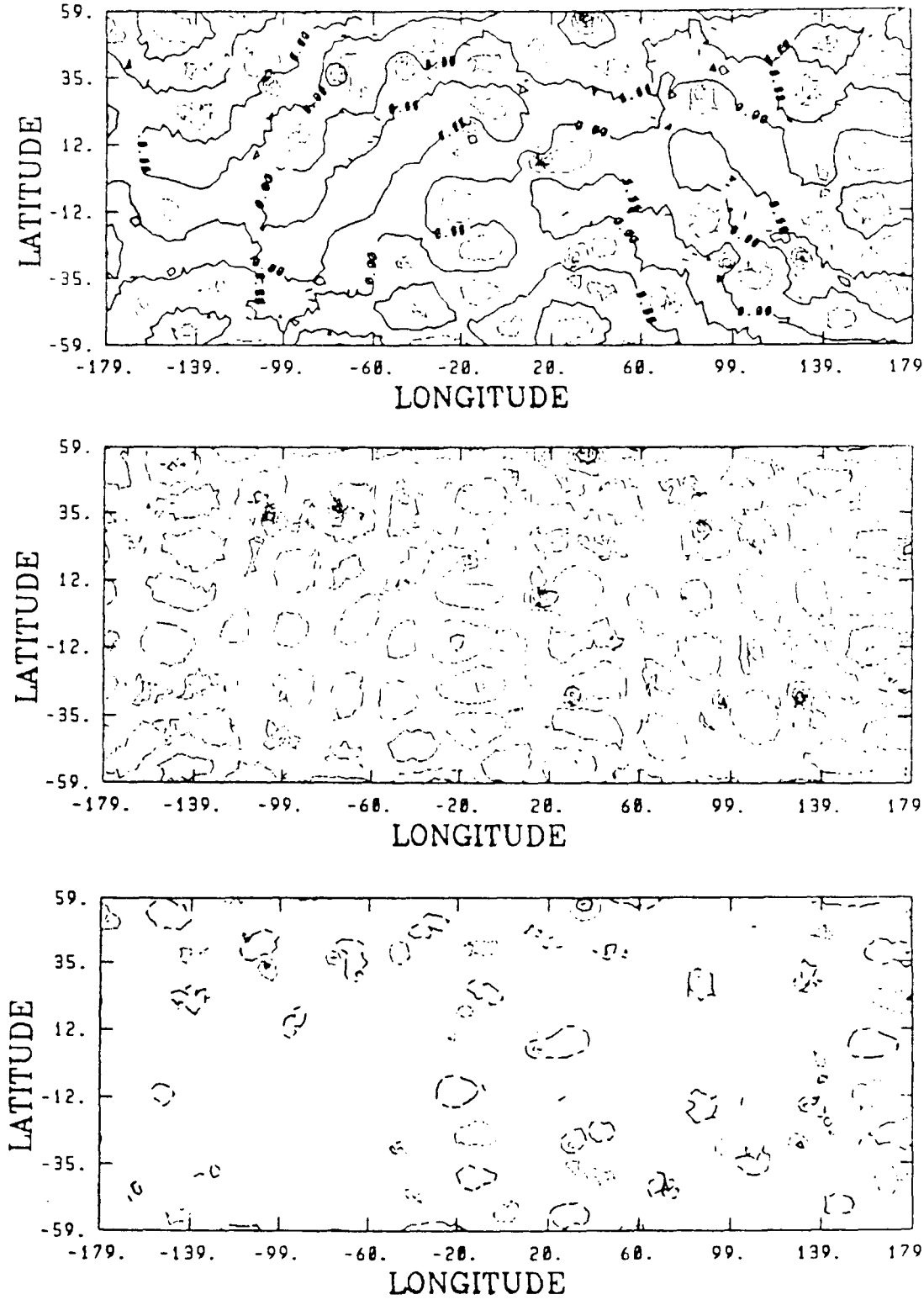

Figure 13. Scalar magnetic anomaly field at an altitude of 400 km from the second simulation. See text for further discussion.

spectrum of these coefficients will produce a fairly white spectrum at the core- mantle boundary. We truncated at degree 17 because the intensity of the magnetic field from higher degrees of harmonic is below the noise level (0.3 nT, Sailor et al., 1982) of MAGSAT data. Figure 14A shows the resulting anomaly field with 2 nT contour intervals after having removed a core field of harmonics 1-13. Figure 14B is contoured at -22, -18, -14, -10, -6, -2, 2, 6, 10, 14, 18, 22 nT, and Figure 14C at -20, -12, -4, 4, 12, 20 nT. In Figure 15 we have hand drafted the -4, -2, 2 and 4 nT, and some of the higher contour levels. This simulation shows not only distortion of the original anomalies but also strong ghost anomalies as repetition of the dipole anomalies along the magnetic latitude. The maximum intensity of many of the ghost anomalies is well above 4 nT.

The power spectrum of the total magnetic field SH-model and the crustal SH-model is shown in Figure 16A. The power spectrum above degree 13 of the anomaly field is that of Langel and Estes (1982) model. However, the anomaly field is also present in the lower degrees of harmonics, which are believed to represent mainly the core field. This shows that the distribution of the dipoles on the surface of the sphere is creating long wavelengths of anomaly. If this is the case, will the magnetic field from local magnetic sources like the dipoles in our model be represented by long wavelengths, i.e. low degrees of harmonic, when expressed by

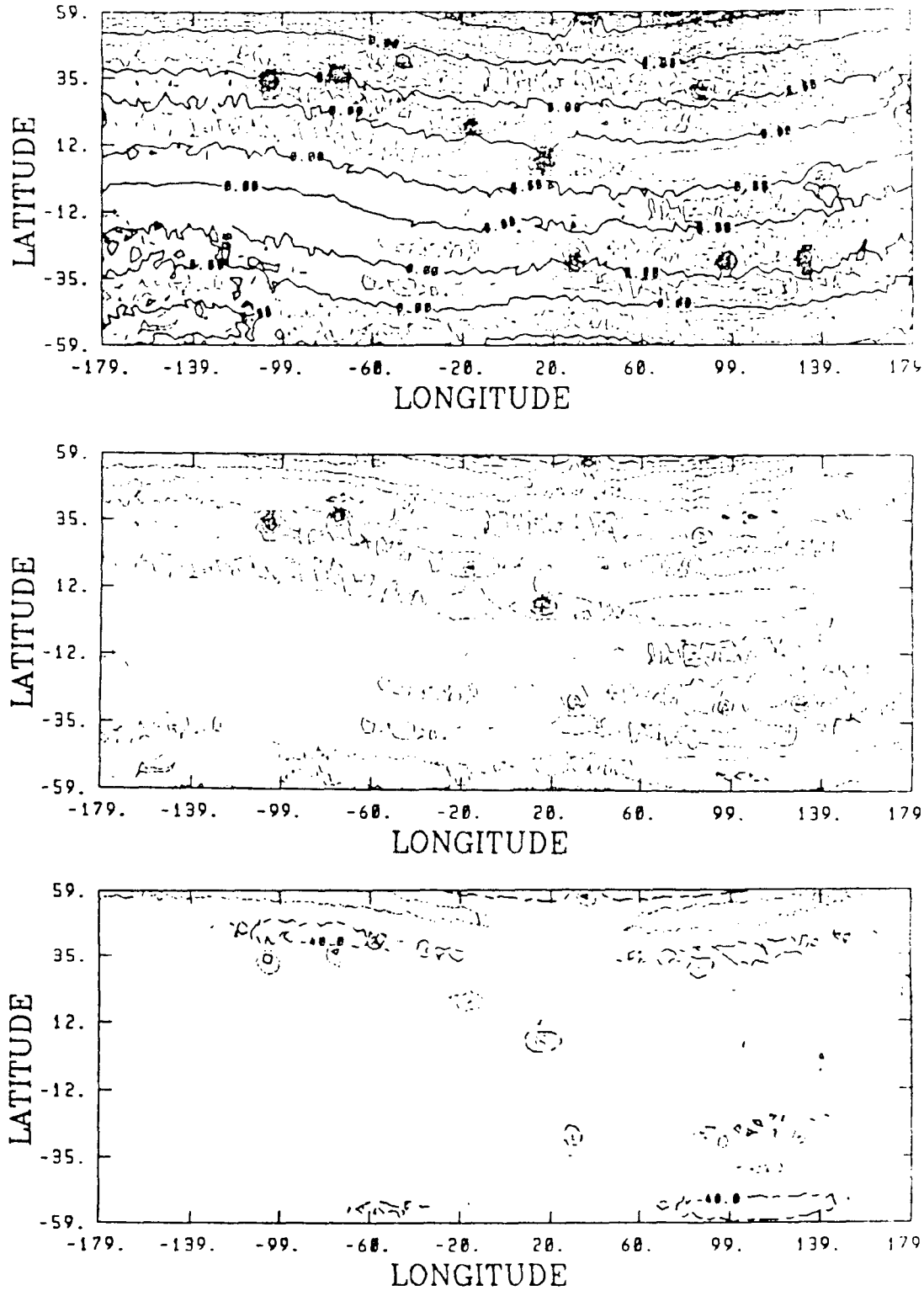

Figure 14. Scalar magnetic anomaly field at an altitude of 400 km from the third simulation. See text for further discussion.

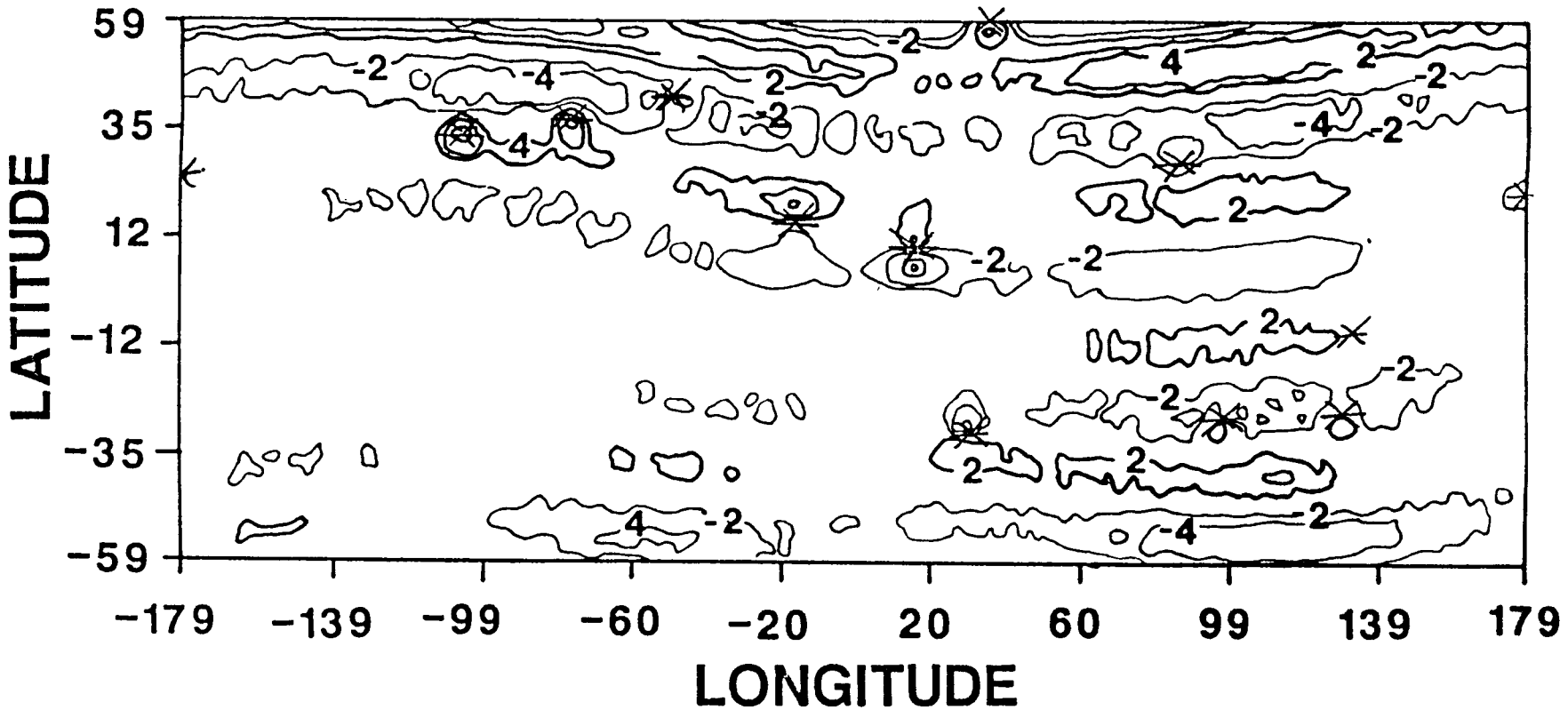

Figure 15. Distortion of scalar magnetic anomalies when using spherical harmonic analysis. Asterisks show position of 12 dipoles used to simulate crustal anomalies. See text for further discussion.

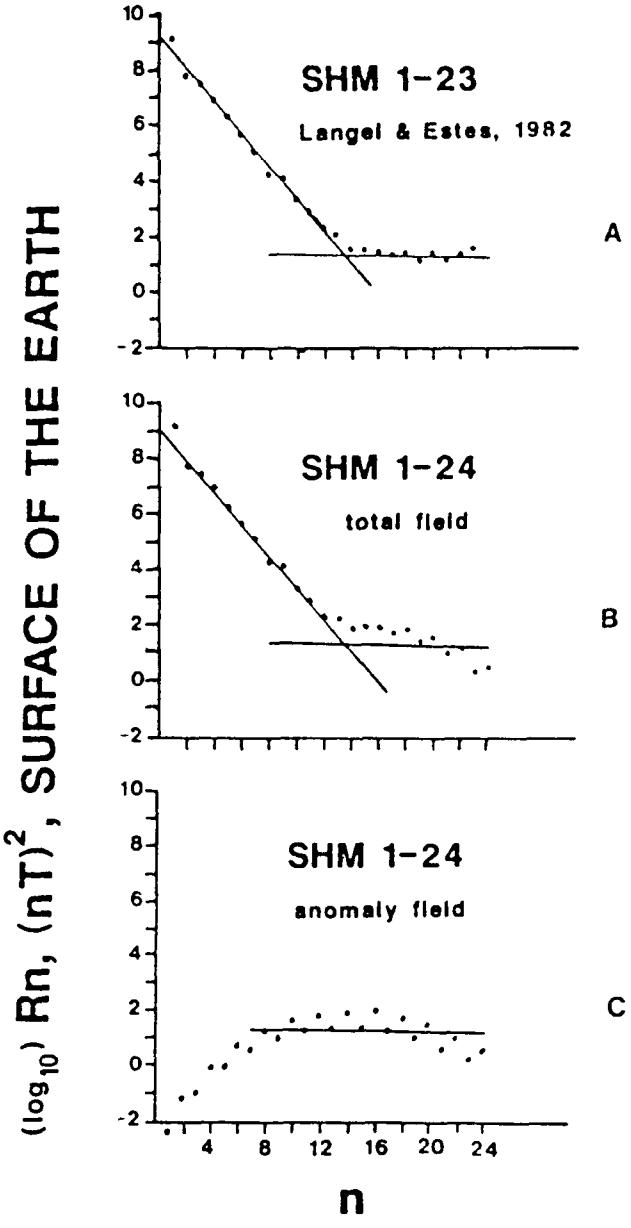

Figure 16. A. Power spectrum of the spherical harmonic model of Langel and Estes. B. Power spectrum of the spherical harmonic model that was fitted to the total magnetic field of the third simulation. C. Power spectrum of the spherical harmonic model that was fitted to the anomaly field of the third simulation.

the power spectrum of a spherical harmonic model, just as good as the magnetic field from spherical caps that are more like continents? It is proposed (Mayer et al., 1983; 1985) that the lack of magnetic signal over continent-ocean boundaries is the result of removing not only the core field with the lower degree terms (degrees 1 through 13) in spherical harmonic models but also the magnetic signal from a magnetization contrast between continents and oceans which is also mainly represented by these low degree SH-terms. Hayling (1987) showed that the few pronounced magnetic anomalies that are found over continent-ocean boundaries in satellite magnetic anomaly maps can be explained by variations in the Curie isotherm in these areas rather than by a difference in vertically integrated magnetization between the continental and oceanic crusts. We will discuss this possibility in Chapter 4.

The power spectrum of the spherical harmonic models of the total field in our last simulation is fairly similar to the power spectrum of Langel et al. (1982). It seems that power from the magnetic field produced by the dipoles in the Earth's crust has leaked into longer wavelengths, when the SH-model was determined, and will distort the anomaly field. Is it possible that long wavelengths will leak power into shorter wavelengths? We investigated this possibility by inverting models of a field generated by SH degrees 1-13 to obtain SH-models up to various degrees higher than 13.

Figure 17 shows the power spectrum of these spherical harmonic models. In the spherical harmonic models up to degree 18 the power spectrum for degrees higher than 13 is very low, but for the higher degree models the spherical harmonic coefficients for n > 13 become more important. It is possible that some of the power in these models is simply caused by rounding errors in the computer. However, the power spectrum of the SHM 1-24 model is of somewhat lower amplitude when compared to the spherical harmonic models of the total and anomaly fields in our simulation (Figure 16). The power spectra are also very similar for the higher degrees in Figure 16. It is also possible that the best least squares fit of the harmonic coefficients to the magnetic field is obtained if some value is given to all harmonic coefficients. We examined this possibility by using only the first 4 degrees of the MGST/81 SH-model to represent the core field. The magnetic field that will be produced by this SH-model was calculated for an altitude of 400 km, and SH models were determined for various degrees higher than 13. The power spectra of these SH models are shown in Figure 18. The power from degrees above 4 show a very low amplitude for all models. However, these power spectra show the same pattern as in the case when we used the SH model consisting of degrees 1-13. The power for the even degree terms is generally higher than for the odd degree terms. The reason for this is not clear.

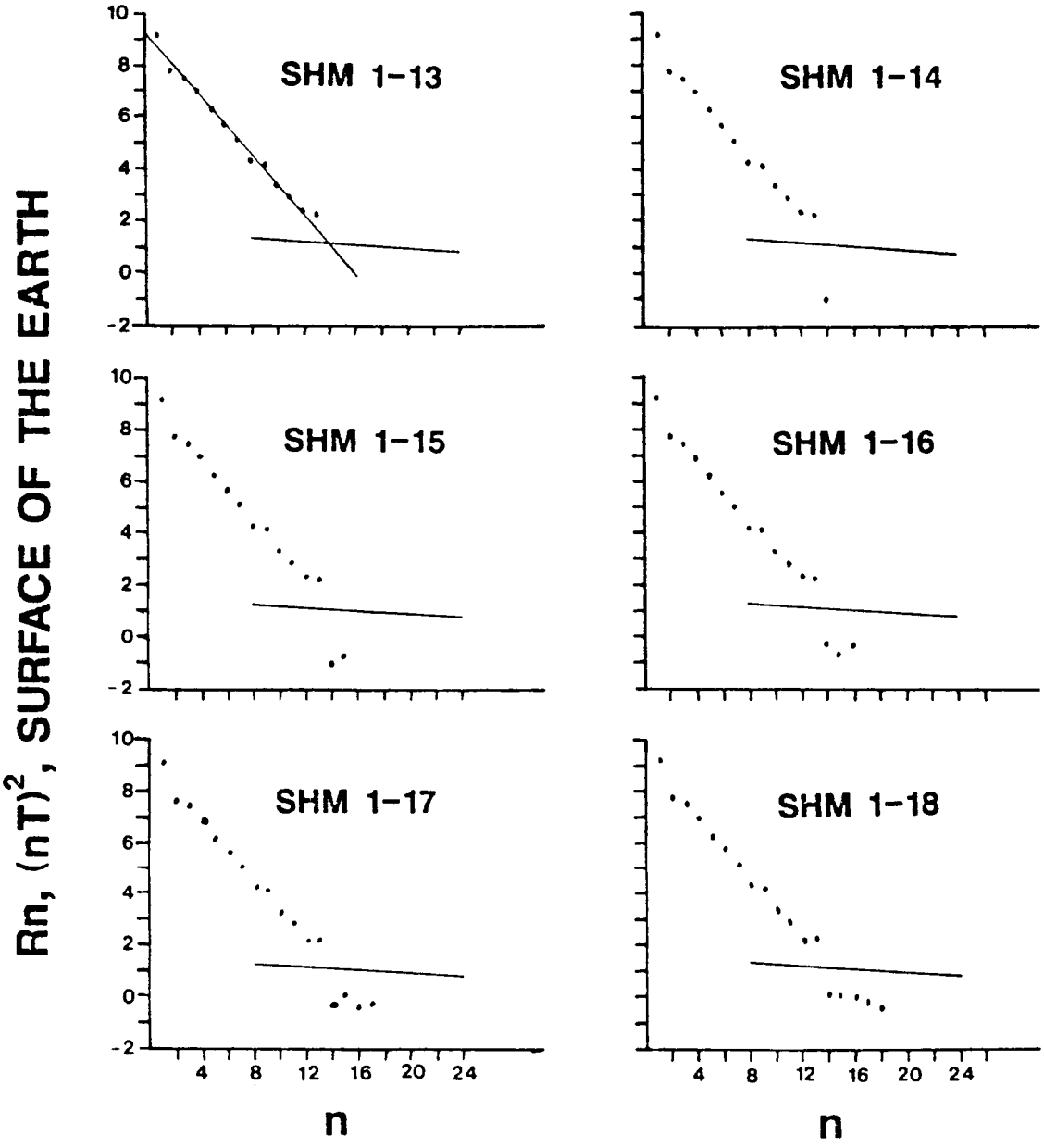

Figure 17. Power spectrum of spherical harmonic models of the core field (Figure 11) that are expanded to different degrees of harmonic.

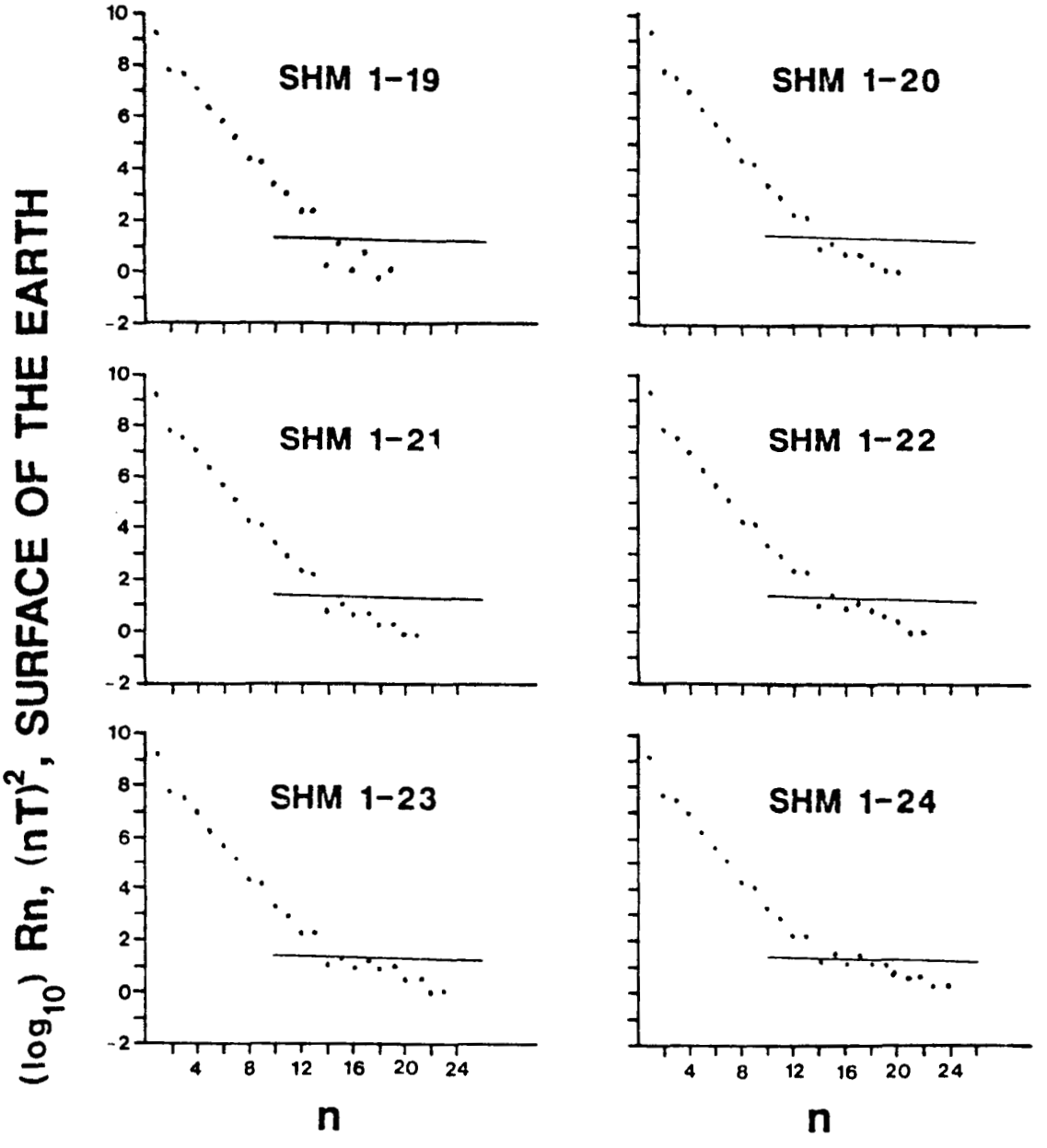

Figure 17 cont.

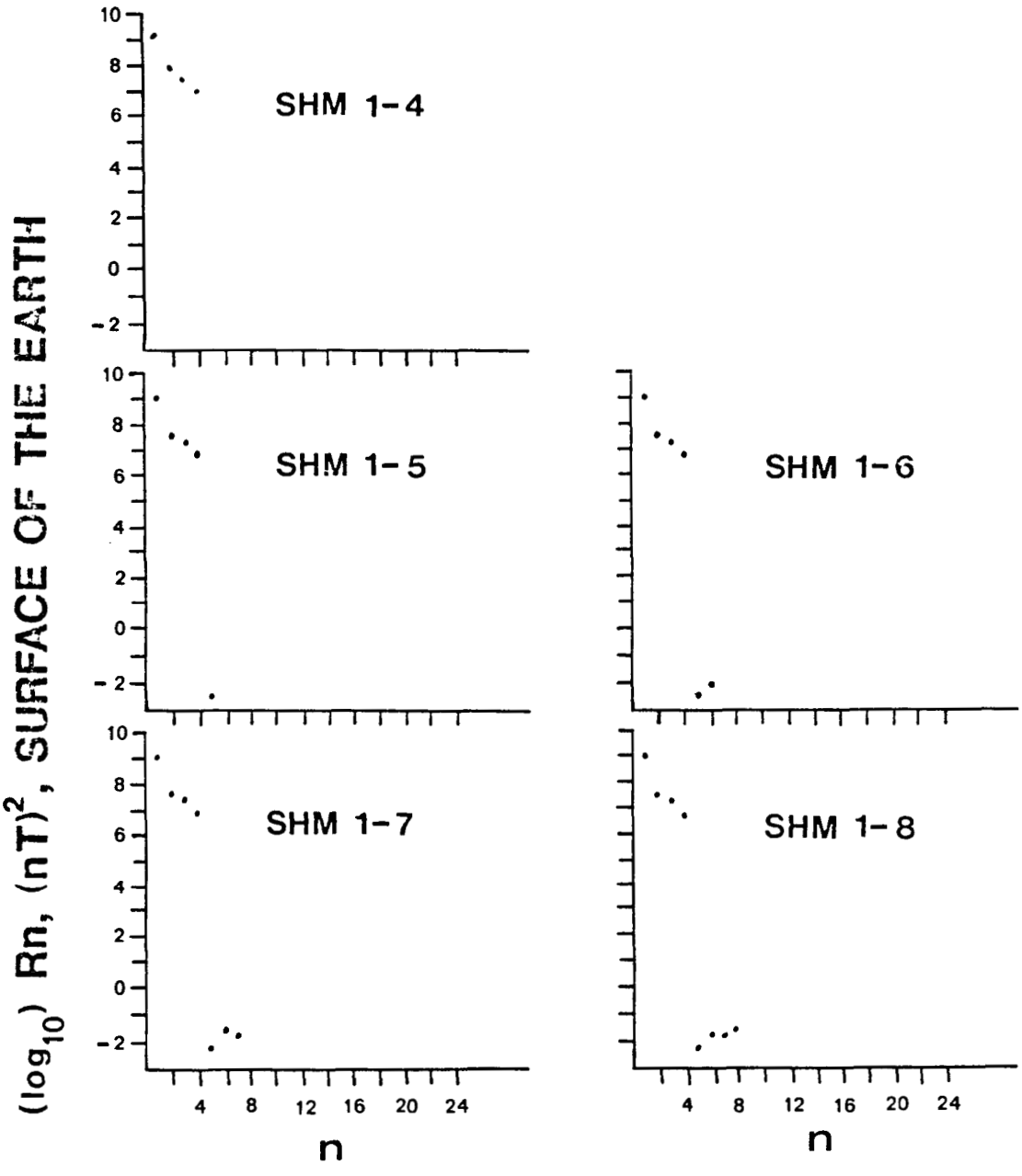

Figure 18. Power spectrum of spherical harmonic models of a magnetic field consisting of the first 4 degrees of harmonic of the core field (Figure 11).

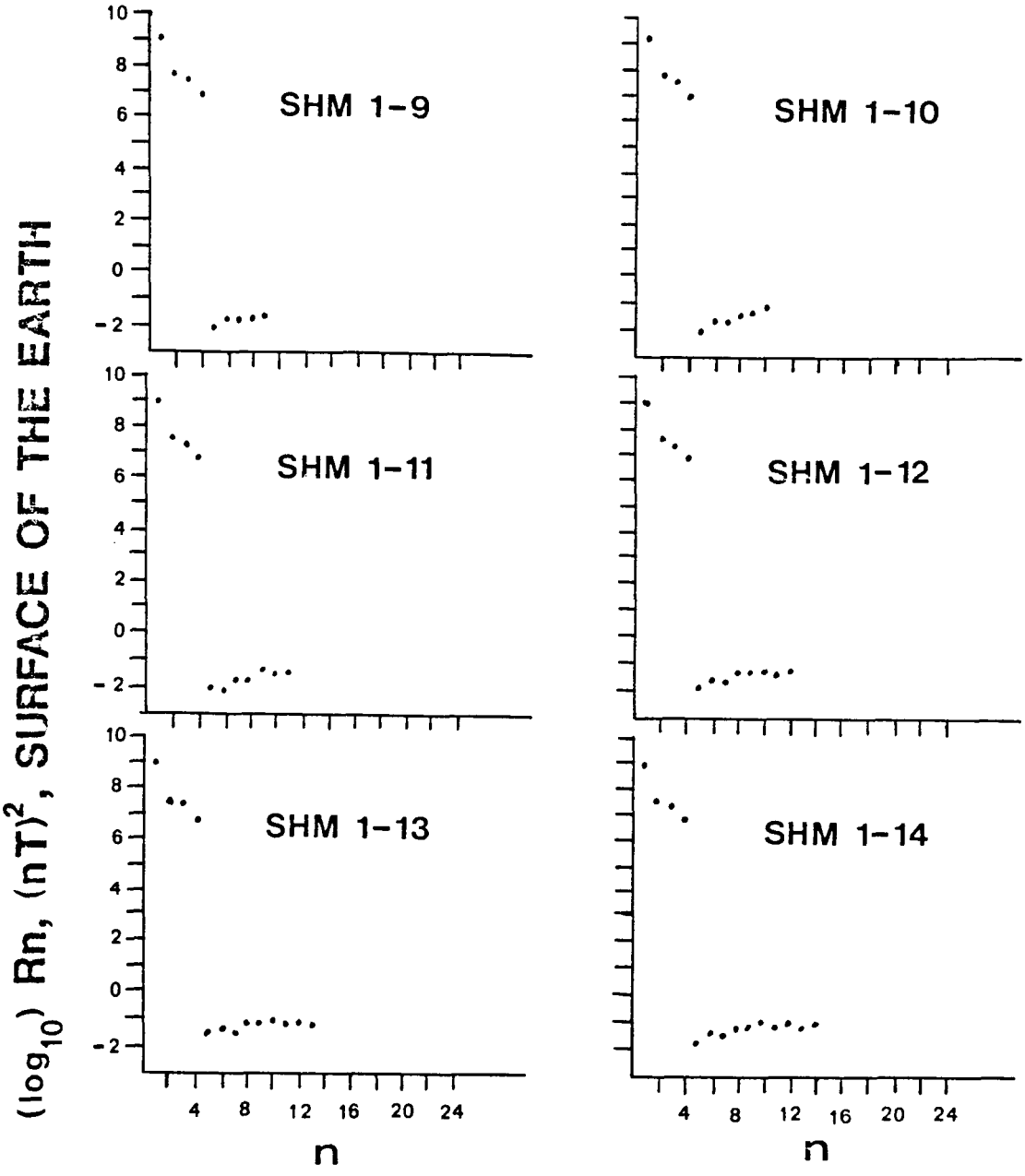

Figure 18 cont.

Further work is needed on this problem. We also have to examine how other magnetic fields will be represented by spherical harmonic models, for example spherical caps that are similar in size to the continents. In order to speed up the inversions and also derive spherical harmonic models of even higher degrees of harmonic, for example up to degree and order 29, a much more powerful computer is needed. The inversion of a spherical harmonic model up to degree 24, with 4 iterations, takes over 20 CPU hours on the VAX at RSMAS.

4. CORRELATION BETWEEN DEPTH TO THE CURIE ISOTHERM AND MAGNETIC ANOMALIES.

In this chapter we will describe how models of the depth to the Curie isotherm(s) can be used in the interpretation process and in the modelling phase of satellite altitude magnetic anomalies. We will investigate how different distributions of magnetic sources in the oceanic lithosphere, and how different thermal properties of the oceanic lithosphere, will affect the magnetic anomaly field at satellite altitude. Possible factors for variations in surface heat flow will be discussed extensively, to examine if the assumptions that we make in our modelling are viable. In the last section we will discuss how modelling of the depth to the Curie isotherm in the oceanic lithosphere can be used to find the strength of the annihilator, which was the initial reason why we started to study if there is a correlation between depth to the Curie isotherm and magnetization in the oceanic lithosphere. If there exists at least one area in the oceanic lithosphere where the effective total magnetization is roughly zero we will know the strength of the annihilator when we adjust magnetization models.

Mayhew (1982a; 1982b; 1985) describes how Curie isotherms correlate with models of magnetization, derived from satellite magnetic data, in the conterminous United States. The correlation in continental crust is fairly

simple, where there is an inverse relationship between surface heat flow and intensity of magnetization. The thickness of the magnetized layer, or the depth to the Curie isotherm, is assumed to be inversely dependent on the surface heat flow. Mayhew found an almost linear relationship between intensity of magnetization and surface heat flow. Similar results have been obtained with aeromagnetic data (Shuey et al., 1973; 1977). A fairly good agreement between surface heat flow and magnetization has also been found to apply over Australia (Mike Mayhew, personal communications). The problem is not this simple in the oceanic crust. It is usually believed that magnetic sources are restricted to the approximately 6 km thick oceanic crust and the upper 1 or 1.5 km of the serpentinized upper mantle. The heat removing agent in the oceanic crust is not only conduction but in some cases convection. Cooling of the lithosphere and sedimentation are other time dependent functions that have to be accounted for in the modelling of the depth to the Curie isotherm in the oceanic lithosphere.

We investigate several possibilities in terms of the physical properties of the oceanic crust and upper mantle, and the possibility of lateral heat flow, the effects of sedimentation, cooling of the lithosphere, and internal generation of heat. We will first describe our modelling technique of the depth to the Curie isotherm and how this

governs the intensity of magnetization in the oceanic lithosphere for our forward modelling of scalar magnetic anomaly fields. We will then examine possible causes for lateral variations in surface heat flow and if the assumptions that we adopt in our modelling are viable.

A. Methods

An outline of the modelling procedure is given in Figure 19. Since the lower limit of the resolution of MAGSAT is in the order of 200 km (Sailor et al., 1982) we divided the study area into 2 by 2 degree blocks. Each block is given values for the age, the sediment thickness, and the surface heat flow. The age is determined from identified magnetic isochrons, with extrapolation between the isochrons. We used maps of Emery and Uchupi (1984), Sclater et al. (1980), and Hayes and Rabinoiwitz (1975). The determination of the age in the equatorial regions is difficult because of the geometry of the situation, but a fairly good knowledge of the amplitude of the ridge crest offset in this area allowed us to model the ages reasonable well. Figure 20 shows the average age within each 2 by 2 degree block. The sediment thickness was taken from the compilation of Emery and Uchupi (1984), and is shown in Figure 21. Heat flow data were compiled from a number of sources and averaged for each block. We used as much information as possible about each heat flow value,

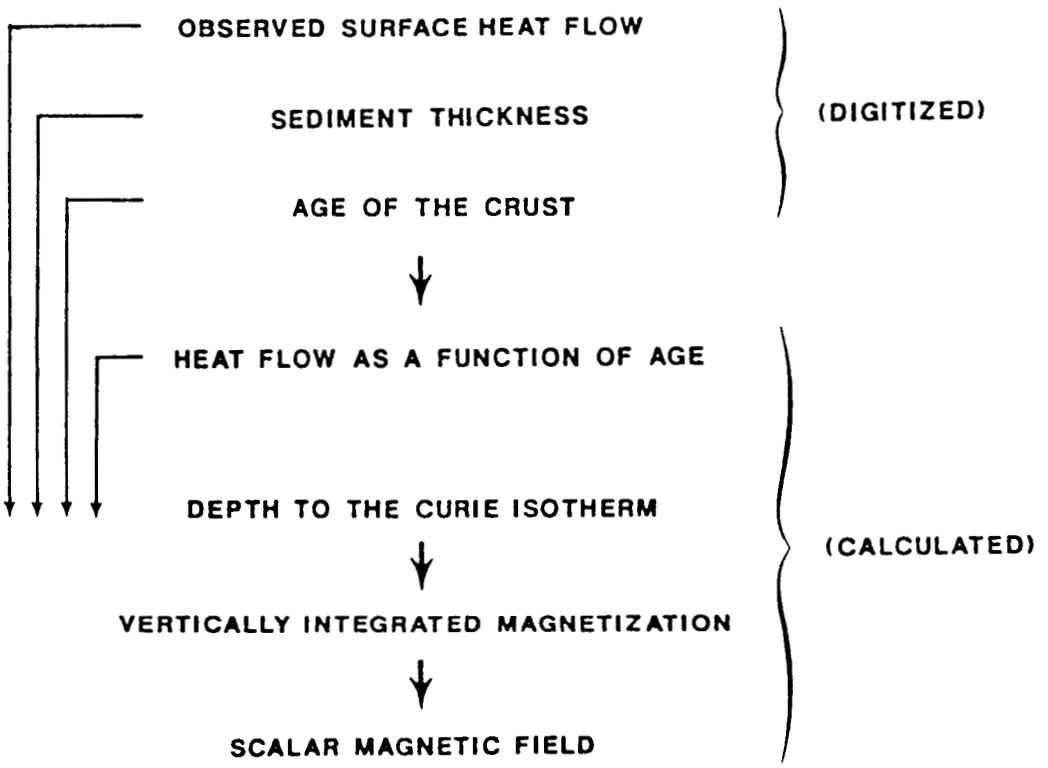

Figure 19. Flowchart of modelling depths to the Curie isotherm, models of vertically integrated magnetization, and the scalar magnetic field at satellite altitude produced by these magnetization models.

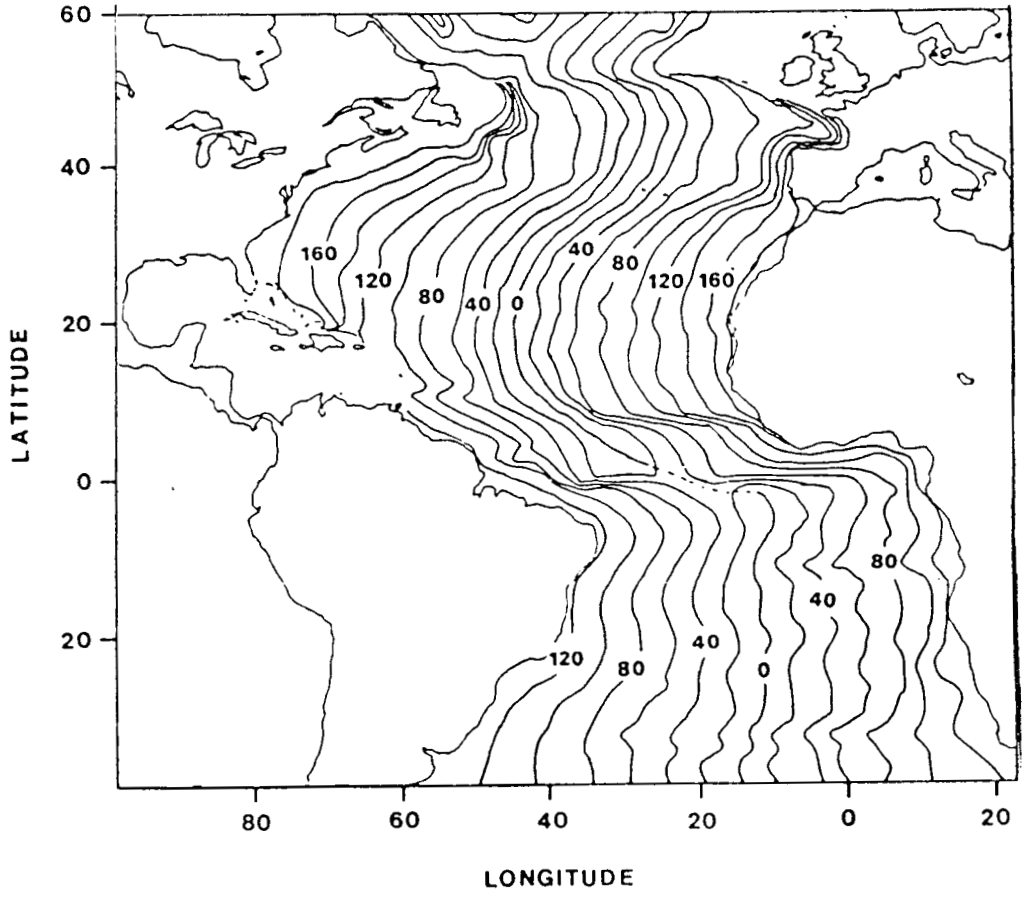

Figure 20. Average age (in MY) of the Atlantic Ocean within 2 by 2 degrees spherical tesserae. 20 MY contour interval.

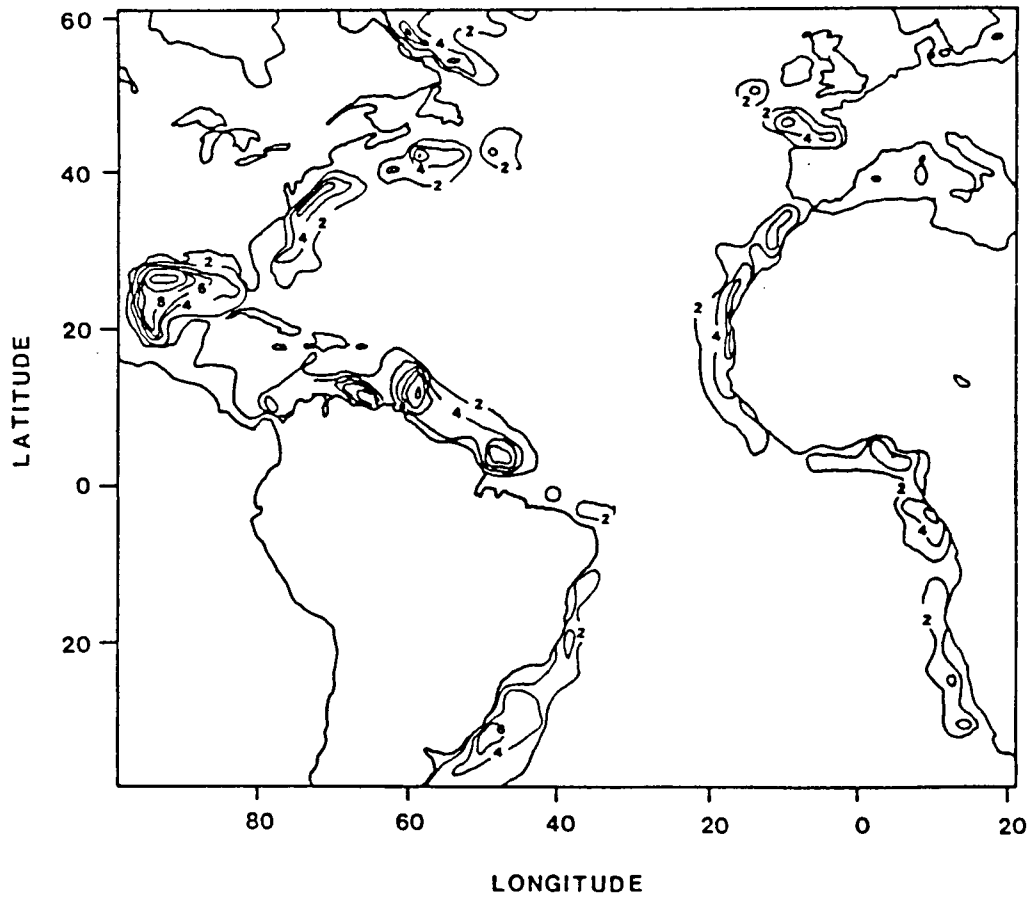

Figure 21. Average sediment thickness (in km) in the Atlantic Ocean within 2 by 2 degrees spherical tesserae. Contour interval is 2 km.

especially the quality of the data points, the number of data points at each location etc. The coverage of surface heat flow data in the study area is poor. To overcome this difficulty, and fill the gaps in this data set, we determined the heat flow that could be expected from the age of the crust, calculated from the cooling of the oceanic lithosphere. We also used the relationship between surface heat flow and age suggested by Parssons and Sclater (1977). The large variations in surface heat flow, even for areas with similar age, produce big undulations in the depth to the Curie isotherm that we have to use a much smoother function for the lateral variation in surface heat flow. We will demonstrate and discuss this in a later section. From the data sets described above we determine the depth to the Curie isotherm by repetitive calculations of the temperature (Equation 6) at the bottom of each layer in which the thermal and magnetic properties can be assumed to be homogeneous. It is possible that the thermal conductivity varies as a function of temperature in the upper mantle (Arkani-Hamed and Strangway, 1985), and we have used an iterative technique to calculate the temperature. The temperature at every 0.5 km is determined with the thermal conductivity of the layer above it. The thermal conductivity for the new temperature is then used to calculate a new temperature until the change in temperature is less than $0.01^{\circ}C$. 2 to 3 iterations were usually needed. The thermal

conductivity is determined by a factor $e^{-(T/836)}$ multiplied with the thermal conductivity at room temperature, and was used when the temperature exceeded 250 °C. An example of the depth to the Curie isotherm in the study area is shown in Figure 22. The intensity of magnetization is then determined for each block, depending on the temperature and the intensity of magnetization for each layer within the block. From the vertically integrated intensity of magnetization in each block the scalar magnetic field is calculated for an altitude of 400 km. The choice of magnetic and thermal properties will be discussed later in this chapter.

B. Oceanic heat flow: Models and observations

The ocean floor is almost always covered with sediments, which makes it an ideal environment to measure heat flow. Thousands of heat flow measurements have been made in the oceans, but the coverage is not sufficient for large scale modelling of the depth to the Curie isotherm over entire ocean basins. However, the observations agree with the surface heat flow that can be expected in oceanic lithosphere of a specific age. Figure 23 shows the cooling curve of Parsons and Sclater (1977) which is a combination of the heat flow predicted from conductive cooling of a semi-infinite half space and observed heat flow. For ages between 60 MY and 125 MY the observed heat flow is in very good agreement with the heat flow predicted from thermal

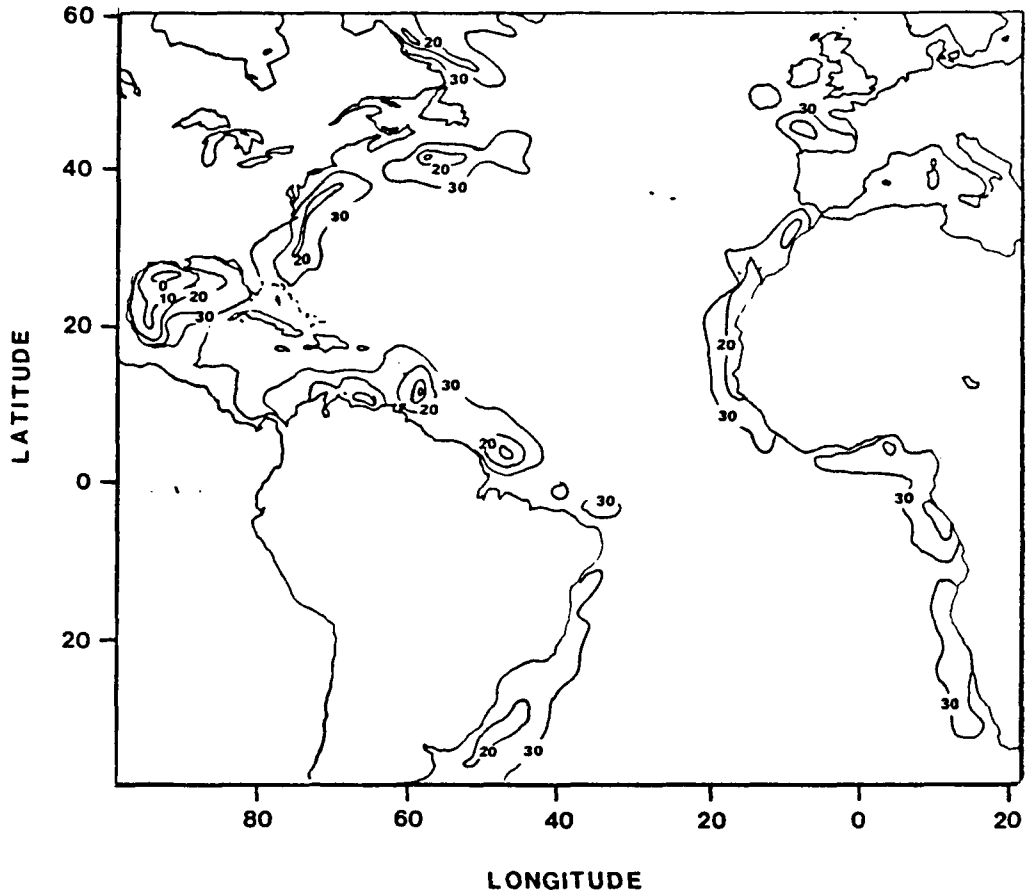

Figure 22. Calculated depths (in km) to the Curie isotherm within 2 by 2 degrees spherical tesserae. The physical properties of Table 3 (page 60) have been used in the calculations. Contour interval is 10 km.

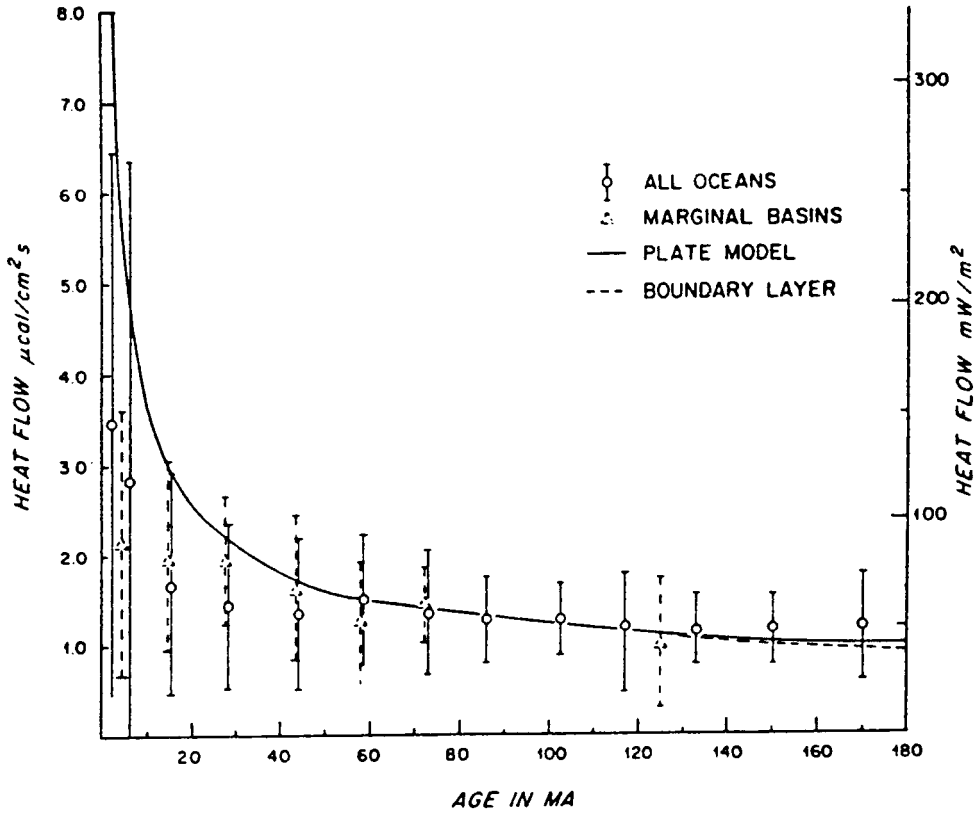

Figure 23. Mean heat flow and standard deviation for all the oceans and for the marginal basins as a function of age. Also shown are the expected heat flow from the plate and boundary layer model of Parsons and Sclater (1977). From Sclater et al. (1980).

models of the oceanic crust. The surface heat flow that is predicted by cooling models, as the crust ages decreeses with some exponential function, and will ultimately become zero as time (t) goes to infinity. The rate of decrease is so low for older crust that it can be modelled by a constant heat flow (50 mW/m^2) for crust >125 MY, in agreement with observations. This heat flow value is close to the heat flow from the Earth's interior and will not change during the life span of an ocean basin. The observed heat flow for very young crust is much less than is expected from a situation of conductive cooling, and this is caused by convective

cooling due to hydrothermal circulation. When the crust ages the observed heat flow gradually approaches the heat flow that is predicted from conductive cooling. These observations do not only tell us that circulation of water is taking place in young oceanic crust but that individual heat flow values cannot be used in regional studies of heat flow and of the temperature at depth in the oceanic lithosphere. Sediment with its low permeability, prohibits circulation of ocean water to and from the oceanic crust. Chemical reactions in the crust seal cracks by secondary mineralization and prohibits circulation of water within the crust. Embley et al. (1983) found that conductive cooling of the crust becomes the leading heat removing agent in the oceanic crust when the thickness of the sediments exceeds 75 m. The average oceanic basin has accumulated this amount of sediments after about 20 MY. In Figure 23 this is the age at which the observed heat flow gradually increases. In areas where it is possible to reach the Curie isotherm in the crust, the thickness of the sediment is blanket several kilometers and if we assume that the sedimentation rate has been constant during the history of the North Atlantic, the crust was sealed of by an approximately 75 m thick sediment cover after only 1.5 MY. Convective cooling within the crust is probably important after the surface is sealed off. The question is how much had the lithosphere cooled compared to the average oceanic crust, and how will this affect the

temperature when the crust has reached the age of the areas that we examine, that is 180 MY in the North Atlantic and 120 MY in the South Atlantic.

C. Thermal properties of the oceanic lithosphere

The thermal properties of the average oceanic lithosphere are taken from Stacey (1977), Turcotte and Schubert (1982) and from Huthchison (1985). Table 3 shows the average values of thermal conductivity, Curie temperature and internal generation of heat that we use in our modelling. The most critical physical property in this modelling is the thermal conductivity of the oceanic rocks. A relatively minor change of the thermal conductivity of the sedimentary layer will drastically change the temperature at depth. If the average thermal conductivity is higher than the value that we have used in our calculations the Curie isotherm will be reached at greater depths which will reduce the effect of sedimentation on magnetic anomaly values.

In our heat flow modelling we have assumed that the internal generation of heat is small. This is most certainly true the for mafic and ultramafic layers of the oceanic lithosphere (e.g. Von Herzen and Uyeda, 1963; Parsons and Sclater, 1976). The concentration of radiogenic elements in pelagic sediments is also very small (e.g. Henderson and Davis, 1983; Wilkens and Handyside, 1985), and it is correct to assume a zero contribution of heat by internal sources in

TABLE 3

Layer	Thick (km)	Induced magn. (A/m)	Remanent magn. (A/m)	Curie point °C	Viscous magn. %	Therm. Cond. W/m°C	Density kg/m³	Heat Capacity J/kg°C	Therm. Diff. m²/s	Heat Gen. μW/m³
1	0-18	0	0		0	1.3	2400	920	0.56	0-1.0
2	1.5	0.380	2.42	150-400	30-50	1.7	2900	1050	0.56	0
3a	3.78	0.686	0.618	520-580	0-10	1.7	2900	1050	0.56	0
3b	0.72	0.686	5.09	580	0-10	1.7	2900	1050	0.56	0
4	1.5	0.686	5.09	580	0	1.9	2900	1050	0.56	0
Mantle	. . . . 580°C	0-0.02	0	580	0	3.9	3300	1160	0.8	0

these sediments. Where the thickest deposits of sediments are found, along the continental margins and in the deep sea fans, the major portion of the sediments are derived from the continents, and it is possible that the concentration of radiogenic elements in these sediments is high enough that we should consider this in our calculations. Lewis and Hyndman (1977) predict that the sediments in the Laurentian Cone, if containing the same amount of radiogenic elements as the continental rocks from which they were derived, will contribute about 10 mW/m^2 (~20%) to the total surface heat flow. This effect can be allowed for in the calculations.

D. Lateral heat flow

The possibility of lateral heat flow within the oceanic crust and between the oceanic crust and the continental crust has been proposed to explain the lateral variations in surface heat flow. Lewis and Hyndman (1977) found that the surface heat flow in the Laurentian Cone varied between 40 and 72 mW/m^2 . They interpreted the observed variations in surface heat flow as being caused by variations in the thermal conductivity within the sediments. The most pronounced conductivity difference is between the normal mixture of continental and oceanic sediments and the salt diapirs that were formed early in the spreading history of the ocean basin. This type of lateral heat flow takes place on a very small scale, and is not important in modelling of

structures that are detectable at satellite altitude. The difference in thermal conductivity between the continental lithosphere and the oceanic lithosphere is a more probable cause for large scale variations in surface heat flow. We have used a simplified model (Figure 24) to determine if lateral heat flow has to be considered when we model the depth to the Curie isotherm. Equations 7 and 8

$$T_{x<0} = \frac{1}{L}\left[zT_1 - \frac{2L(T_2 - T_1)K_1}{\pi(K_1 + K_2)} \sum_{n=1}^{\infty} \frac{(-1)^n}{n} \sin\frac{n\pi y}{L}\, e^{npx/L}\right] \tag{7}$$

$$T_{x>0} = \frac{1}{L}\left[zT_1 - \frac{2L(T_2 - T_1)K_2}{\pi(K_1 + K_2)} \sum_{n=1}^{\infty} \frac{(-1)^n}{n} \sin\frac{n\pi y}{L}\, e^{-npx/L}\right] \tag{8}$$

with the following boundary conditions

$$T = 0 \qquad z = 0 \qquad - < x <$$

$$T = 0 \qquad z = L \qquad x > 0$$

$$T = T \qquad z = L \qquad x < 0$$

is a slight modification of a similar problem solved by Carslaw and Jaeger (1978). The parameters are explained in Figure 24. We have computed the temperature with two sets of boundary conditions. The selection of boundary conditions for the first set of calculations were made after the model of Sclater et al. (1980) of the continental and oceanic geotherms (Figure 25). They propose that an equilibrium ocean basin and an Archean continent have similar

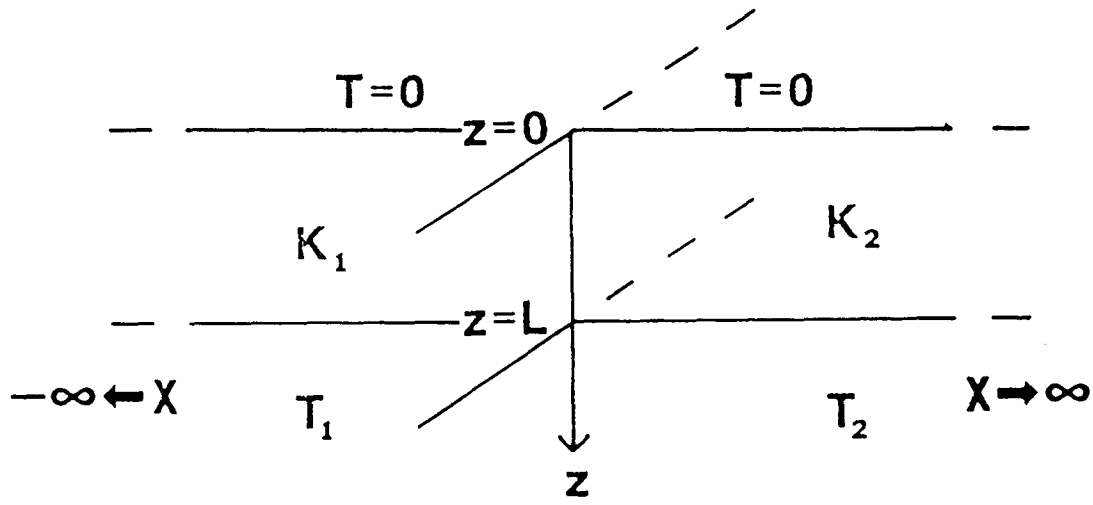

Figure 24. Lateral heat heat flow in an infinite strip. The temperature at the surface of the plate (z=0) is the same for both parts of the plate. K_1 and K_2 are the thermal conductivities in the continental and oceanic crusts respectively. T_1 and T_2 are the temperatures at the bottom of the oceanic and continental layers respectively.

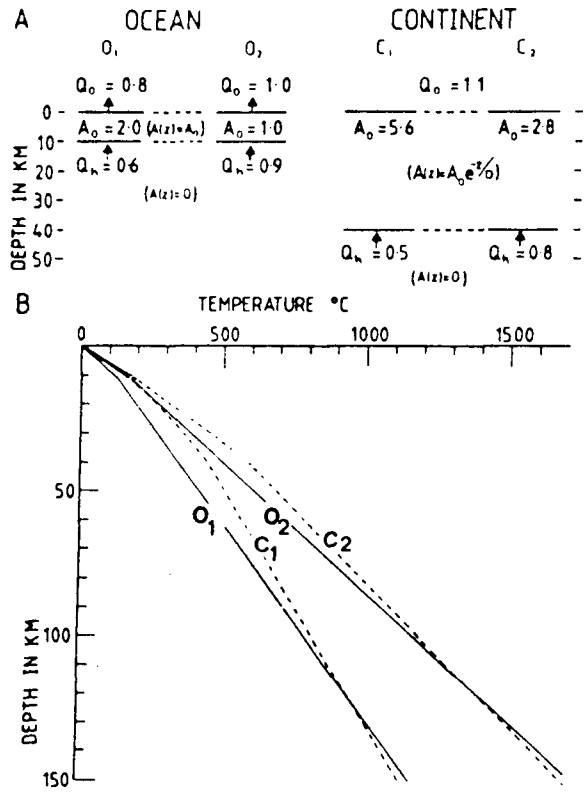

Figure 25. Continental and oceanic geotherms. A. Models used to compute the range of geotherms beneath an 'equilibrium' ocean O_1 and O_2 and an old stable continent C_1 and C_2. B. Predicted range in old continental (C_1 and C_2) and 'equilibrium' oceanic (O_1 and O_2) geotherm. From Sclater et al. (1980), who also give a detailed discussion of these models.

temperature structures at depth, and that this depth is between 100 and 150 km. The thick line is the geotherm in the oceanic plate, and the continental geotherms C_1 and C_2 are for continental lithospheric models with higher and lower concentrations of radiogenic elements in the crust. Sclater et al. give a more detailed discussion of these models. The largest temperature difference between the oceanic and continental geotherms arise if we chose curves C_2 and O_2 in Figure 25. This difference is fairly well described by a gradient of 5 °C per km for the upper 50 km and a constant difference of 250 °C between 50 and 150 km. In Figure 26 we have plotted the difference in temperature between a case with no lateral heat and lateral heat flow (Equations 7 and 8, with L = 150km) plotted as a function of depth and distance from the continent-ocean boundary. In our second calculation we used 12 km as the lower boundary of the strip. The thermal conductivities of oceanic sediments and rocks are much lower when compared to continental rocks. There will be a substantial temperature difference between the two types of crust at this depth. Figure 27 shows the temperature difference between cases with and without lateral heat flow.

The decrease in temperature in the oceanic lithosphere that is suggested by our models of lateral heat flow is only important at a distance of some tens of kilometers from the continent-ocean boundary. If we would have used the C_1

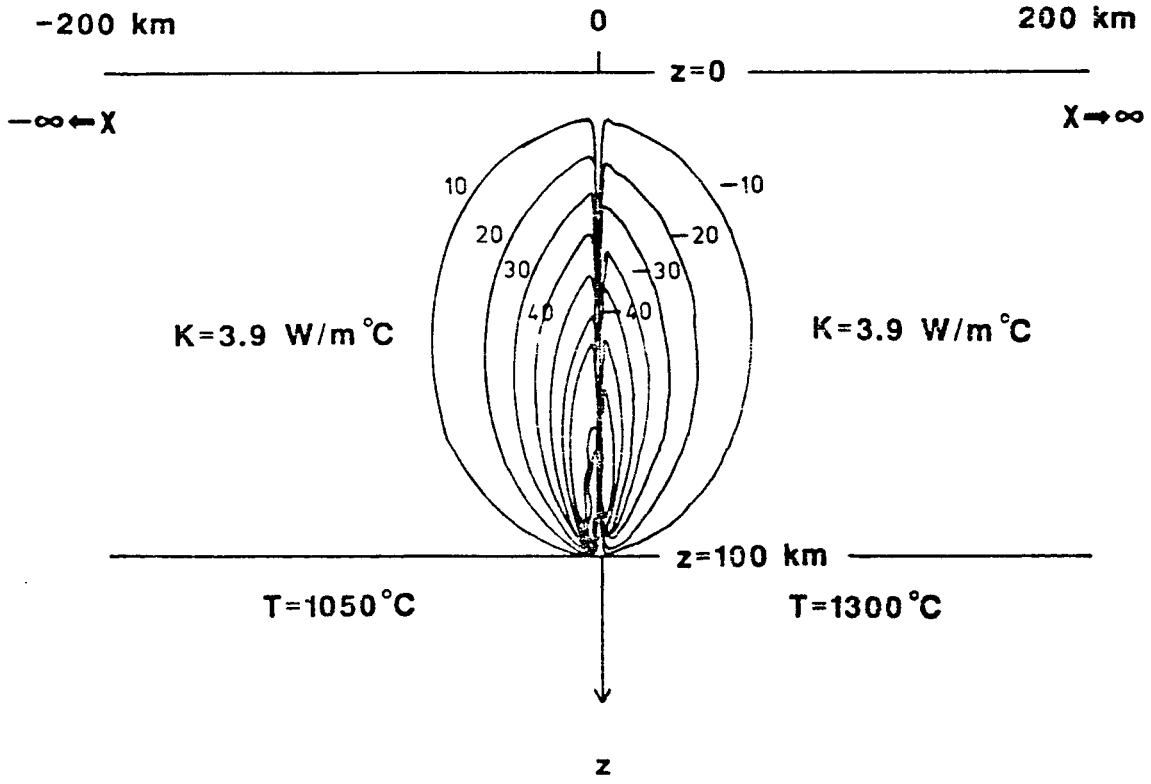

Figure 26. Temperature difference with depth from lateral heat flow across continent-ocean boundary. The difference in temperature with depth between a situation of no lateral heat flow and the change in temperature with lateral heat flow determined by Equations 7 and 8 and with a T of 250 °C at a depth of 100 km. The thermal conductivity is 3.9 W/m °C in the continental as well as in the oceanic lithospheres.

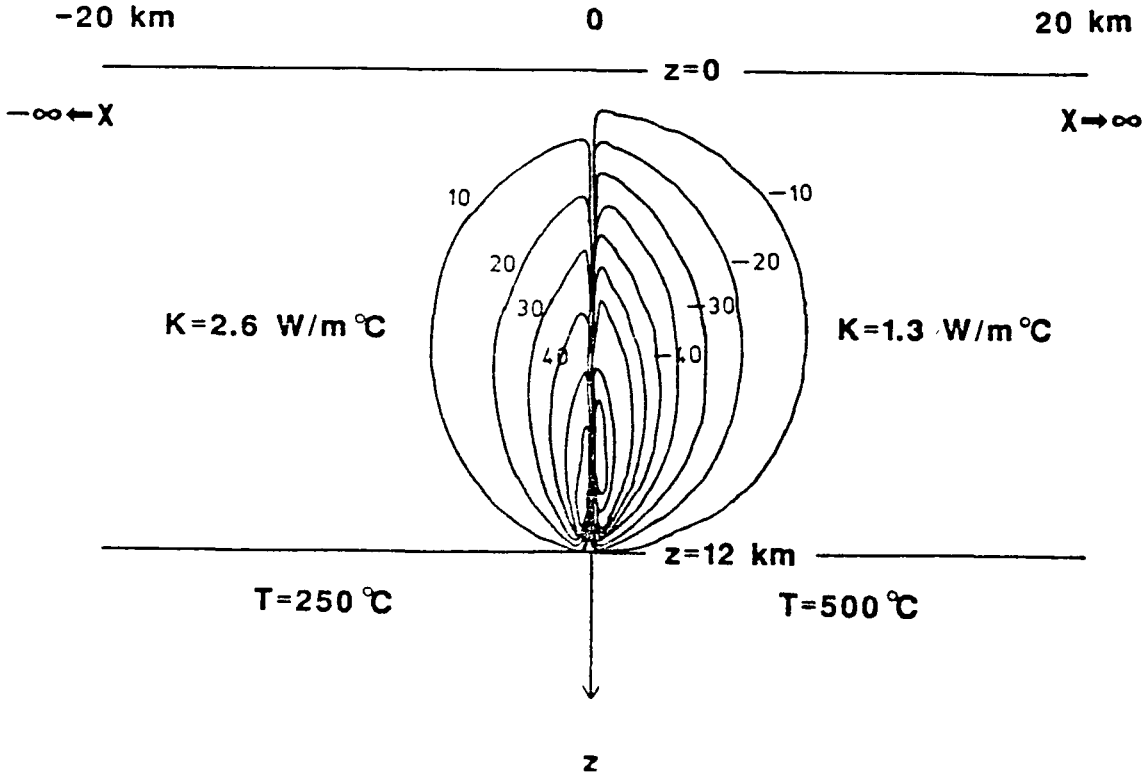

Figure 27. Temperature difference in a model where the thermal conductivity is 1.3 W/m °C in the oceanic sediments and 2.6 W/m °C in the continent. The temperature at the bottom of the strip (12 km) is 500 °C and 250 °C in the oceanic and continental crusts, respectively.

continental geotherm of Sclater et al. (Figure 24) the change in temperature difference from lateral heat flow is practically zero. We conclude that lateral heat flow can only be a very minor source for lateral variations in surface heat flow on the length scale that is of interest when studying satellite altitude magnetic anomalies.

E. The effect of sedimentation

When we model conductive heat flow it is important to examine how much of the surface heat flow that is observed in an oceanic area has its origin in the global flux of heat from the Earth's interior, from cooling of the oceanic lithosphere and from internal heat generation. In the previous section we showed that lateral heat flow is of minor importance in large scale studies of the depth to the Curie isotherm. Another alternative is that the excess heat from the decay of radiogenic elements in the sediments is consumed when the sediments are heated from a temperature that at the time of deposition was the same as the ocean bottom waters, about 4 $^{\circ}$C. In this section we will discuss different mathematical methods that can be used to determine this effect.

Von Herzen and Uyeda (1967) made some calculations concerning the possibility of explaining variations in surface heat flow in the Pacific Ocean. They concluded that only very rapid sedimentation (>100 m/MY) can cause

important changes in the surface heat flow. We have made some further calculations of this problem and not only determined the change in surface heat flow due to sedimentation, but more important for our modelling, how the temperature in the accreting sediment layer and in the magnetic layers will change as a function of sedimentation rate, thermal conductivity and internal generation of heat. The equation of heat transfer in a moving medium (this equation is derived in Appendix B) is

$$\frac{\partial^2 T}{\partial z^2} = \frac{U}{\kappa}\frac{\partial T}{\partial z} + \frac{1}{\kappa}\frac{\partial T}{\partial t} - \frac{A}{K} \qquad (10)$$

where T is the temperature, z is the depth, U is the sedimentation rate, κ is the thermal diffusivity, t is the time, A is the amount of heat generated per unit volume and time, and is the thermal conductivity. With the following boundary conditions,

$$T = z \quad \text{at} \quad z > 0, \quad t = 0$$
$$T = bt \quad \text{at} \quad z = 0, \quad t > 0$$

the temperature gradient in a sediment layer with constant rate of sedimentation is

$$\frac{\partial T}{\partial z} = a + \frac{1}{2U}\left[aU - \frac{\kappa A}{K}\right]\left[e^{Uz/\kappa}\left(1 + \frac{Uz}{\kappa} + \frac{U^2 t}{\kappa}\right)\operatorname{erfc} X - \operatorname{erfc} Y + e^{Uz/\kappa}\, X\left(-\frac{\partial}{\partial X}\operatorname{erf} X\right) - Y\left(-\frac{\partial}{\partial Y}\operatorname{erf} Y\right)\right] \qquad (11)$$

where $X = \frac{z + Ut}{2(kt)^{1/2}}$ $Y = \frac{z - Ut}{2(kt)^{1/2}}$

This solution is given by Von Herzen and Uyeda (1963).

In Figure 28 we have plotted the relative change in surface heat flow in a 12 km thick sediment layer as a function of time of deposition and as a function of the thermal conductivity of the sediments. We have only plotted the time range that is interesting for sedimentation in the Atlantic Ocean. The y-axis is a linear scale representing the thermal conductivity and the x-axis is the time plotted on a logarithmic scale. The time spans from 10 MY to 1000 MY. The vertical dashed lines are the approximate ages of the South Atlantic (~120 MY) and the North Atlantic (~180 MY). For the average thermal conductivity of the sediments, 1.3 mW/m^2, there is a relative decrease in surface heat flow in the Amazon and Congo Cones to approximately 0.77 of the undisturbed gradient. This means that about 20% of the observed surface heat flow comes from some other source(s), if the surface heat flow is similar to the average heat flow in the oceans (50 mW/m^2). The most probable one is from internal generation of heat from radiogenic isotopes (as discussed earlier). This calculation suggest that the amount of internal heat generation is approximately what Lewis and Hyndman (1977) predicted. In our calculation of the depth to the Curie isotherm this amount of internal heat

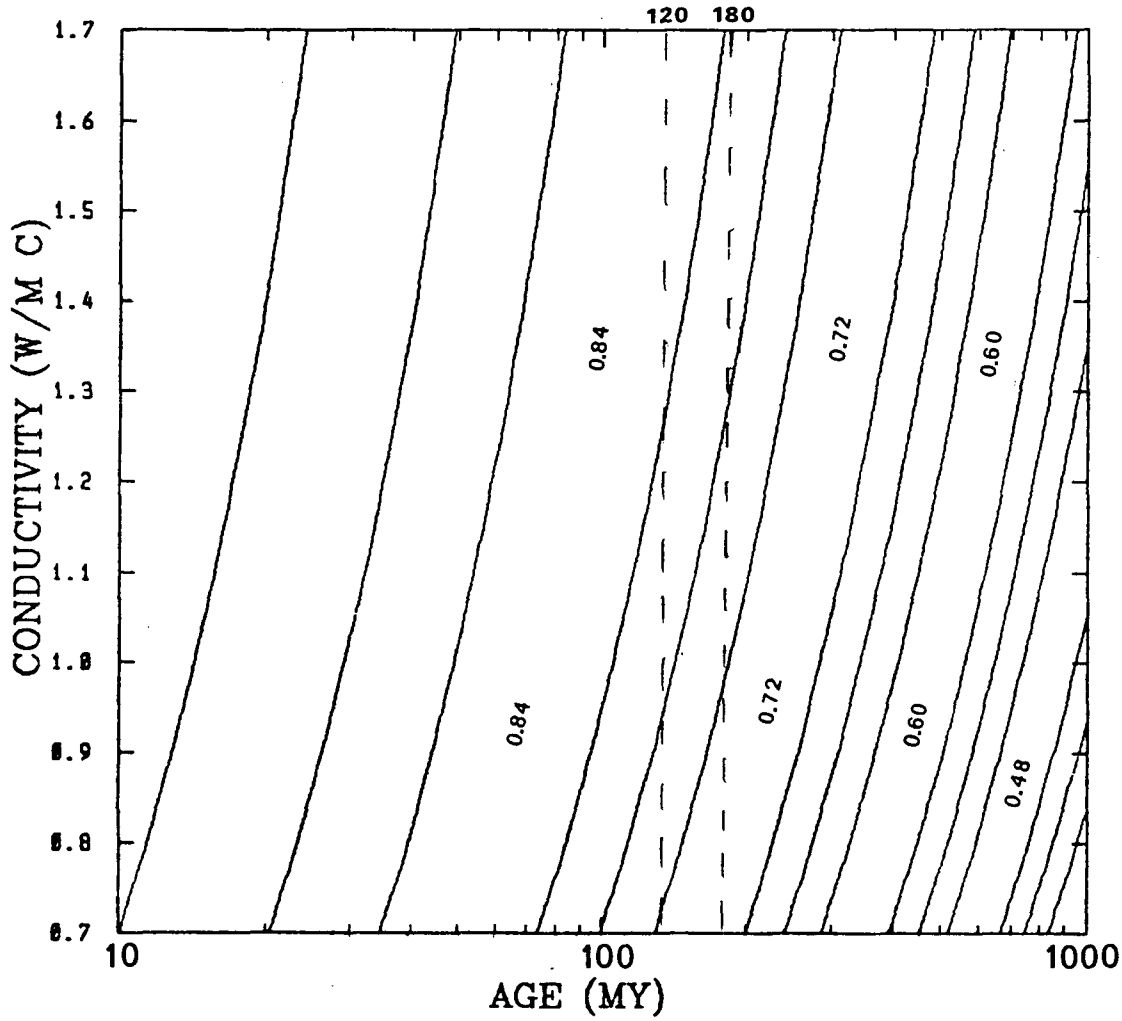

Figure 28. The effect of sedimentation on surface heat flow. The difference between a steady state case with one dimensional conductive heat flow (Equation B1, Appendix B) and a case where the surface heat flow is reduced due to the heating of the sediments, that at the time of deposition had the same temperature as the oceanic bottom waters (Equation 11). The heat flow is calculated for a depth of 100m, with a constant sedimentation rate of 12 km per 180 MY. The surface heat flow is reduced by approximately 20%, which is approximately equal to the heat flow produced by a concentration of radiogenic elements that is similar to continental rocks from which the sediments are derived.

generation will increase the depth to this isotherm by about 1.5 km.

In the calculations that we have done of the depth of the depth to the Curie isotherm we have used surface heat flow in a steady state situation to determine the temperature at certain depths in the lithosphere. Instead of solving Equation 10 for the surface heat flow, we can solve for the temperature at different depths. The solution of Equation 10 in a situation of conductive heat flow in a moving medium with the following initial and boundary conditions

$$T = T_0 + az \quad \text{at} \quad z > 0,\ t = 0$$
$$T = T_0 + bt \quad \text{at} \quad z = 0,\ t > 0$$

where a is the undisturbed temperature gradient and b is a time dependent temperature function. The rest of the symbols are the same as in Equation 11, is

$$T = T_0 + az + (\kappa A_0 t/K) - aUt + \frac{1}{2}(T_1 - T_2)\left[\text{erf } X + e^{Uz/\kappa}\text{erfc } X\right] + \frac{1}{2U}\left[b + aU - \frac{\kappa A_0}{K}\right]\left[(z + Ut)e^{Uz/\kappa}\text{erfc } X + (Ut - z)\text{erfc } Y\right] \quad (12)$$

where X and Y are the same as in Equation 11. From Equation 12 we can see that any positive value of A will increase the temperature. However, the heat generation is not time

dependent in Equation 12 and if we use a value of heat generation in the sediments that will produce a surface heat flow of 10 mW/m^2 ($\sim 0.5 \mu W/m^3$) the temperature at the bottom of the sediments will be over 1000 °C. We can only conclude that the temperature will increase if A is greater than 0. Hutchison (1985) determined by finite element analysis, that internal generation of heat will reduce the difference in surface heat flow, caused by sedimentation, by about 40%. We will discuss this method further later in this section.

In Figure 29 we have plotted the temperature difference as a function of conductivity of the sediments. The sedimentation rate in the calculations is again taken to be 12 km per 180 MY. We can see that for a thermal conductivity of 1.3 W/m °C the difference in temperature at the bottom of the sediment layer, which also is the top of the magnetic crust, the temperature difference is about 90 °C. This will put the Curie isotherm about 2.8 km deeper compared to a case of no heat expendature to the sediments. Naturally, if radiogenic elements are present in the sediments a substantial amount of heat will be released during the time of sedimentation, especially for the lowermost layers.

In the calculations above we have assumed that sedimentation took place on the oceanic lithosphere with a steady input of heat from the mantle of 50 mW/m^2. This boundary condition is certainly correct when the sedimentation rate is what we usually find in the oceans,

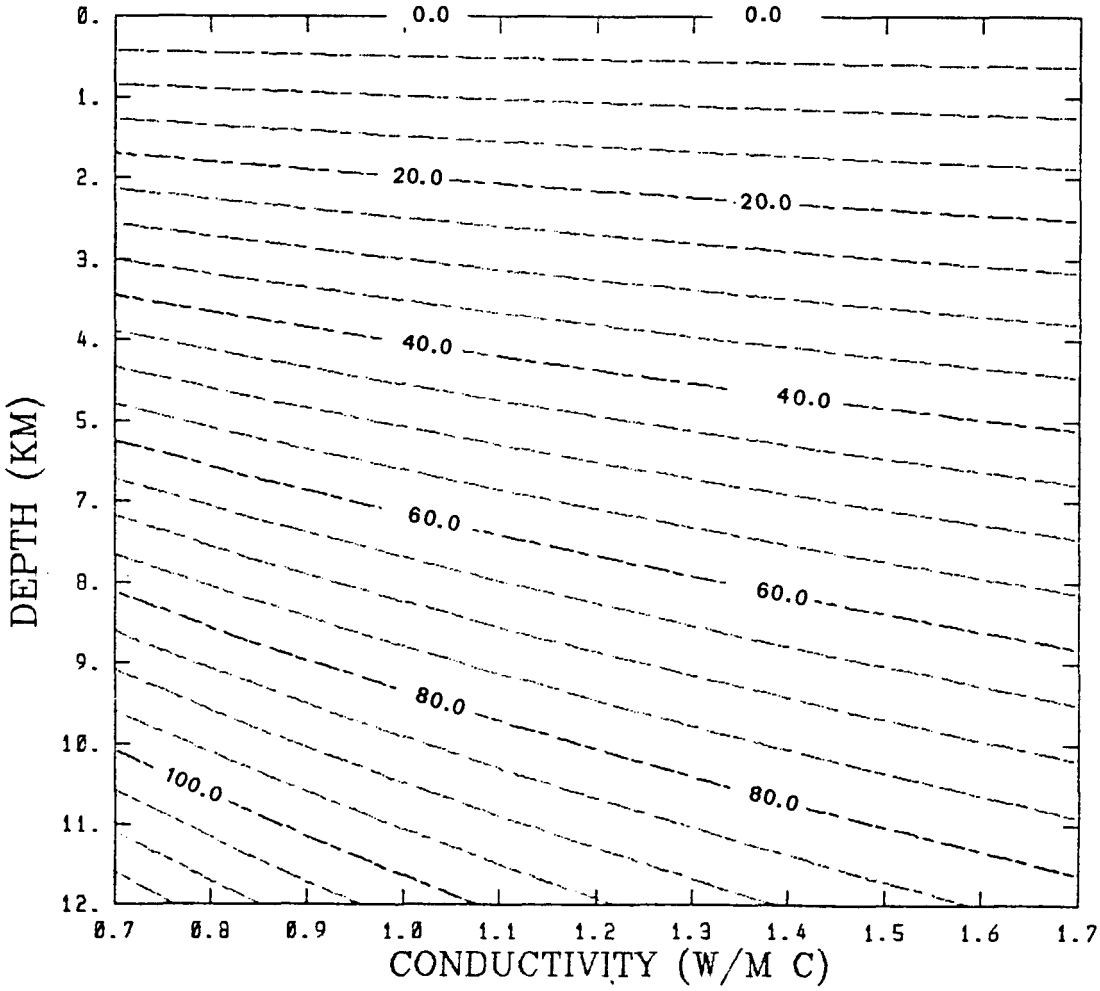

Figure 29. The effect of sedimentation on the temperature at depth in a 12 km thick deposit of sediments. The contour interval is 5 °C and shows the difference between the temperatures calculated with a simple heat flow model (Equation B1, Appendix B) and Equation 12.

let us say approximately 5 m/MY. At the age at which the sediment cover has reached such thickness that the leading heat removing agent is conduction, the oceanic lithosphere has cooled so much from hydrothermal circulation that this boundary condition is fairly correct. In areas where the sediment blanket is several kilometers thick, the hot lithosphere at the time that conductive heat flow became dominant, has perhaps not cooled down enough that we can make this assumption which has to be allowed for in the calculations. We also have to allow for the internal heat generation to be time dependent and for the effect of compaction of the sediments. To be able to make analytical solutions to these problems the assumptions that have to be made are so severe that only simple analytical models which describe depositional histories can be made (Hutchison, 1985). I order to allow for the processes discussed above, Hutchison used finite element analysis to determine the effects of sedimentation on surface heat flow and temperature in oceanic sediments. The differential terms in the heat flow equation was approximated by expressions involving finite differences in depth and in time. (The reader is referred to the Appendix in Hutchison (1985) for a detailed description of this method). Corrections for a cooling plate, radioactive heating and bottom water temperature changes was allowed for in Hutchison's calculations, and he compared these results with a constant

flux model. He found that a cooling plate has a very small effect after about 50 MY, about 5%. A variation in surface temperature of 20 °C during a time period of 10 MY, which can be compared to the higher bottom water temperatures during the Cretaceous, had practically no effect after 60 MY since the increase in surface temperature had ceased. Finally, radiogenic heat production in the sediments will compensate the effect of sedimentation by about 40%.

With the analytical method (Equation 12 and Figure 28) we estimated that the difference in the depth to the Curie isotherm between a model of simple heat flow model and a case of heat expendature to the sediments of 2.8 km. When we regard the results of Hutchison (1985), that all will compensate for the sedimentation effect, we believe that it safe to use a simplified heat flow to determine the temperature in the oceanic crust in the Atlantic.

F. Results

In Chapter 2 we described the average magnetization in of the oceanic crust and in Section C of this chapter we examined the thermal properties of the oceanic crust and upper lithosphere. There are quite large areas for some of the physical properties in the oceanic crust and there is a possibility that magnetic sources are present in the upper mantle. In this section we will examine the scalar magnetic anomaly field that will result from different models of the

physical properties in the oceanic lithosphere, first by presenting the physical properties and then by examining how the depth to the Curie isotherm and different intensities of magnetization in the oceanic lithosphere correlates with the scalar magnetic anomaly field at satellite altitude. Further discussion of these results is made in Chapter 5. To make it easier to compare the anomaly maps that we will present in this section, an enlarged map of the MAGSAT scalar magnetic anomaly field over the Atlantic Ocean is shown in Figure 30.

For the first model of an oceanic lithosphere (Figure 31) have used the magnetic properties from Table 3. Figure 32 shows the scalar magnetic anomaly field from an oceanic lithosphere with no viscous magnetization and no magnetic sources in the upper mantle. The magnetic fields produced by the remanent magnetization over the Cretaceous quiet zones dominates the anomaly map. Some similarity with the MAGSAT field can be seen in the North Atlantic Ocean but the anomalies in the Equatorial and South Atlantic are only similar in a few areas to the MAGSAT map. Note the reversed sign of the anomalies from the remanent magnetization in the Equatorial regions. The amplitude of the anomalies in Figure 30, produced by the remanent magnetization, is about 5 times smaller when compared to the MAGSAt field. Interestingly there is an anomaly over the Amazon delta, which demonstrates how a "hole" in the remanently magnetized slab will produce magnetic anomalies. Another important

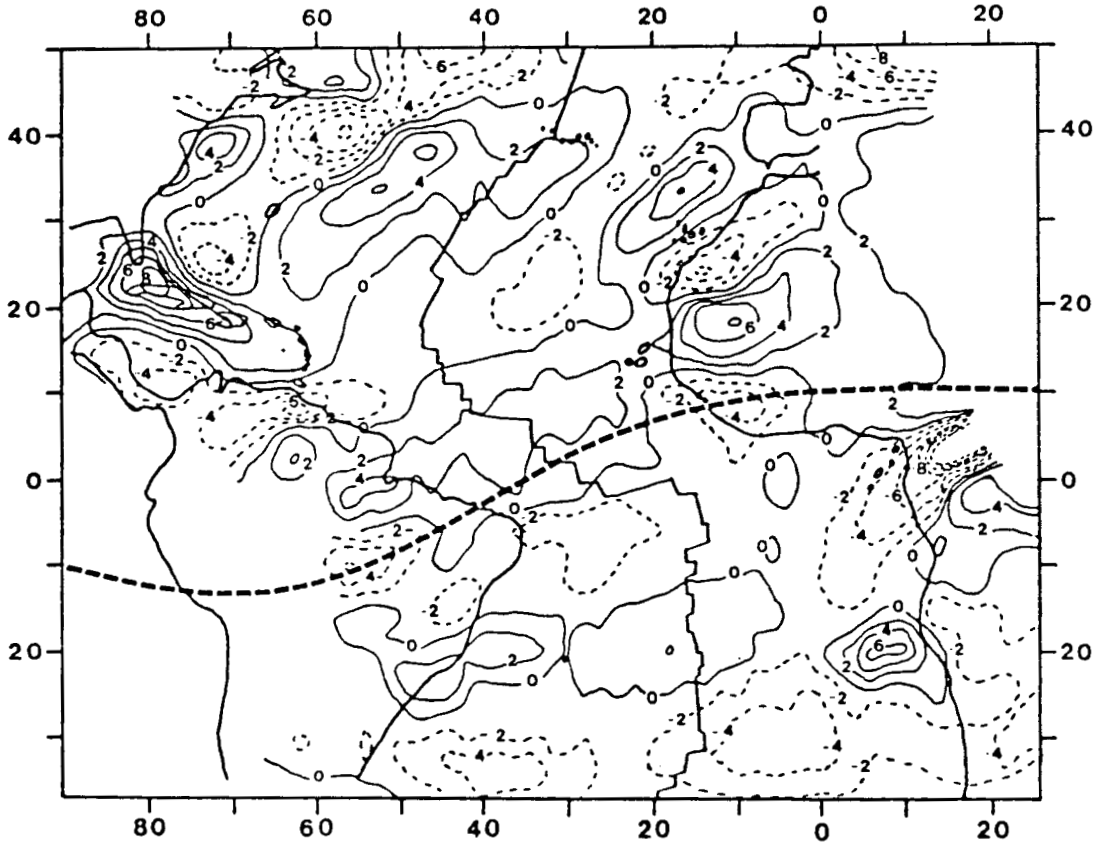

Figure 30. MAGSAT scalar magnetic field over the Atlantic Ocean. After Langel et al. (1982). Contour level is 2 nT.

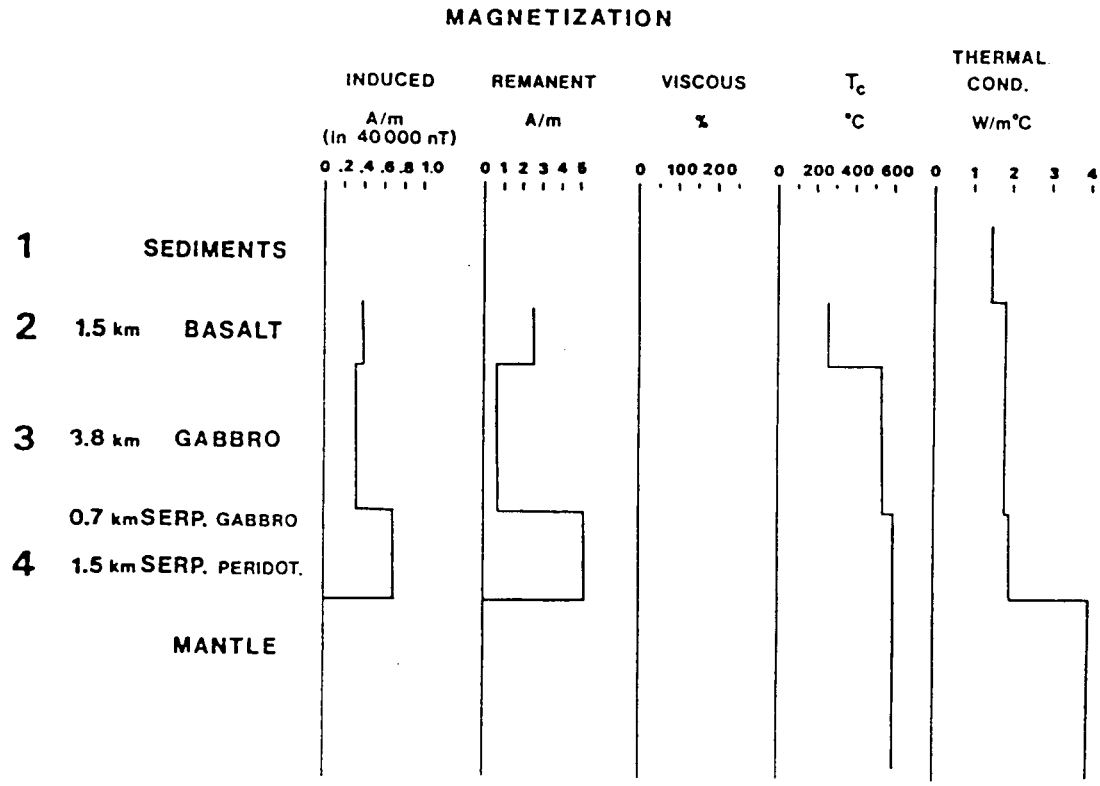

Figure 31. Magnetization model of the oceanic lithosphere inferred from oceanic rock samples. Average remanent magnetization and susceptibility in the crust is included.

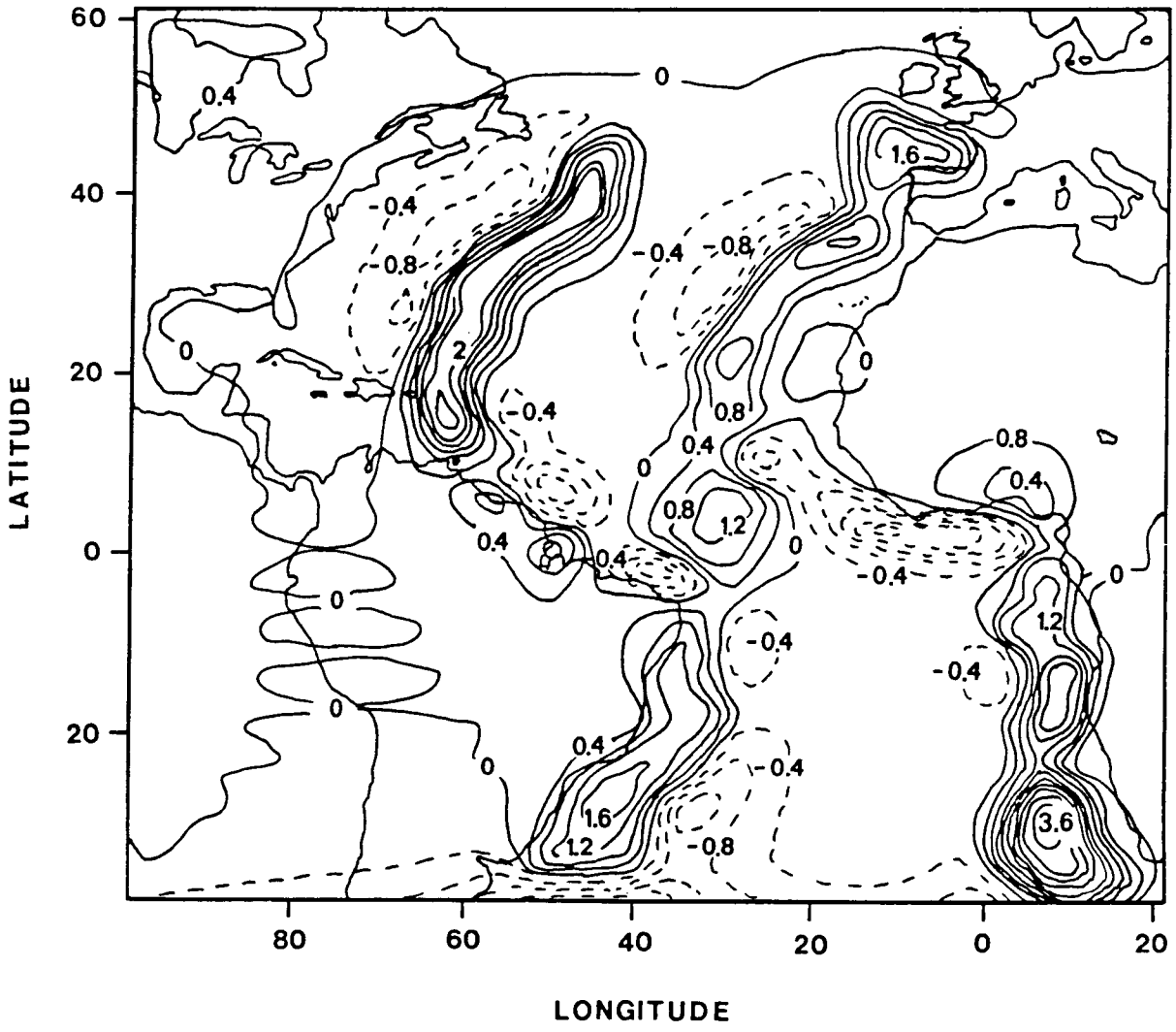

Figure 32. Scalar magnetic field at satellite altitude, from an oceanic crust with an average susceptibility and remanent magnetization that has been inferred from oceanic rock samples (Figure 31). Contour level is 0.4 nT.

difference between Figure 32 and the MAGSAT field is the lack of anomalies along the east coast of the United States, in the Greenland Sea, and in the Gulf of Mexico.

In the next model we keep the thermal properties the same as in Figure 31, but we assume 50% viscous magnetization in the basalt layers and 10% viscous magnetization in the gabbro layer (Figure 33). The scalar magnetic field from this model is shown in Figure 34. The field from remanent magnetization in the Cretaceous quiet zones is still present but does not dominate the overall character of the field. The negative anomaly over the Gulf of Mexico that is very pronounced in the MAGSAT map is present as well as the anomaly over the Laurentian Cone. Discrete magnetic anomalies can also be seen along the northern part of South America and along the north western coast of Africa. The strong anomaly over South Africa and adjacent ocean basins may be caused by the edge effect that arise from going to zero magnetization outside the map. Edge effects can also be seen along the lower and upper borders of the map. We should also note the low amplitude of the magnetic anomalies relative to MAGSAT.

Several investigators of satellite magnetic anomalies have suggested that viscous magnetization is the dominating source for oceanic magnetic anomalies. (e.g. Frey, 1985; Thomas, 1987). In the third model we have allowed for a viscous component that is much higher than what has been

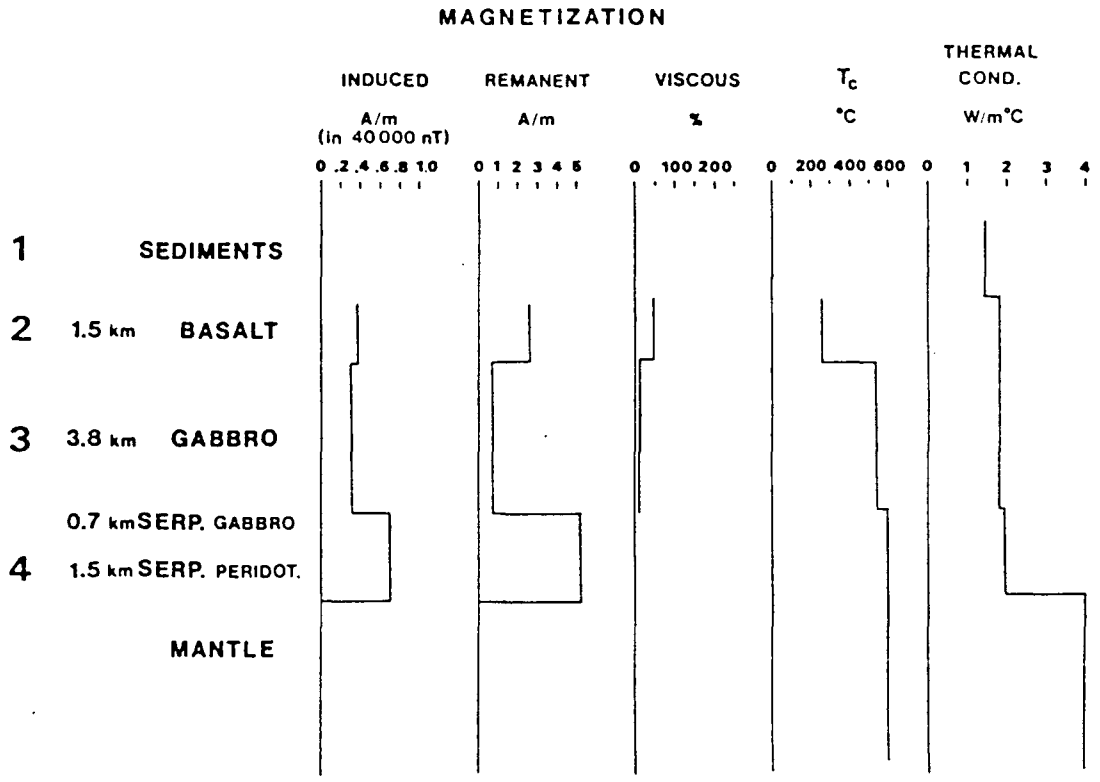

Figure 33. Magnetization model of the oceanic lithosphere inferred from oceanic rock samples. The same as Figure 31 with the addition of viscous magnetization in the basalts (Lowrie and Kent, 1978) and in the gabbros (Dunlop, 1983).

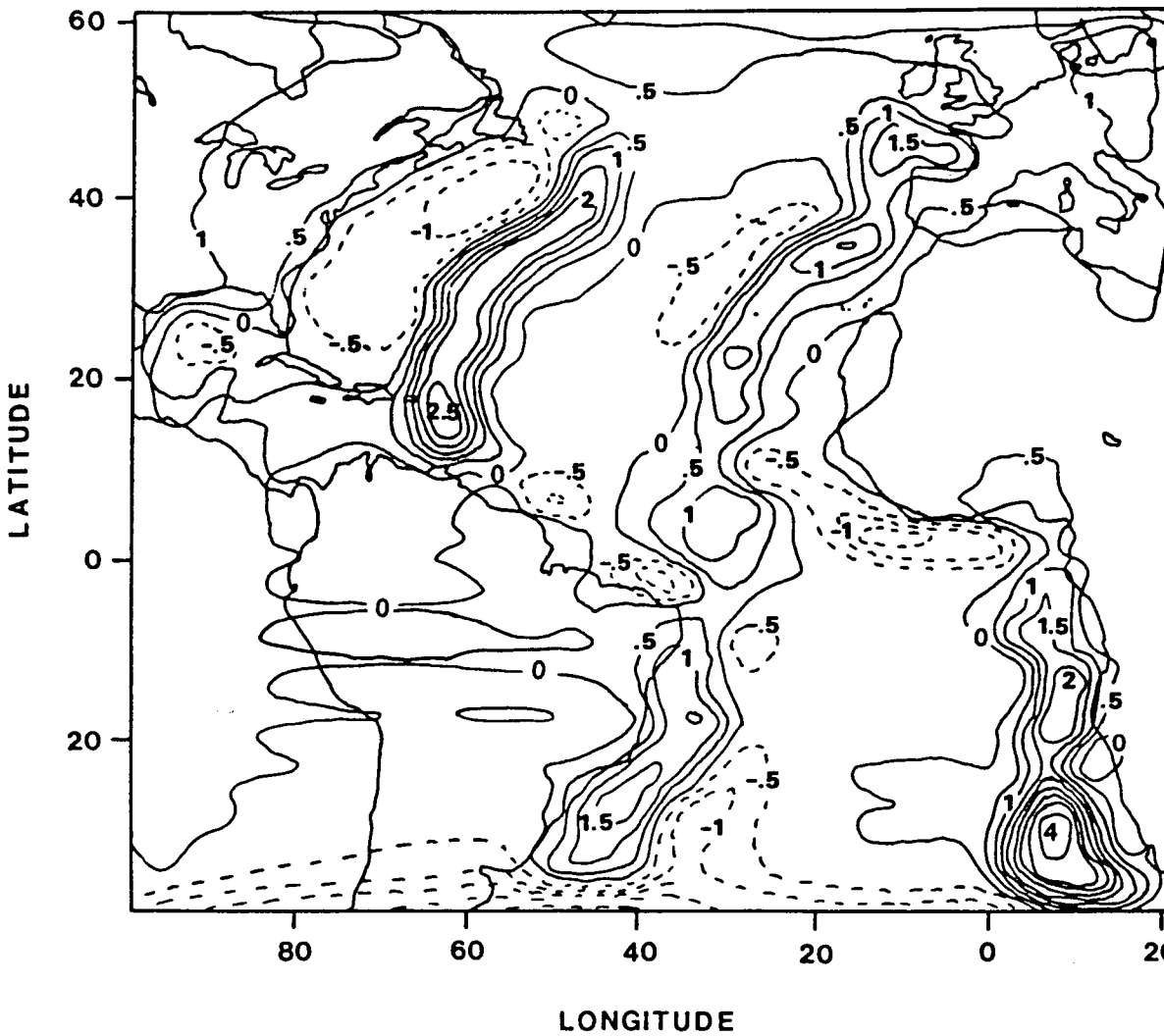

Figure 34. Scalar magnetic field at satellite altitude, from an oceanic crust with the average susceptibility and remanent magnetization that has been inferred from oceanic rock samples with the addition of 50% viscous magnetization of the basalts and 10% viscous magnetization of the gabbros (Figure 33). Contour level is 0.5 nT.

found in laboratory studies of this phenomenon (e.g. Dunlop, 1983). The anomaly field from a source layer that is dominated by viscous magnetization (Figure 35) is shown in Figure 36. The magnetic anomalies associated with the deep sea fans are apparent, especially in the Gulf of Mexico. The Cretaceous quiet zones are easily detected, but are not as dominating as in Figure 33. However, the relative amplitude between the anomalies from remanent magnetization and the anomalies from induced magnetization is about the same as in the MAGSAT field.

So far we have only considered models that include magnetic sources in the oceanic crust. The magnetic anomalies produced by these models anly show resemblance with the MAGSAT field in a few cases, and the amplitude of the anomalies is much lower than those seen in Figure 31. In our third model we have assumed that serpentinized peridotites are fairly abundant in the upper mantle, and not restricted to the approximately 1 km thick layer suggested by Lewis and Snydsman (1977). Arkani-Hamed and Strangway (1985) found that 20% serpentinization in a 20 km thick upper mantle, together with some enhanced magnetization due to the Hopkinson effect, will produce magnetic anomalies that are similar to MAGSAT anomalies over subduction zones. The average susceptibility of the upper mantle is about 0.0085 SI units (Figure 37). In a 40 μT inducing field the vertically integrated magnetization from this source will be

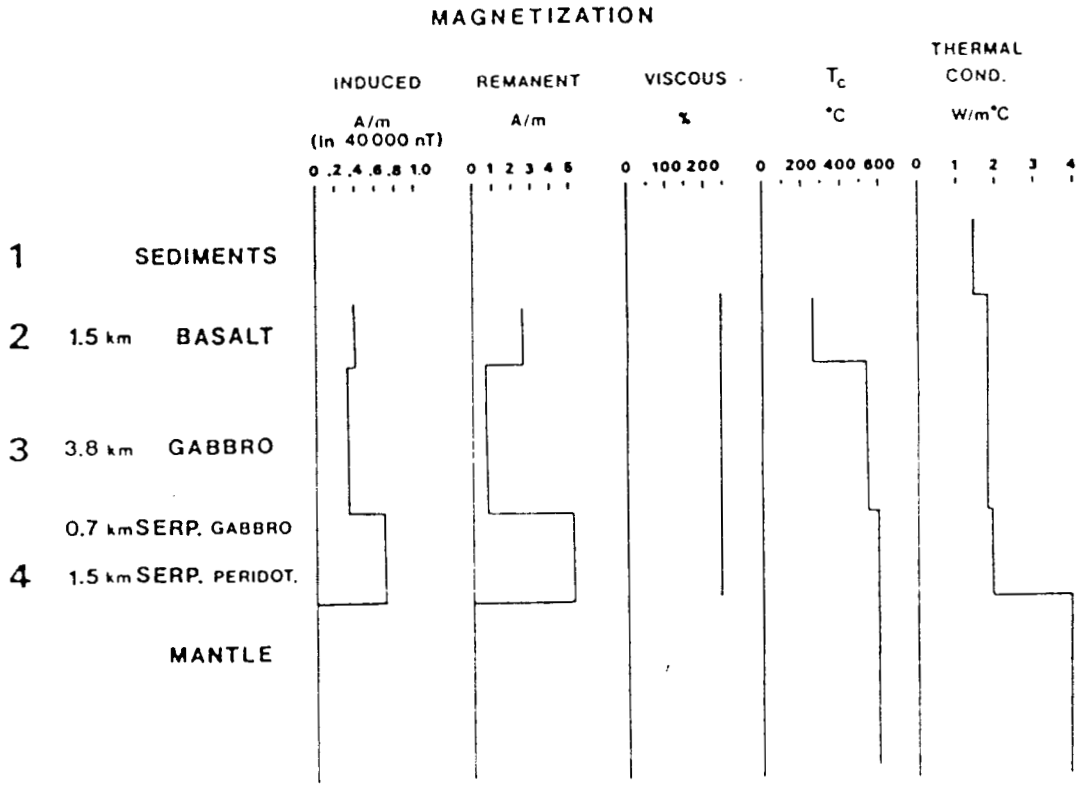

Figure 35. Magnetization model of the oceanic lithosphere with a viscous magnetization that is several times stronger than induced magnetization.

C-2

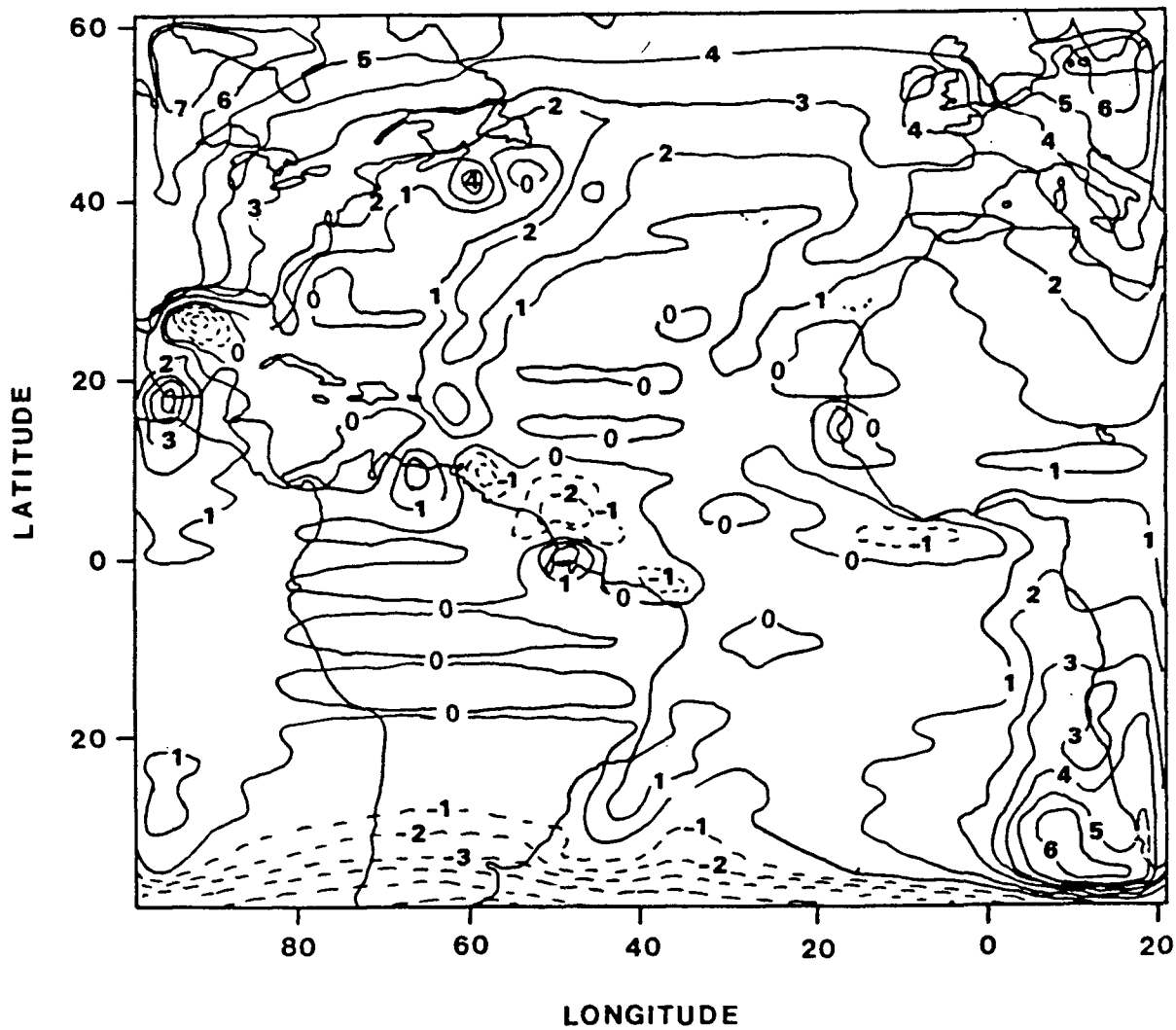

Figure 36. Scalar magnetic field at satellite altitude when the viscous magnetization is strong enough (Figure 35) to produce magnetic anomalies that are similar in strength to those observed by MAGSAT. Contour level is 1 nT.

many times stronger than the average magnetization inferred from studies of oceanic rock samples. The magnetic field (Figure 38) from the Cretaceous quiet zones in the North Atlantic is still dominating, but some of the magnetic signal along the east coast of North America is present. Anomalies, still fairly weak, can also be seen over the Amazon delta and in the Gulf of Mexico. Strong anomalies are also present over the east coast of Brazil and along the south-western Africa-Atlantic coast. However, the amplitude of these anomalies is several times lower than MAGSAT.

In the next model we have increased the susceptibility of the upper mantle to 0.02 SI units (Figure 39), which is so high that the magnetic anomalies produced by the elevated Curie isotherm beneath areas with thick deposits of sediments are similar in strength to MAGSAT anomalies. We have used the same contour interval (2 nT) in Figure 40 as in the MAGSAT map. The characteristic anomaly in the north-western Atlantic, that can be seen in the MAGSAT field, shows the same low values over the Laurentian Cone and of the coast of Georgia and Florida. The negative anomaly in this area is closer to the coast when compared to the MAGSAT field. The negative anomaly in the Gulf of Mexico is also similar to what is observed by MAGSAT. There is a strong anomaly over the Lesser Antilles Trench in Figure 38 that is not present in the MAGSAT field. The reason for this is probably the compensation of the relative low

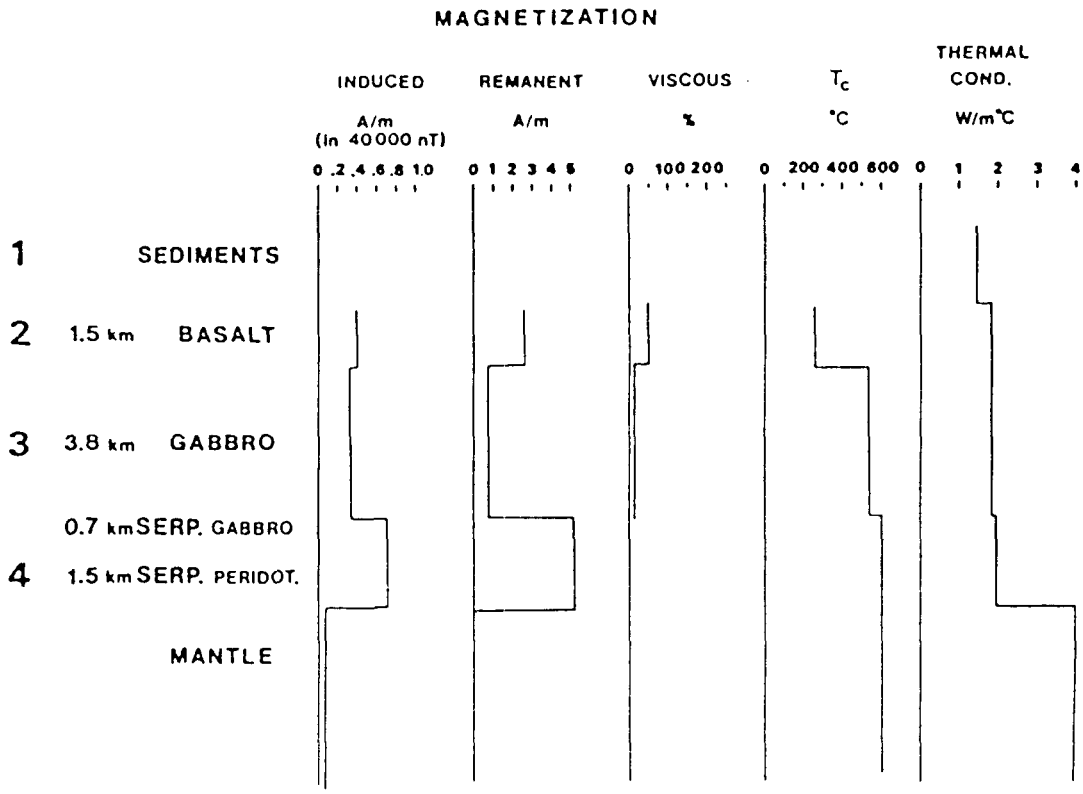

Figure 37. Magnetization model of the oceanic lithosphere with remanent magnetization, susceptibility and viscous magnetization inferred from oceanic rock samples, and with a susceptibility of 0.008 SI units in the part of the upper mantle that is situated below the 1.5 km of serpentinized peridotites and the Curie isotherm.

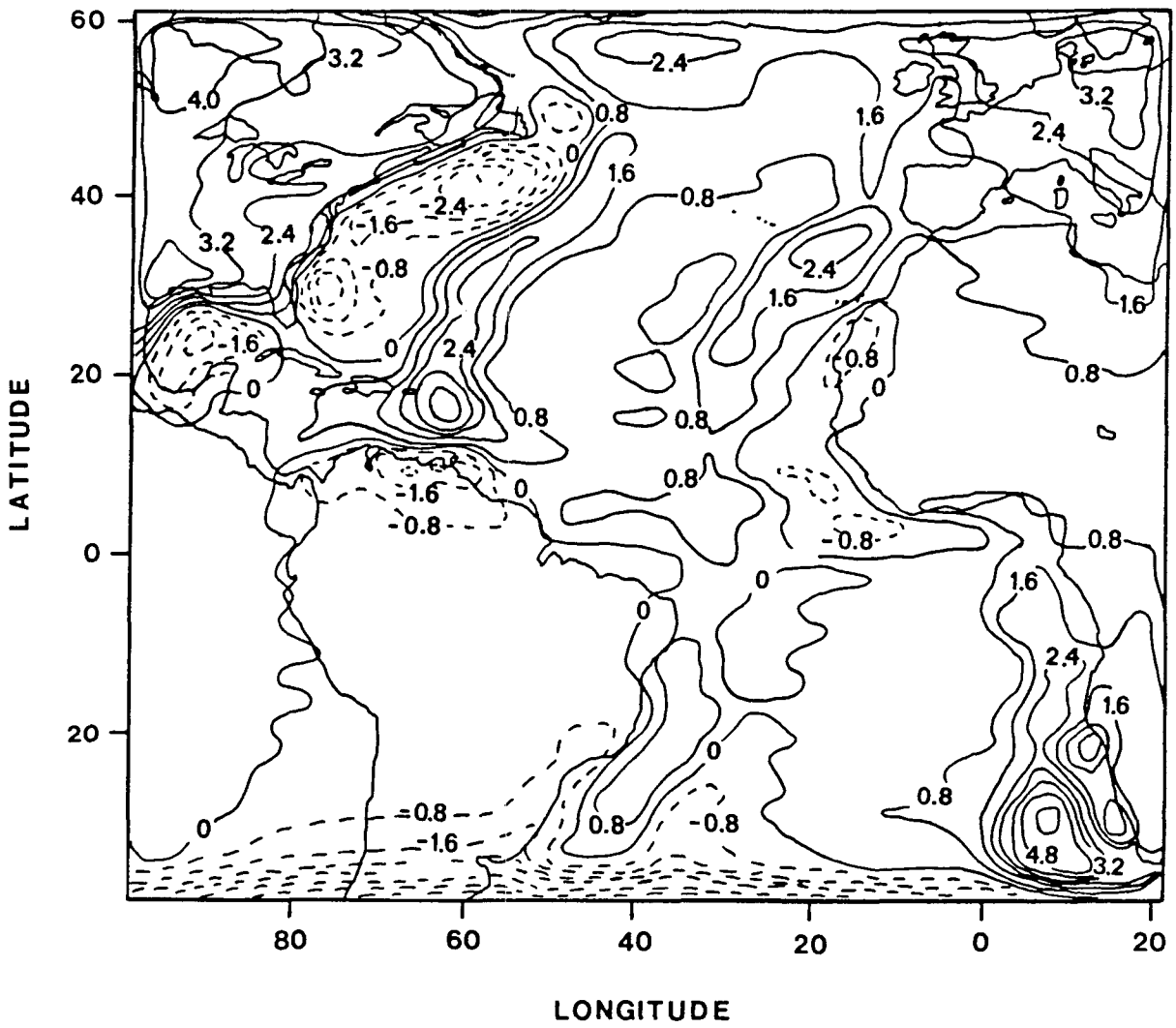

Figure 38. Scalar magnetic field at satellite altitude, from magnetic sources in the crust and in the upper mantle (Figure 37). The susceptibility in the part of the upper mantle is 0.008 SI units. Contour interval is 0.8 nT.

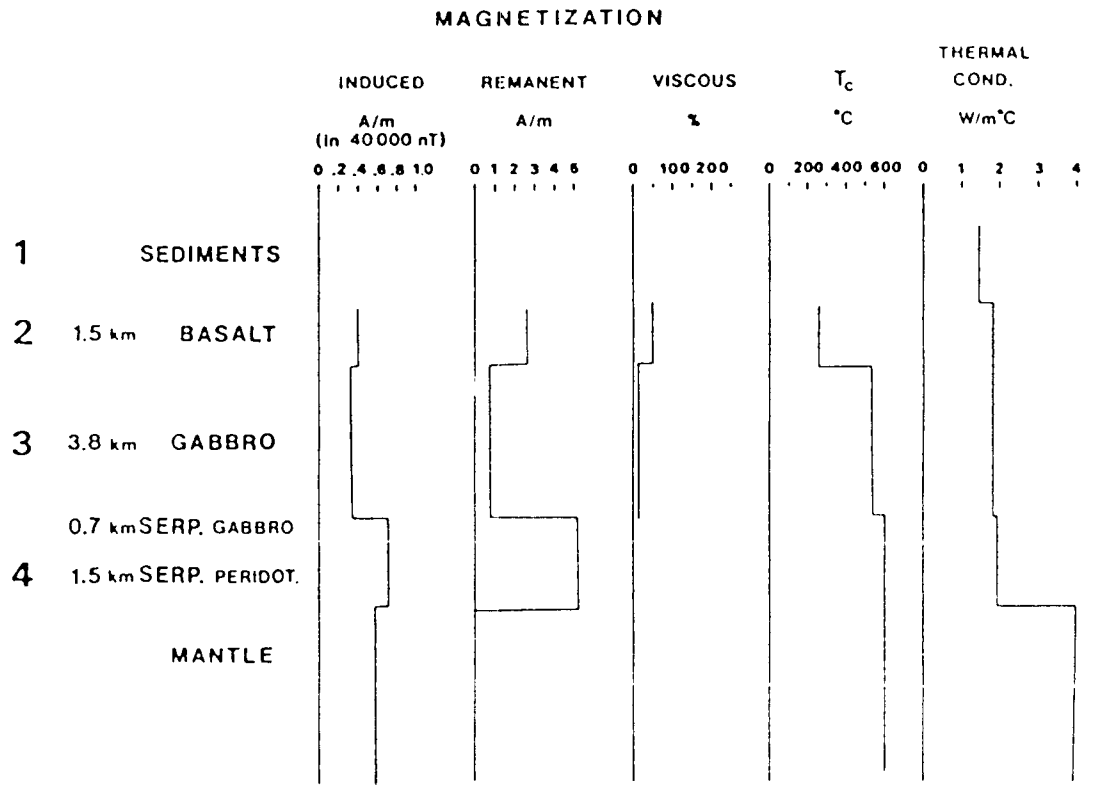

Figure 39. Magnetization model of the oceanic lithosphere with remanent magnetization, susceptibility and viscous magnetization inferred from oceanic rock samples, and with a susceptibility of the upper mantle of 0.02 SI units.

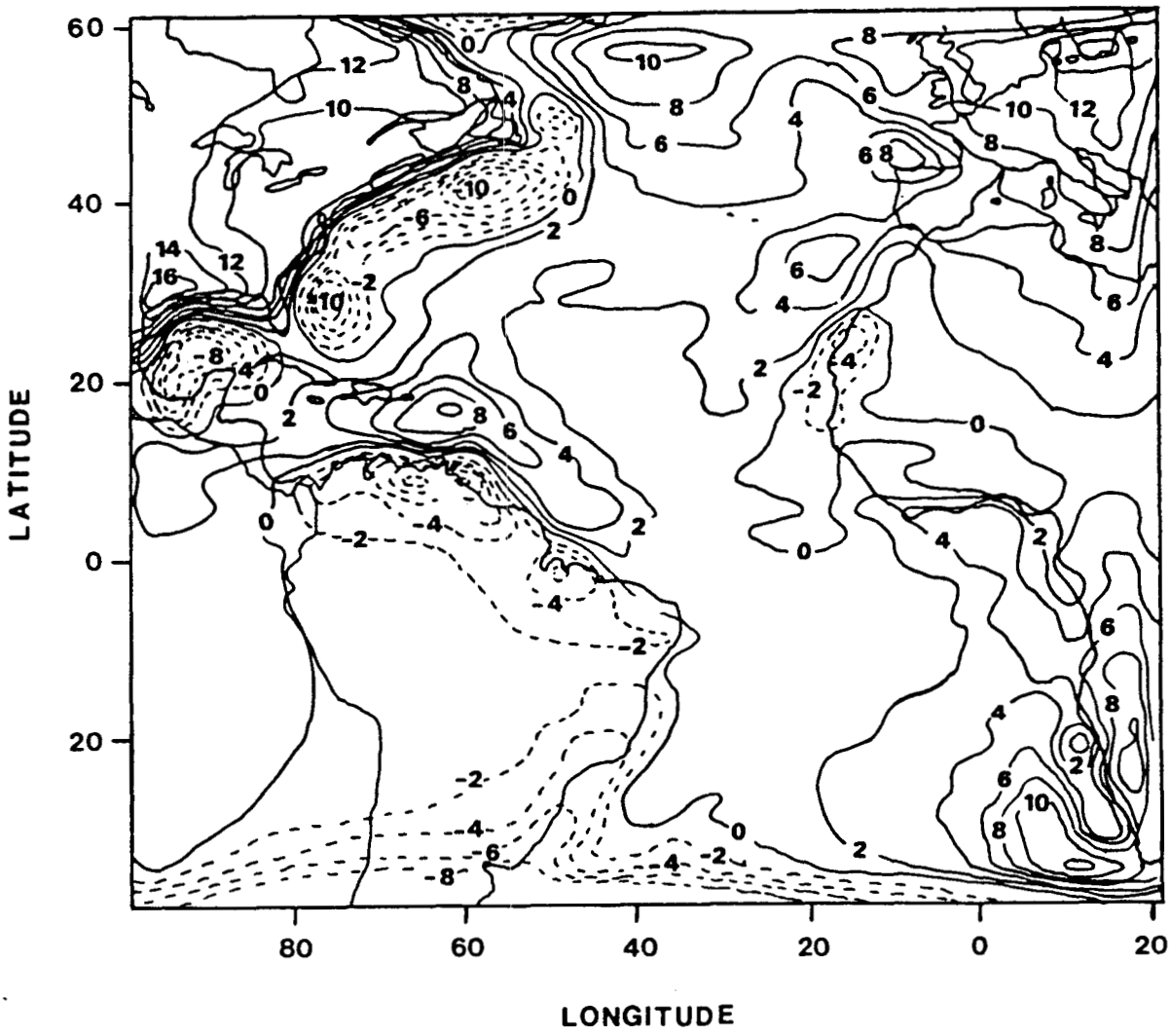

Figure 40. Scalar magnetic field at satellite altitude when the upper mantle has strong enough susceptibility (Figure 39) to produce magnetic anomalies that are similar in amplitude to MAGSAT anomalies. Contour level is 2 nT.

magnetization from the thick sediment cover, by an increase in vertically integrated magnetization from the subducting slab. Subduction zones are often associated with high magnetizations (e.g. Vasicek et al, 1984; Frey, 1985; Arkani-Hamed and Strangway, 1986). A negative anomaly can also be seen in the Greenland Sea. The anomaly over the Amazon delta is not as strong as in the MAGSAT map. It is possible that the Amazon aulacogen enhances the relative low magnetization, which will increase the amplitude of this anomaly. The lack of an anomaly over the Congo Cone is probably the result of the relatively small lateral extension of the thick sediment cover in this area. It is possible that the map that we have used to digitize sediment thickness is less accurate in this area. The number of seismic lines over the Congo Cone is much less than over the Amazon, Mississippi, and Laurentian deep sea fans. It is possible that the full extent of the Congo delta has not been adequately measured yet.

We mentioned earlier that much attention has been given the the lack of long wavelength anomalies over the continent-ocean boundary, and the possibility that some of this signal is removed when the magnetic field from the Earth's core is subtracted from the measurements. In order to see what kind of magnetic anomalies that will be produced by a difference in magnetization between the continents and the oceans, we calculated the scalar magnetic anomaly field

from a model where the vertically integrated intensity of magnetization is higher in the continental lithosphere than in the oceanic lithosphere. Figure 41 shows this anomaly field from a contrast in vertically integrated magnetization of a factor 2. We have not included any effect from sedimentation in this model. Strong anomalies are present along all continental margins. At high magnetic latitudes the anomalies are positive and at low magnetic latitudes the anomalies are negative. The magnetic anomaly over the Greater Antilles is similar to the MAGSAT anomaly field over this area. This characteristic anomaly supports a model of a stronger magnetization in the continental lithosphere. Hayling and Harrison (1986) discuss other explanations for this anomaly, such as thickening of the oceanic crust when this moved over a hot spot.

The magnetization model that we produced magnetic anomalies most similar to MAGSAT is a model that includes magnetic sources in the upper mantle. A similar magnetic anomaly field will also be produced by very strong viscous magnetization. This type of magnetization is a very popular contender for the magnetic source, being able to make up for the discrepancy between the intensity of magnetization inferred from studies of oceanic rock samples and magnetic anomalies, both for satellite altitude and for near surface observations. However, this requires that the thermal properties that we have used in our calculations are

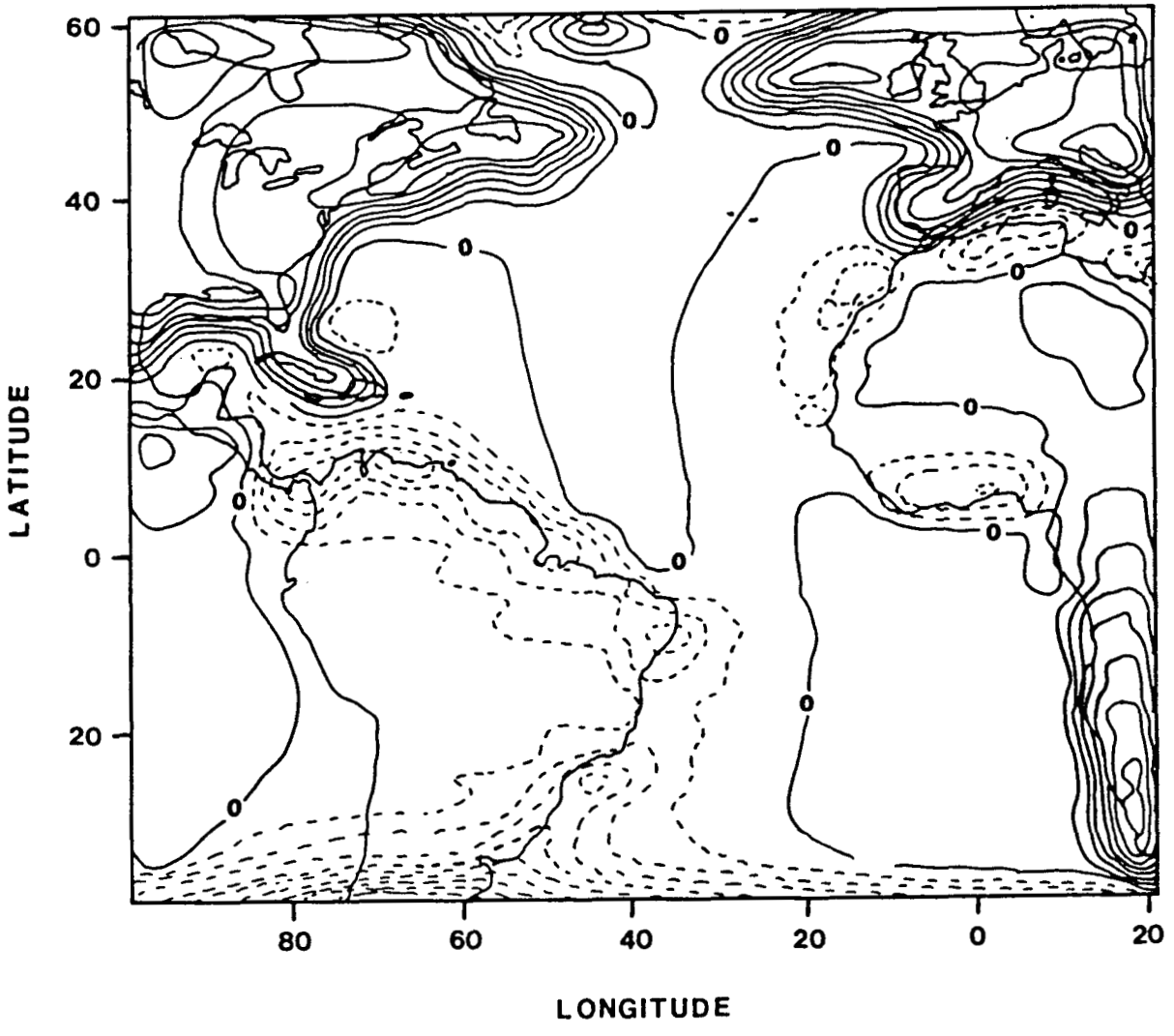

Figure 41. Scalar magnetic field at satellite altitude that is produced if the vertically integrated magnetization contrast in the continental crust is twice that of the oceanic crust. The contour level is arbitrary.

approximately correct. In a case of a magnetized upper mantle, if for some reason the Curie isotherm is deeper than we propose because of higher conductivity or internal generation of heat, it is still possible to produce magnetic anomalies that are similar to MAGSAT anomalies (Figure (39). In the latter case we cannot explicitly determine a zero level to be used when we choose the strength of the annihilator, but have to make the annihilator strong enough that the minimum intensity of magnetization in the final model is approximately the same as the average magnetization of the oceanic crust, or about 0.58 A/m.

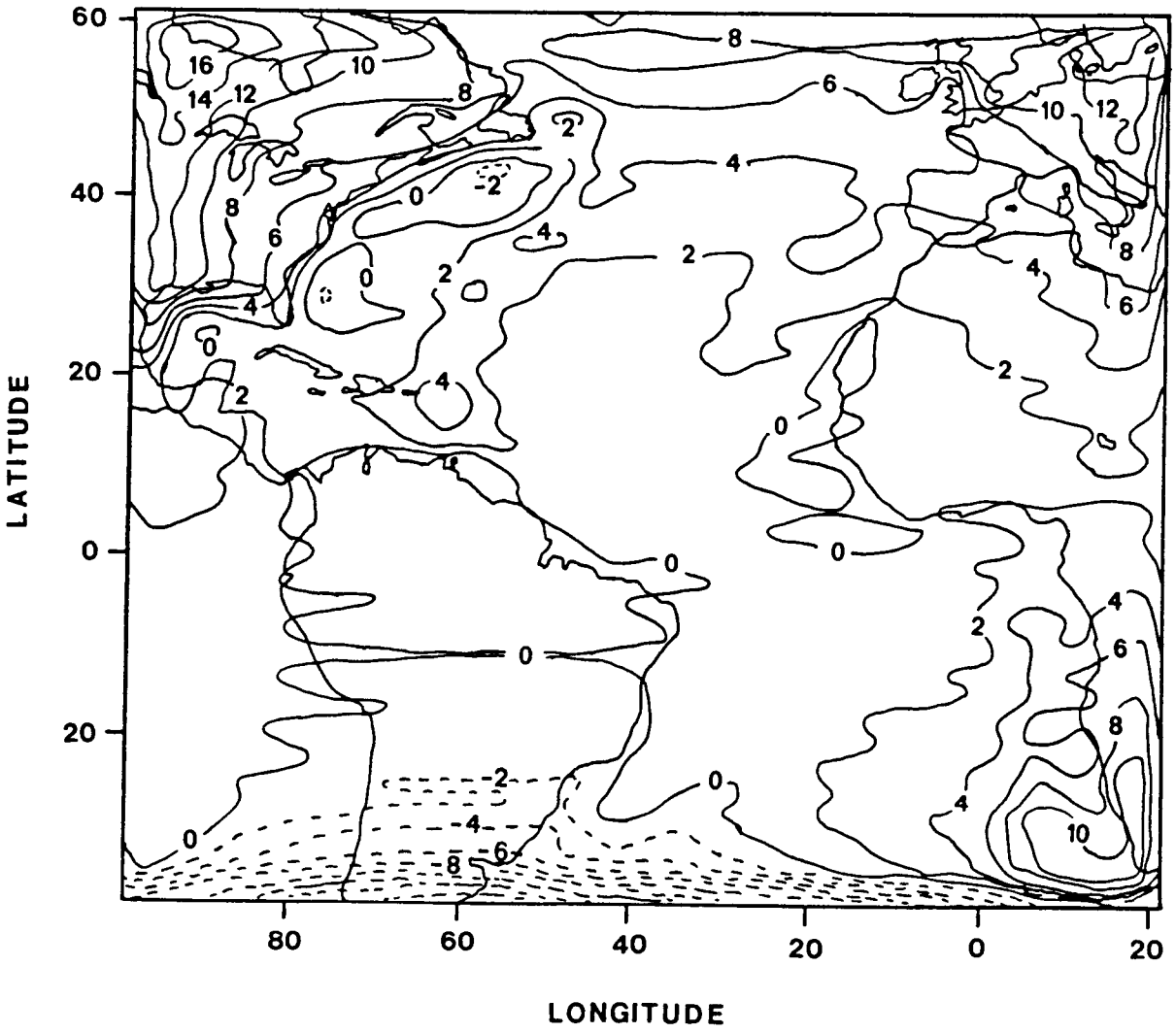

Figure 42. Scalar magnetic field at satellite altitude, with magnetic sources in the crust and upper mantle, but with a high enough thermal conductivity in the sediments that the Curie isotherm never reaches the crust. Contour interval of 2 nT.

5. DISCUSSION

We have shown that some of the signal in magnetic anomaly maps can be artifacts of the algorithms that have been used to extract the anomaly field. These results agree with the prediction of Alldredge (1983) concerning the subtraction of a core field to obtain anomaly fields. Alldredge concludes that the spherical harmonic content of extended (several hundreds of kilometers) crustal sources will overlap so much with the core field that subtraction of a core field model up to only degree 10 will distort the anomaly field so badly that interpretation in terms of geologic sources will be difficult. We have shown that also small (dipoles) magnetic sources in the crust will distort the anomaly field. The result from analysis of power spectra of the spherical harmonic models of the total field and the anomaly field is puzzling. When we determined spherical harmonic models of the core field alone, it seems that all harmonic coefficients that are fitted to the data set will aquire some value. It is obvious that some of the power in the high degrees of harmonic comes from the crustal field, because the power for high degrees is greater in the power spectra of the total and anomaly fields compared to the core field. We need to determine how much of the high degrees of harmonic in the simulated total and anomaly fields that is produced by crustal anomalies. Much work remains to be done with this problem, but we believe that it is important that

investigators working with modelling of satellite magnetic anomaly fields are aware of the possibility that some of the magnetic signal, especially weak anomalies, may not be caused by large scale variations in vertically integrated magnetization in the Earth's lithosphere.

Much of the discussion about the depth to the Curie isotherm and scalar magnetic anomalies from different magnetic sources in the oceanic lithosphere has been done in the previous chapter. The characteristic magnetic anomalies along the east coast of North America that are seen in most satellite anomaly maps are effectively produced by variations in vertically integrated magnetization. These variations are produced by fluctuations in the depth to the Curie isotherm. A magnetized upper mantle produce anomalies that correlate well with MAGSAT anomalies. Although similar amplitudes of these anomalies can be obtained with an increase in viscous magnetization the closer correlation between the field from a magnetized upper mantle suggests a magnetized mantle as the source for these anomalies. Correlation between depth to the Curie isotherm and satellite magnetic anomalies is shown to be useful in the modelling of satellite magnetic anomalies and in the investigation of possible magnetic sources in the Earth's lithosphere.

A zero level, to be used when magnetization models are calculated, can be determined if the thermal conductivity of

oceanic rocks and sediments is equal to or less than what we have used in our calculations of the depth to the Curie isotherm. The necessity to adjust magnetization models with annihilators has been discussed above. The minimum amount of annihilator, needed to produce physically plausible magnetization models, is given by the final magnetization model. Negative magnetizations can not be allowed. The average intensity of magnetization in the oceanic lithosphere is increased when an annihilator is added. The average intensity of magnetization, implied from modelling of MAGSAT anomalies, is very similar for all oceans. This value, about 4 A/m, has also been suggested from rock studies (e.g. Thomas, 1987). The most important components in his model are viscous magnetization and thermal enhance ment. We have used several assumptions when we modelled the depth to the Curie isotherm, the vertically integrated intensity of magnetization in the oceanic lithosphere and the magnetic anomalies produced by these models of magnetization. However, we have shown by different methods that these assumptions are reasonable. The results from this simulation have again raised the question about the source for intermediate wavelength anomalies over the oceans. The rock samples that have been studied so far is possibly a good representation of the upper part of the crust where most of the DSDP rocks have been sampled. It is probably not reasonable to expect that the data set of

magnetic rock samples from the oceanic crust will drastically change our rock magnetic models of the oceanic crust. Some of this information can be found from studies of magnetic anomalies with additional geophysical information, for example the thermal state of the oceanic lithosphere. The danger in using rock samples alone is well demonstrated by Bleil and Petersen (1983), who propose a model of the variation of magnetization in the oceanic crust over a time span of over 100 MY from as little as 4 rock samples for a time period of over 10 MY.

In our modelling of the depth to the Curie isotherm the most important physical properties are the thermal conductivities in the different layers of the oceanic lithosphere. A general increase in the thermal conductivity will push the Curie isotherm deeper and at a certain point the oceanic crust will not be affected by thermal destruction of the magnetic minerals. But if the upper mantle is magnetic, magnetic anomalies will be produced from variations in the depth to the Curie isotherm. If this is the case we cannot find a zero level to determine the strength of the annihilator. The strength of the annihilator in such a case has to be set to in such a way that the minimum intensity of magnetization, after adjustment with an annihilator, is greater or equal to the average magnetization of the approximately 6 km thick oceanic crust. If we use values from direct studies of

oceanic rock samples this is about 0.5 A/m, which will increase the average intensity of magnetization in the upper mantle by the same amount in order for this source to produce magnetic anomalies with the same amplitude as the case when the crust was affected by thermal destruction of its magnetic minerals. The effective susceptibility of the upper mantle will then be about 0.02 SI units, which is almost three times the value proposed by Arkani-Hamed and Strangway (1986b). Naturally a choice of thermal conductivities that will increase the depth to the Curie isotherm even more, will require an additional susceptibility in the upper mantle in order to produce the same amplitude of the magnetic anomalies.

6. CONCLUSIONS

Scalar magnetic anomaly fields, derived by subtracting a core field that is represented by spherical harmonics, can be severely distorted. The power spectra of spherical harmonic models of core and crustal fields does not correctly represent the true spectrum of these anomalies.

The depth to the Curie isotherm, mainly governed by the thickness of the insulating sediment cover, correlates well with the intensity of magnetization in the oceanic lithosphere. The most pronounced magnetic anomalies over the continent-ocean boundaries in the Atlantic Ocean are produced by undulations in the depth to the Curie isotherm and an magnetized upper mantle with a susceptibility of about 0.02 SI-units.

Finding the depth to the Curie isotherm also indicates where the effective magnetization is approximately zero, which can be used to find the strength of the annihilator when magnetization models are adjusted.

APPENDIX A: Spherical harmonic analysis

The magnetic field at some location, given in geocentric coordinates (r,θ,ϕ) is defined as the gradient of the potential and is fairly easy to determine from a spherical harmonic model of magnetic potential

$$V = a \sum_{n=1}^{N} \left[\frac{a}{r}\right]^{n+1} \sum_{m=0}^{n} (g_n^m \cos m\phi + h_n^m \sin m\phi)\, P_n^m(\theta) \qquad \text{(A1)}$$

The magnetic field components in latitudinal, longitudinal and vertical directions are determined by Equations A2, A3 and A4.

$$F_\theta = -\frac{1}{r}\frac{\partial V}{\partial \theta} = -\sum_{n=1}^{N} \left[\frac{a}{r}\right]^{n+2} \sum_{m=0}^{n} (g_n^m \cos m\phi + h_n^m \sin m\phi)\, \frac{\partial P_n^m(\theta)}{\partial \theta} \qquad \text{(A2)}$$

$$F_\phi = -\frac{1}{r\sin\theta}\frac{\partial V}{\partial \phi} = \frac{1}{\sin\theta} \sum_{n=1}^{N} \left[\frac{a}{r}\right]^{n+2} \sum_{m=0}^{n} (g_n^m \sin m\phi - h_n^m \cos m\phi)\, P_n^m(\theta) \qquad \text{(A3)}$$

$$F_r = -\frac{\partial V}{\partial r} = \sum_{n=1}^{N} \left[\frac{a}{r}\right]^{n+2} (n+1) \sum_{m=0}^{n} (g_n^m \cos m\phi + h_n^m \sin m\phi)\, P_n^m(\theta) \qquad \text{(A4)}$$

The Gauss coefficients, g_n^m and h_n^m, are determined by integration of the expressions above

$$\begin{matrix} A_n^m \\ B_n^m \end{matrix} = \frac{2n+1}{4\pi} \int_0^{\pi}\int_0^{2\pi} f(\theta,\phi)\, P_n^m(\theta) \begin{matrix} \cos m\theta \\ \sin m\theta \end{matrix} \sin\theta\, d\theta\, d\phi \qquad \text{(A5)}$$

where $f(\theta,\phi)$ is the functional of A_n^m and B_n^m . A_n^m and B_n^m are spherical harmonic coefficients of potential. The Gauss coefficients are determined by dividing with the distance square to make the coefficients come out in units of magnetic field. A detailed discussion of spherical harmonic analysis in geomagnetism is given by Chapman and Bartels (1962, Chapter 17).

When spherical harmonic models are determined from discrete values of the magnetic field, the gauss coefficients are determined by least squares fit of the coefficients to the observed field values. Simplified, the matrix consists of the functions $f_i\ (r,\theta,\phi)$ of $g_n^m$and h_n^m, and the observed field values $O_l\ (l = 1,\ldots,k)$

$$\begin{matrix} f_{1,1} & \ldots & f_{n,1} & O_1 \\ \cdot & \cdots & \cdot & \cdot \\ f_{1,} & \ldots & f_{n,l} & O_l \end{matrix}$$

Schmitz and Cain (1983) describe in detail the iterative method that usually is used when spherical harmonic models of the Earth's magnetic field are determined. In general, no set of parameters of the spherical harmonic model will satisfy all observations, but if the initial model is close enough to reality any corrections of the model can be assumed to be linear. A brief description of this method follows.

Let O_i be observed values and C_i calculated values, of the

magnetic field, at the i:th observation point (i = 1,...,I).

$$\varepsilon^2 = \sum_{i}^{I} \left[O_i - C_k(p_k; r, \theta, \phi) \right]^2 w_i \qquad \text{(A6)}$$

where p_k (k = 1,...,K) may be any of the parameters g_n^m and h_n^m. The functional form f may be non-linear in the parameters and we expand f in a Taylor series about the approximate solution C_i

$$\varepsilon^2 = \sum_{i}^{I} \left[O_i - C_i - \sum_{k=1}^{n} \frac{\partial C}{q p_k} \Delta p_k - \frac{1}{2!} \sum_{j,k=1}^{n} \frac{\partial^2 C}{\partial p_j \, \partial p_k} \Delta p_j \, \Delta p_k, \ldots \right]^2 w_i \qquad \text{(A7)}$$

Assuming that the needed corrections are linear, we truncate after the first order term. The problem is now to minimize

$$\sum_{i=1}^{n} \left[O_i - C_i - \sum_{k=1}^{K} \frac{\partial f}{\partial p_k} \Delta p_k \right]^2 w_i = 0 \qquad \text{(A8)}$$

The adjustment made is found by determining the differential of the calculated value with respect to the variables, using this as the divisor with the difference between observed and calculated field value as dividend. We also assign weights (W_i) to each field value.

$$\sum_{i}^{I} w_i \sum_{j=1}^{n} \Delta p_j \frac{\partial f}{\partial p_j} \frac{\partial f}{\partial p_k} = \sum_{i}^{I} w_i (O_i - C_i) \frac{\partial f}{\partial p_k} \qquad \text{(A9)}$$

and

$$\Delta p_j = \left[\sum_{j=1}^{K} \sum_{i=1}^{I} w_i \sum_{k=1}^{n} \frac{\partial f}{\partial p_j} \frac{\partial f}{\partial p_k} \right]^{-1} \left[\sum_{j=1}^{K} \sum_{i=1}^{I} w_i (O_i - C_i) \frac{\partial f_i}{\partial p_j} \right] \quad \text{(A10)}$$

In matrix form (A17) becomes $P = (X^T W X)^{-1} X^T W Y$. P is the column vector with the unknown adjustment. The weights are arranged in the diagonal matrix W. The derivatives of the functions with respect to the parameters are included in an I by K matrix X and the vector (Y) of difference between observed calculated field values.

$$P = \begin{vmatrix} \Delta p_1 \\ \cdot \\ \Delta p_K \end{vmatrix} \qquad W = \begin{vmatrix} W_1 & \cdots & 0 \\ & \cdot & \\ 0 & \cdots & W_I \end{vmatrix}$$

$$X = \begin{vmatrix} \frac{\partial f_1}{\partial p_1} & \cdots & \frac{\partial f_1}{\partial p_K} \\ & \cdot & \\ \frac{\partial C_I}{\partial p_1} & \cdots & \frac{\partial C_I}{\partial p_K} \end{vmatrix} \qquad Y = \begin{vmatrix} O_1 - C_1 \\ \cdot \\ O_I \quad C_I \end{vmatrix}$$

APPENDIX B: Conductive heat flow

Conductive heat flow per unit area is directly proportional to the temperature gradient. Fourier's law, in one dimension, is given by

$$q = - K \frac{\partial T}{\partial T} \qquad \text{(B1)}$$

where q is the surface heat flow, κ is the thermal conductivity of the material, T is the temperature, and z is the distance in the direction of the flow of heat. z is taken positive downwards.

In order to determine the flow of heat as a function of sedimentation rate, we introduce a time dependent expression of heat flow. The change in temperature with time within a small volume of the sediment layer will depend upon the net flow of heat across its surface, the rate of heat generation and the thermal capacity of the sediments. The change in temperature as a function of the flow of heat with time is equal to the difference in heat flow between the top and the bottom of the small volume divided by the ability of the material to store heat, which is equal to the heat capacity (k) times the density (ρ). Internal generation of heat (A) will increase the temperature with time as a function of how fast the heat is conducted away.

$$\frac{\partial T}{\partial t} = \frac{1}{\varrho c} \frac{\partial q}{\partial z} + \frac{A}{\varrho c} \qquad \text{(B2)}$$

In a simulation of sedimentation we consider the sediment layer moving with a velocity (U) in the positive vertical direction. The flow of heat that we will observe when moving with the medium will depend on the temperature gradient (Equation B1) plus a convective term due to the motion.

$$q = - K \frac{\partial T}{\partial z} + \varrho c T U \tag{B3}$$

Using (B3) in (B2) gives

$$\frac{\partial T}{\partial t} = - \frac{1}{\varrho c} \frac{\partial}{\partial z} \left(- K \frac{\partial T}{\partial z} + \varrho c T U\right) + \frac{A}{\varrho c} \tag{B4}$$

Combining the constants K, c and ρ (density) to thermal diffusivity $k = K/\rho c$, and differentiating (B4) gives

$$\frac{1}{k} \frac{\partial T}{\partial t} = \frac{\partial^2 T}{\partial z^2} - \frac{U}{\kappa} \frac{\partial T}{\partial z} + \frac{A}{K} \tag{B5}$$

We are interested in how much the thermal gradient at the surface varies for different situations and rearrange to

$$\frac{\partial^2 T}{\partial z^2} = \frac{U}{\kappa} \frac{\partial T}{\partial z} + \frac{1}{\kappa} \frac{\partial T}{\partial t} - \frac{A}{K} \tag{B6}$$

with the following boundary conditions

$$T = az \quad \text{at} \quad z > 0,\ t = 0$$

$$T = 0 \quad \text{at} \quad z = 0,\ t > 0$$

the temperature gradient in a sediment layer with constant rate of sedimentation (U) is

$$\frac{\partial T}{\partial z} = a + \frac{1}{2U}\left[aU - \frac{\kappa A}{K}\right]\left[e^{Uz/\kappa}\left(1 + \frac{Uz}{\kappa} + \frac{U^2 t}{\kappa}\right)\operatorname{erfc} X - \operatorname{erfc} Y + e^{Uz/\kappa}\, X\left(-\frac{\partial}{\partial X}\operatorname{erf} X\right) - Y\left(-\frac{\partial}{\partial Y}\operatorname{erf} Y\right)\right] \tag{B7}$$

where

$$X = \frac{z + Ut}{2(kt)^{1/2}} \qquad Y = \frac{z - Ut}{2(kt)^{1/2}}$$

This solution is given by Von Herzen and Uyeda (1963).

A time dependent boundary condition for the surface temperature can be included

$$T = bt \quad \text{at} \quad z = 0,\ t > 0$$

giving us the possibility to determine the effect on the thermal gradient when the surface temperature is allowed to vary with time. For example during the Cretaceous the bottom water temperature was about 15 °C.

REFERENCES

Alldredge, L.R., Core and crustal geomagnetic fields, J. Geophys. Res., 88, 1229-1234.

Arkani-Hamed, J., and D.W. Strangway, Bandlimited global magnetic anomaly map of the earth derived from Magsat data, J. Geophys. Res., 91, 8193-8203, 1986a.

Arkani-Hamed, J., and D.W. Strangway, Interpretation of magnetic signals of subduction zones detected by Magsat, Geophys. Res. Lett., 13, 999-1002, 1986b.

Arkani-Hamed, J., W.E.S. Urquhart, and D.W. Strangway, Scalar magnetic anomalies of Canada and northern United States derived from Magsat data, J. Geophys. Res., 90, 2599-2608, 1985.

Banerjee, S.K., Magnetism of the oceanic crust: Evidence from ophiolite complexes, J. Geophys. Res., 85, 3557-3566, 1980.

Beckenbach, E.F., Applied combinatorial mathematics, J. Wiley and Sons, New York, 608 pp., 1964.

Bergren, W.A., D.V. Kent, J.J. Flynn, and J.A. Van Couvering, Cenozoic geochronology, Geol. Soc. Am. Bull., 96, 1407-1418, 1985.

Beske-Diehl, S., and S.K. Banerjee, An example of magnetic properties as indicators of alteration in ancient oceanic lithosphere - The Othris ophiolite, Earth Planet. Sci. Lett., 44, 451-462, 1979.

Bleil, U., and N. Petersen, Variations in magnetization intensity and low-temperature titanomagnetite oxidation of ocean floor basalts, Nature, 301, 384-388, 1983.

Bott, M.H.P., Solution of the linear inverse problem in magnetic interpretation with application to oceanic magnetic anomalies, Geophys. J. Roy. Astr. Soc., 13, 313-323, 1967.

Bozorth, R.M., Ferromagnetism, Van Nostrand, 968 pp., New York, 1964.

Cain, J.C., D.R. Schmitz, and L.Muth, Small scale features observed by Magsat, J. Geophys. Res., 89, 1070-1076, 1984.

Carle, H.M., Modeling oceanic crustal magnetization using Magsat derived scalar anomalous field data, Thesis, University of Miami, 58 pp., 1983.

Carle, H.M., and C.G.A. Harrison, A problem in representing the core magnetic field of the earth, Geophys. Res. Lett., 9., 265-268, 1982.

Carslaw, H.S., and J.C. Jaeger, Conduction of heat in solids, 2 nd ed., Oxford University Press, 510 pp., Oxford, 1978.

Clark, S.C., Modelling satellite magnetic anomalies: Subduction zones, EOS, AGU, 64, 215, 1983.

Dunlop, D.J., Thermal enhancement of magnetic susceptibility, J. Geophys. Res., 40, 439-451, 1974.

Dunlop, D.J., Viscous magnetization of 0.04-100 μm magnetites, Geophys. J. Roy. Astr. Soc., 74, 667-687, 1983.

Dunlop, D.J., and M. Prevot, Magnetic properties and opaque mineralogy of drilled submarine intrusive rocks, Geophys. J. Roy. Astr. Soc., 69, 763-802, 1982.

Embley, R.W., M.A. Hobart, R.N. Anderson, and D. Abbot, Anomalous heat flow in the northwest Atlantic: A case for continued hydrothermal circulation in 80 m.y. crust, J. Geophys Res., 88, 1967-1074, 1983.

Emery, K.O., and E. Uchupi, The geology of the Atlantic Ocean, Springer Verlag, 1050 pp., New York, 1984.

Fox, P.J., and N.F. Opdyke, Geology of the oceanic crust: Magnetic properties of oceanic rocks, J. Geophys. Res., 78, 5139-5154, 1973.

Frey, H., POGO and Magsat anomalies and the oceanic crust, EOS, AGU, 66, 359-360, 1985.

Harrison, C.G.A., Magnetization of the oceanic crust, Geophys. J. Roy. Astr. Soc., 47, 257-283, 1976.

Harrison, C.G.A., Marine magnetic anomalies - the origin of the stripes Ann. Rev. Earth Planet. Sci., 15, 505-543, 1987a.

Harrison, C.G.A., The crustal field, in J.A. Jacobs, Geomagnetism, Academic Press, London, 1987b.

Harrison, C.G.A., H.M. Carle, and K.L. Hayling, Interpretation of satellite magnetic anomalies, J. Geophys. Res., 91, 3633-3650, 1986.

Harrison, C.G.A., and T.B. Lindh, A polar-wandering curve for North America during the Mesozoic and Cenozoic, J. Geophys. Res., 87, 1903-1920, 1982.

Heyes, D.E., and P.D. Rabinowitz, Mesozoic lineations and the magnetic quiet zone off northwest Africa, Earth Planet. Sci. Lett., 28, 105-115, 1975.

Hayling, K.L., Magnetic anomalies at satellite altitude over continent-ocean boundaries, IUGG General Assembly, IAGA Session 1.7, Vancouver, 9-22 August.

Hayling, K.L., Heat flow and magnetization in the oceanic crust, and the possibility to determine a zero level for magnetic models derived from satellite altitude magnetic anomalies, EOS, AGU, 67, 264, 1986.

Hayling, K.L., and C.G.A. Harrison, Examination of noise in Magsat data from equivalent source modeling, EOS, AGU, 66, 255, 1985.

Hayling, K.L., and C.G.A. Harrison, Magnetization modeling in the North and Equatorial Atlantic Ocean using Magsat data, J. Geophys. Res., 91, 12423-12443, 1986.

Henderson, J., and E. Davis, An estimate of the heat flow in the western North Atlantic at Deep Sea Drilling Project Site 504, In Sheridan, R.E., et al., Init. Repts. DSDP 76: Washington (U.S. Govt. Printing Office), 719-724, 1983.

Hutchison, I., The effect of sedimentation and compaction on oceanic heat flow, Geophys. J. Roy. Astr. Soc., 82, 439-459, 1985.

Irving, E., W.A. Robertson, and F. Aumento, The Mid-Atlantic Ridge near 45 N, VI, Remanent intensity, susceptibility and iron content of dredged samples, Can. J. Earth Sci., 7, 226-238, 1970.

Kent, D.V., and F.M. Gradstein, A Cretaceous and Jurassic Geochronology, Geol. Soc. Am. Bull., 96, 1419-1427, 1985.

Kent, D.V., B.M. Honnorez, N.D. Opdyke, and P.J. Fox, Magnetic properties of dredged oceanic gabbros and the source of marine magnetic anomalies, Geophys. J. Roy. Astr. Soc., 55, 513-537, 1978.

Klumpar, D.M., and D.M. Greer, A technique for modeling the magnetic perturbations produced by field-aligned current systems, Geophys. Res. Lett., 9, 361-364, 1982.

LaBrecque, J.L., and C.A. Raymond, Seafloor spreading anomalies in the Magsat field of the North Atlantic, J. Geophys. Res., 90, 2565-2557, 1985.

Langel, R.A., J. Berbert, T. Jennings, and R. Horner, Magsat data processing: An interim report for investigators, NASA Tm, 82160, 1981.

Langel, R.A., and R.H. Estes, A geomagnetic field spectrum, Geophys. Res. Lett., 9, 250-253, 1982.

Langel, R.A., and R.A., Sweeney, Asymmetric ring current at twilight local time, J. Geophys. Res., 76, 4420-4427, 1971.

Lewis, J.F., and R.D. Hyndman, Oceanic heat flow measurements over the continental margins of eastern Canada, Can. J. Earth Sci., 13, 1031-1038, 1976.

Lewis, B.T.R., and W.E. Snydsman, Evidence for a low velocity layer at the base of the oceanic crust, Nature, 266, 340-344, 1977.

Lowes, F.J., Mean square value on the sphere of spherical harmonic vector fields, J. Geophys. Res., 71, 2179, 1966.

Lowes, F.J., Spatial power spectrum of the main geomagnetic field, and extrapolation to the core, Geophys. J. Roy. Astr. Soc., 36, 717-730, 1974.

Lowrie, W., Oceanic basalt magnetic properties and the Vine and Matthews hypothesis, J. Geophysics, 40, 513-536, 1974.

Lowrie, W., and D.V. Kent, Characteristics of VRM in oceanic basalts, J. Geophysics, 44, 297-315, 1978.

Luyendyk, B.P., and R. Day, Paleomagnetism of the Somail ophiolite, Oman, 2, The Wadi Kadir gabbro section, J. Geophys. Res., 87, 10903-10917, 1982.

Luyendyk, B.P., and W.G. Melson, Magnetic properties and petrology of rocks near the crest of the Mid-Atlantic ridge, Nature, 215, 147-149, 1967.

Mauersberger, P., Das Mittel der Energiedichte des geomagnetischen Hauptfeldes an der Erdoberfläche, and seine säkulare Änderung, Gerlands Beitr. Geophys., 65, 207-215, 1956.

Mayhew, M.A., Application of satellite magnetic anomaly data to Curie isotherm mapping, J. Geophys. Res., 87, 4846-4854, 1982a.

Mayhew, M.A., An equivalent layer magnetization model for the United States derived from satellite-elevation magnetic anomalies, J. Geophys. Res., 87, 4837-4845, 1982b.

Mayhew, M.A., Curie isotherm surfaces inferred from high-altitude magnetic anomaly data, J. Geophys. Res., 90, 2647-2654, 1985.

Mayhew, M.A., B.D. Johnson, and R.A. Langel, An equivalent source model of the satellite-altitude magnetic anomaly field over Australia, Earth Planet. Sci Lett., 51, 189-198, 1980.

Minster, J., and T. Jordan, Present day plate motions, J. Geophys. Res., 83, 5331-5354, 1978.

Moore, W.A., Amazon and Mississippi river concentrations of uranium, thorium, and radium isotopes, Earth Planet. Sci. Lett., 2, 231-234, 1967.

Opdyke, N.D., and T. Hekinian, Magnetic properties of some igneous rocks from the Mid-Atlantic ridge, J. Geophys. Res., 72, 2257-2260, 1967.

Parker, R.L., and S.P. Heustis, The inversion of magnetic anomalies in the presence of topography, J. Geophys. Res., 79, 1587-1593, 1974.

Parsons, B., and J.G. Sclater, An analysis of the variation of ocean floor bathymetry and heat flow with age, J. Geophys. Res., 82, 803-827, 1977.

Raitt, R.W., The crustal rocks, in The Sea, vol. 3, M.M. Hill ed., 85-102, J. Wiley and Sons, New York, 1963.

Raymond, C.A., and J.L. LaBrecque, Magnetization of the oceanic crust: TRM or CRM?, J. Geophys. Res., 92, 8077-8088, 1987.

Sailor, R.V., A.R. Lazarewicz, Magsat investigation of crustal magnetic anomalies in the eastern Indian Ocean, unpublished report prepared for NASA, Goddard Space Flight Center, Greenbelt, Maryland, 1983.

Sailor, R.V., A.R. Lazarewicz, and R.F. Brammer, Spatial resolution and repeatability of Magsat crustal anomaly data over the Indian Ocean, Geophys. Res. Lett., 9, 289-292, 1982.

Sheridan, R.E., L.G. Bates, T.H. Shipley, and J.T. Crosby, Seismic stratigraphy in the Blake-Bahama Basin and the origin of Horizon D, In Sheridan, R.E., et al., Init. Repts. DSDP, 76: Washington (U.S. Govt. Printing Office), 667-683, 1983.

Shuey, R.T., D.K. Shellinger, E.H. Johnson, and L.B. Alley, Aeromagnetics and the transition between the Colorado and the Basin Range province, Geology, 1, 107-110, 1973.

Shuey, R.T., D.K. Shellinger, A.C. Tripp, and L.G. Alley, Curie depth determination from aeromagnetic spectra, Geophys. J. Roy. Astr. Soc., 50, 75-101, 1977.

Schmitz, D.R., and J.C. Cain, Geomagnetic spherical harmonic analysis 1. Techniques, J. Geophys. Res., 1222-1228, 1983.

Smith, B.M., Magnetic viscosity of some doleritic basalts in relation to the interpretation of the oceanic magnetic anomalies, Geophys. Res. Lett., 11, 213-216, 1984.

Stacey, F.D., Physics of the Earth, 414 pp., J. Wiley and Sons, New York, 1977.

Swift, B.A., and H.P. Johnson, Magnetic properties of the Bay of Islands ophiolite suite and implications for the magnetization of oceanic crust, J. Geophys. Res., 89, 3291 -3308, 1984.

Thomas, H.H., 1985, A model of ocean basin crustal magnetization appropriate for satellite elevation anomalies, J. Geophys. Res., 92, 11609-11613, 1987.

Tucholke, B.E., R.E. Houtz, and W.J. Ludwig, Sediment thickness and depth to basement in western North Atlantic ocean basin, Am. Assoc. Petr. Geol. Bull., 66, 1384-1395, 1982.

Turcotte, D.L., and G. Schubert, Geodynamics, J. Wiley and Sons, New York, 450 pp., 1982.

Vasicek, J., H. Frey, and H. Thomas, Satellite-altitude magnetic anomalies over subduction zones: The Middle American trench, EOS, AGU, 65, 202, 1984.

Vine, F.J., and E.M. Moores, Model of gross structure, petrology, and magnetic properties of oceanic crust, Geol. Soc. Am. Mem., 132, 195-205, 1972.

Von Herzen, R.P., and S. Uyeda, Heat flow through the eastern Pacific Ocean floor, J. Geophys. Res., 68, 4219-4250, 1963.

Wilkens, R.H., and T. Handyside, Physical properties of equatorial Pacific sediments, in Mayer, L., et al., Init. Repts. DSDP, 85: Washington (U.S. Govt. Printing Office), 839-847, 1985.

Yanagisawa, M., and M. Kono, Magnetic anomaly maps obtained by means of the mean ionospheric field correction, J. Geomag. Geoelectr., 36, 417-441, 1984.

Yanagisawa, M., M. Kono, T. Yukutake, and N. Fukushima, Preliminary interpretation of magnetic anomalies over Japan and surrounding areas, Geophys. Res. Lett., 9, 322-324, 1982.

VITA

Kjell Lennart Hayling was born [redacted] to Lennart and Virginia Hayling in [redacted]. Primary education was received at the Torpa skolan in Gothenburg, Sweden. Secondary education was obtained at the Munkebacks Gymnaiet in Gothenburg. In 1974 he entered the University in Gothenburg from which he graduated in 1981.

In August 1981 he was admitted to the University of Miami Rosenstiel School of Marine and Atmospheric Science. He was granted the degree Master of Science in December 1986. In December 1988 he was granted the degree Doctor of Philosophy by the University of Miami, Coral Gables.

Permanent address: Pl. 4575A, S-43400 Kungsbacka, Sweden.